CMS Draft Analysis Note

The content of this note is intended for CMS internal use and distribution only

2011/04/26
Head Id: 52123
Archive Id: 52174M
Archive Date: 2011/04/26
Archive Tag: trunk

Measurement of Transverse Momentum Distribution within Jets in pp Collisions at $\sqrt{s}$=7 TeV using reconstructed Particles

Anwar A Bhatti[1], Vivain, O'Dell[2], Kenichi Hatakeyama[3], Ozdemir Kadri[4], and Pelin Kurt[5]

[1] The Rockefeller University, New York, NY 10065, USA
[2] Fermi National Accelerator Laboratory, Batavia IL 60510, USA
[3] Baylor University, Waco, TX 76706, USA
[4] Cukurova University, Adana, Turkey
[5] Vanderbilt University, Nashville, TN 37235, USA

DRAFT

Abstract

Using 36.1 pb^{-1} of pp collisions at center of mass energy of 7 TeV collected by CMS detector at the Large Hadron Collider at the CERN, we have measured the jet shapes, defined as the fractional transverse momentum distribution as a function of the distance from the jet axis using the particle reconstructed and calibrated using PF algorithm. We compare the results with predictions of the QCD inspired event generators PYTHIA and HERWIG++. For Pythia predictions, various underlying event tunes and showering models are studied.

This box is only visible in draft mode. Please make sure the values below make sense.

PDFAuthor: Anwar A Bhatti
PDFTitle: Measurement of Transverse Momentum Distribution within Jets in pp Collisions at sqrts=7 TeV using reconstructed Particles
PDFSubject: CMS
PDFKeywords: CMS, physics, QCD, JetShapes

Please also verify that the abstract does not use any user defined symbols

DRAFT

Contents

1 Introduction . . . 1
2 Definition of Jet Shapes . . . 2
3 Dataset . . . 6
4 Particle Reconstruction . . . 6
5 Cleaning . . . 10
5.1 Vertex Selection Criteria . . . 10
6 Trigger Efficiency . . . 10
7 Jet Reconstruction . . . 12
8 Validation of PF Recontrunction Alorithm . . . 13
9 Gen and reconstructed Jetshape Distributions . . . 17
10 Validation of QCD Parton Shower Modelling . . . 19
10.1 Particles Multiplicity and Momentum Distributions . . . 19
10.2 Jet Fragmentation Functions . . . 38
10.3 Single Jet Mass Distributions . . . 40
11 Jet Shapes . . . 44
12 Unfolding of the jetshapes . . . 44
13 Systematic Uncertainties . . . 46
13.1 Jet Energy Scale . . . 46
13.2 PF Particle Calibration . . . 46
13.3 Jet Energy Resolution . . . 46
13.4 Unfolding Uncertainty . . . 46
14 Jet Shapes . . . 46
15 Conclusions . . . 48

1 Introduction

The transverse momentum profile of a jet, jet shapes [1, 2], is sensitive to multiple parton emissions from the primary outgoing parton and provides a good test of the parton showering description of Quantum Chromodynamics (QCD), the theory of strong interactions. Historically the jet shape has been used to test perturbative QCD (pQCD) α_s^3 calculations [3, 4]. These leading order calculations, with only one additional parton in a jet, showed good agreement with the observed jet shapes. While confirming the validity of pQCD calculations, jet shape studies also indicated that jet clustering, underlying event contribution and hadronization effects must be considered. Currently, these effects can be modeled accurately only within the framework of full-event generators. Current Monte Carlo (MC) event generators use pQCD inspired parton shower models, in conjunction with hadronization and underlying event models, to generate final state particles. MC generators are used extensively to model signal and background events in most analyses at hadron colliders. Jet shapes can be used to tune phenomenological parameters in these MC generators. QCD predicts broader gluon jets than quark jets. The structure of quark and gluon jets can be investigated by comparing measurements of the jet shapes in different processes enriched with either quark or gluon initiated jets in the final state. As shown in Fig. 1, in QCD jet production, the gluon jet contribution changes with the transverse momenta of the jets. Previously, jet shapes have been measured in $p\bar{p}$ collisions at Tevatron and ep collisions at HERA [3–7].

DRAFT

In this paper, we present a study of jet shapes measured using CMS detector at $\sqrt{s} = 7$ TeV using integrated luminosity of 36.1 pb^{-1}. and compare the results obtained with various MC generators. The sensitivities of jet shapes to the underlying event (UE) model and to the flavor of the initiating parton are also explored. To reconstruct jetshapes, we use PF particles which are indivitually reconstructed using tracker, electromagnetic calorimeter, hadron calorimeter and muon system. These particles are individually calibrated and can be directly compared to "true" i.e generated particles. A previous study at CMS using tracks and the calorimeter towers is described in [8, 9]. In addition to jetshapes.we describe the multiplicity and momenta of the particles in a jet. We also present a study of jet fragmentation function, the second moments of jet η and ϕ distributions and jet mass distributions.

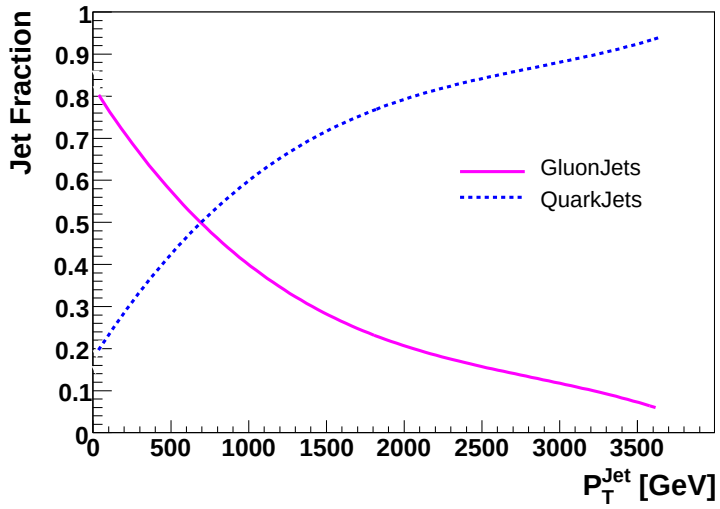

Figure 1: Fraction of the quark or gluon initiated jets as a function of jet p_T for $|y| < 1$ (from PYTHIA DWT) in pp scattering at $\sqrt{s} = 14$ TeV

2 Definition of Jet Shapes

The jet shape is defined as the average fraction of the jet transverse momentum within a cone of a given size r around the jet axis, $r = \sqrt{(y_i - y_j)^2 + (\phi_i - \phi_j)^2}$, where i refers to the particle and j to the jet. Jet shapes can be studied by using an integrated or a differential distribution. In the present study only two leading jets within $|y| < 1$ are considered per event. All particles and calorimeter towers within distance $R = \sqrt{(\Delta y)^2 + (\Delta\phi)^2} = 0.7$ from the jet axis are used . This large cone size ensures that most of the parent parton energy is included in the jet. The differential distribution, $\rho(r)$, is illustrated in Fig. 5. It is defined as the fraction of the jet transverse momentum contained inside an annulus of inner radius $r - \delta r/2$ and outer radius $r + \delta r/2$ around the jet axis, such that $0 \leq r \leq R$:

$$\rho(r) = \frac{1}{\delta r}\frac{1}{N_{jet}}\sum_{jets}\frac{p_T(r - \delta r/2, r + \delta r/2)}{p_T(0, R)}. \tag{1}$$

Above, N_{jet} denotes the total number of selected jets. In the numerator p_T is the sum of all particles in the distance range $(r - \delta r/2, r + \delta r/2)$ from the jet axis. In the denominator, $p_T(0, R)$ is the scalar sum of transverse momenta of all the particles, tracks or towers within the cone of radius R.

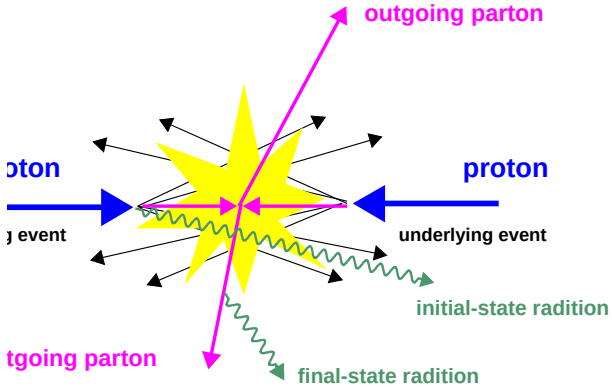

Figure 2: Illustration of a typical proton-proton two parton hard scattering event including initial and final state radiation and beam-beam remnants.

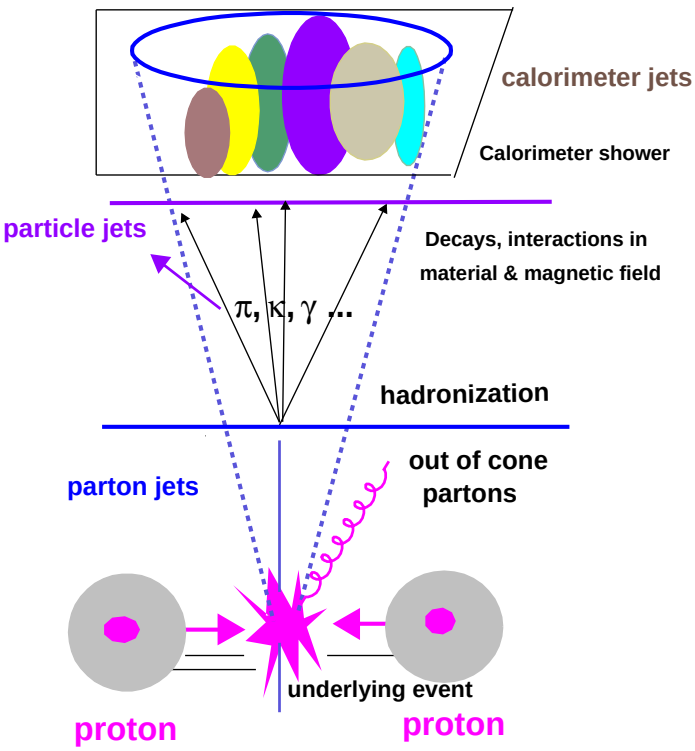

Figure 3: Schematic of jet evolution and detection. Parton jets hadronize into particle jets which interact in the calorimeter forming calorimeter jets.

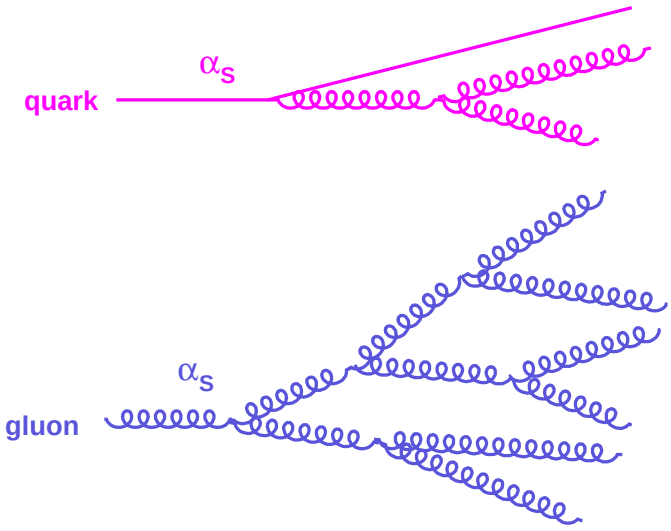

Figure 4: Examples of the structure of quark and gluon initiated jets

Similarly, the integrated jet shape (see Figure 6), $\psi(r)$, is defined as:

$$\psi(r) = \frac{1}{N_{jets}} \sum_{jets} \frac{p_T(0,r)}{p_T(0,R)} \tag{2}$$

where $p_T(0,r)$ is the scalar sum of transverse momenta of all particles within the distance r from the jet axis with $\psi(r = R) \equiv 1$.

To calculate the jet shapes, we made histograms of transverse momentum in the appropriate bin of r divided by the transverse momentum in the cone $R = 0.7$. The mean value of these histograms was then plotted as function of r. The statistical uncertainty on each point was calculated as $rms/\sqrt{N}$, using the rms of the corresponding histogram and the number N of jets in the bin. For the integrated shape the uncertainties at different r points are partially correlated.

Similarly, the integrated jet shape (see Figure 6), $\psi(r)$, is defined as:

$$\psi(r) = \frac{1}{N_{jets}} \sum_{jets} \frac{p_T(0,r)}{p_T(0,R)} \tag{3}$$

where $p_T(0,r)$ is the scalar sum of transverse momenta of all particles within the distance r from the jet axis with $\psi(r = R) \equiv 1$.

The datasets used in this analysis are listed in Table 1, followed by the clean-up and event selections cuts.

To calculate the jet shapes, we made histograms of transverse momentum in the appropriate bin of r divided by the transverse momentum in the cone $R = 0.7$. The mean value of these histograms was then plotted as function of r. The statistical uncertainty on each point was calculated as $rms/\sqrt{N}$, using the rms of the corresponding histogram and the number N of jets in the bin. For the integrated shape the uncertainties at different r points are partially correlated.

DRAFT

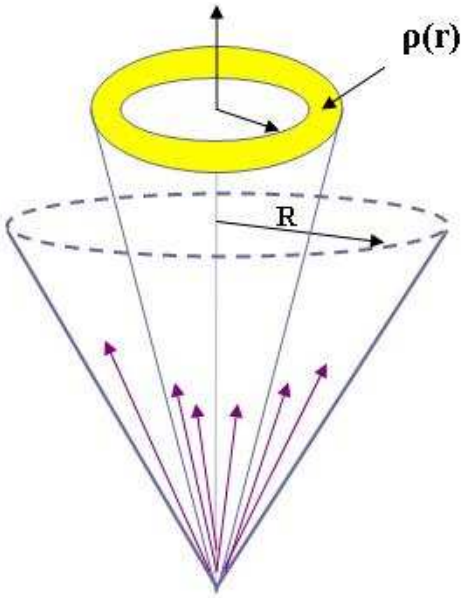

Figure 5: Definition of the differential jet shape, $\rho(r)$.

DRAFT

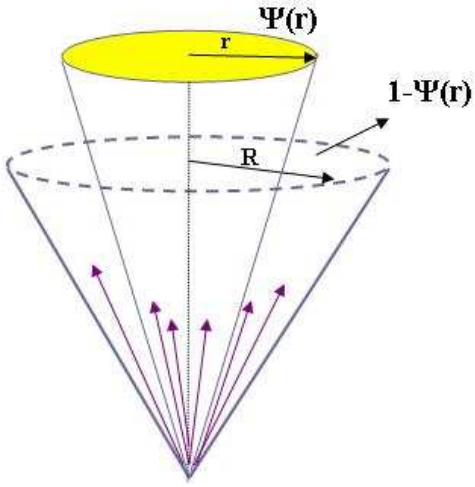

Figure 6: Definition of the integrated jet shape, $\psi(r)$.

3 Dataset

We use Nov4Reco datasets for the jet triggers which are used for the jet $p_T \geq 60$ GeV. For lower jet p_Ts, HLT_L1_BscMinBiasOR_BptxPlusORMinus triggers from the Commissioning10 data are used. These data have the same jet energy scale calibration as the Nov4Reco datasets. For comparison with QCD-inspired event generators, various Fall10 datasets are used. These datasets are listed in Table 1.

The list of good runs and luminosity sections used in given in
Cert_136033-149442_7TeV_Nov4ReReco_Collisions10_JSON.txt
which corresponds to integrated luminosity of 36 pb^{-1}.

The jet trigger were prescaled and appropriate new unprescalled triggers were added to the menu as the instantaneous luminosity increased with time. We combine all these trigger to use maximal data for each p_T bin. For $p_T \leq 40$ GeV/c, we use MinBiasPixel_SingleTrack trigger which triggers on presence of a track in the pixel system and is very efficienct and thus almost unbiased. For $40 \leq p_T \leq 70$ GeV, we use Jet15 and Jet30 triggers from Run2010A-Nov4ReReco datasets (JetMetTau and JetMET). Currently, we are not using Run2010B-Nov4ReReco datasets as these triggers were heavily prescaled during that data taking period. For the $p_T > 70$ GeV/c bins, we use the full data available combining various triggers. Jet50 trigger was available through whole run whereas Jet70, Jet100 and Jet140 were added over time and thus are included in the analysis based on run numbers accordingly. The list of triggers used for different p_T bins is given in 2.

The list of the datasets in given in Table 1. The MC samples include PYTHIA with tune Z2 and tune D6T, PYTHIA 8, herwig6 and herwig++. PYTHIA-D6T sample was generated in range $15 \leq p_T \leq 300$ GeV range but low p_T region can be covered by Minimum bias sample. HERWIG6 samples were generated in $15 \leq p_T \leq 300$ GeV range and no minimum bias sample is avaiable. These event generators use LO matrix elements, supplemented with leading-log parton showering algorithms, to generate an event at parton level. These partons are combined into color-singlet particles using phenomenological hadronization models. These generators use different parton showering algorithms, different hadronization models and different underlying event models.

4 Particle Reconstruction

The PF-particles are reconstructed by combining the information from the tracker, electtromagnetic calorimeter, hadron calorimeter and muon system. Briefly, local energy deposits in EM and hadronic calorimeters are clustered and linked to the reconstructed tracks. If a track is linked to both EM local cluster and HAD local cluster, it is labledas charged hadron. The clusters in the electromagnetic calorimeter which are neither linked to a track of local cluster on hadron calorimeter are labled as photons. The EM calorimeter is very linear ahd fully calibrated using photons using photons produced from decay of pi^0, ρ mesons. These reconstructed particles are fully calibrated and will be collectively labled as PF-particles.

The p_T of charged hadrons in the tracking coverage region is known to accuracy of 1%. In central region, $|\eta| < 1.3$, the energy scale for the photons is known to the accuracy of 1%. The energy of neutral hadrons which are reconstructed from deposit energy in the hadron and EM calorimeters is known to 3%.

In the Endcap calorimeter, all the EM calorimeter calibration were not used in Nov4 ReReco. To correct this ommission, the photons in $|\eta| > 1.3$ were scaled by the 1.027 in the analysis.

DRAFT

Table 1: Name of the datasets used to measure the internal structure of the jets

Collider data
JetRun2010B-Nov4ReReco_v1RECO
JetMETRun2010A-Nov4ReReco_v1RECO
JetMETTauRun2010A-Nov4ReReco_v1/RECO
MinimumBiasCommissioning10-GOODCOLL-Jun14thSkim_v1RECO

Monte Carlo Data (Fall10-START38-V12-v1)
QCD_Pt_0to5_TuneZ2_7TeV_pythia6
QCD_Pt_5to15_TuneZ2_7TeV_pythia6
QCD_Pt_15to30_TuneZ2_7TeV_pythia6
QCD_Pt_30to50_TuneZ2_7TeV_pythia6
QCD_Pt_50to80_TuneZ2_7TeV_pythia6
QCD_Pt_80to120_TuneZ2_7TeV_pythia6
QCD_Pt_120to170_TuneZ2_7TeV_pythia6
QCD_Pt_170to300_TuneZ2_7TeV_pythia6
QCD_Pt_300to470_TuneZ2_7TeV_pythia6
QCD_Pt_470to600_TuneZ2_7TeV_pythia6
QCD_Pt_600to800_TuneZ2_7TeV_pythia6
QCD_Pt_800to1000_TuneZ2_7TeV_pythia6
QCD_Pt_0to15_Tune1_7TeV_pythia8
QCD_Pt_15to30_Tune1_7TeV_pythia8
QCD_Pt_30to50_Tune1_7TeV_pythia8
QCD_Pt_50to80_Tune1_7TeV_pythia8
QCD_Pt_80to120_Tune1_7TeV_pythia8
QCD_Pt_120to170_Tune1_7TeV_pythia8
QCD_Pt_170to300_Tune1_7TeV_pythia8
QCD_Pt_300to470_Tune1_7TeV_pythia8
QCD_Pt_470to600_Tune1_7TeV_pythia8
QCD_Pt_600to800_Tune1_7TeV_pythia8
QCD_Pt_800to1000_Tune1_7TeV_pythia8
MinBias_TuneD6T_7TeV-pythia6
QCD_Pt-15to30_TuneD6T_7TeV-pythia6
QCD_Pt-30to50_TuneD6T_7TeV-pythia6
QCD_Pt-50to80_TuneD6T_7TeV-pythia6
QCD_Pt-80to120_TuneD6T_7TeV-pythia6
QCD_Pt-120to170_TuneD6T_7TeV-pythia6
QCD_Pt-170to300_TuneD6T_7TeV-pythia6
QCD_Pt-15to30_7TeV-herwig6
QCD_Pt-30to50_7TeV-herwig6
QCD_Pt-50to80_7TeV-herwig6
QCD_Pt-80to120_7TeV-herwig6
QCD_Pt-120to170_7TeV-herwig6
QCD_Pt-170to300_7TeV-herwig6
QCD_Pt-15To3000_Tune23_Flat_7TeV-herwigpp

DRAFT

Table 2: The triggers contributing to the jet p_T bins. The jet p_T binning is used for all rapidity bins.

PtMin	PtMax	Trigger	Run range	Njets (Data) in —y—¡1
15	20	HLT_L1_BscMinBiasOR_BptxPlusORMinus	-	285722
20	25	HLT_L1_BscMinBiasOR_BptxPlusORMinus	-	93816
25	30	HLT_L1_BscMinBiasOR_BptxPlusORMinus	-	33892
30	40	HLT_L1_BscMinBiasOR_BptxPlusORMinus	-	20793
40	50	HLT_L1_BscMinBiasOR_BptxPlusORMinus	-	5206
50	60	HLT_L1_BscMinBiasOR_BptxPlusORMinus	-	1814
60	70	Jet_15U	136035-148058	24785
70	80	Jet_15U	136035-148058	11506
80	90	Jet_15U	136035-148058	5932
90	100	Jet_30U	136035-148058	40524
100	110	Jet_30U	136035-148058	24135
110	125	Jet_30U	136035-148058	19634
125	140	Jet_50U,Jet50U_v3	136035-149294	97314
140	160	Jet_50U,Jet50U_v3	136035-149294	65730
160	180	Jet_50U,Jet_70U,Jet70U_v2,Jet70U_v3	136035-149294	70036
180	200	Jet_50U,Jet_70U,Jet70U_v2,Jet70U_v3	136035-149294	36420
200	225	Jet_50U,Jet_100U,Jet100U_v2,Jet100U_v3	136035-149294	48399
225	250	Jet_50U,Jet_100U,Jet100U_v2,Jet100U_v3	136035-149294	25271
250	300	Jet_50U,Jet_100U,Jet140U_v1,Jet140U_v3	136035-149294	33165
300	400	Jet_50U,Jet_100U,Jet140U_v1,Jet140U_v3	136035-149294	16353
400	500	Jet_50U,Jet_100U,Jet140U_v1,Jet140U_v3	136035-149294	3182
500	600	Jet_50U,Jet_100U,Jet140U_v1,Jet140U_v3	136035-149294	774
600	1000	Jet_50U,Jet_100U,Jet140U_v1,Jet140U_v3	136035-149294	333

A systematic uncertainty of 3% on photon energy is assumed in this region. Dijet balancing studies show that the jet energy scale in data is different than the one in the MC simulation. Assumming that the charged hadron calibration, coming from the track measurement, is same over whole $|\eta| < 2.4$, the neutral hadron calibration can be derived using

$$C_{\text{neutral}} = (C_{Jet} - C_\gamma \times f_\gamma - C_{\text{charged}} \times f_{\text{charged}})/f_{\text{neutral}}$$

where C_{JES} is the residual relative jet energy corrections, C_γ, C_{charged} and C_{neutral} are the residual scaling factors for the photons, charged hadrons and neutral hadrons and f_γ, $f_{charged}$ and f_{neutral} are the fractions of jet p_T carried by the photons, charged hadrons and the neutral hadrons. For $1.3 < |\eta| < 2.3$, the C_{charged} is assumed to be 1.0.

For $|\eta| > 2.4$, the tracking information is not available and both charged and neutral hadrons are measured using calorimeter and thus scaling factor for hadrons can be measured using

$$C_{\text{hadrons}} = (C_{Jet} - C_\gamma \times f_\gamma - C_{\text{hadron}} \times f_{\text{hadron}})/f_{\text{hadron}}.$$

Above equations are approximations as C_{Jet} measured using di-jet balancing is averaged over the jet area. More over, we use η of the particles which is also averaged over detector η, though a very small region, by vertex smearing. As the scaling factors differ from 1.0 by only a few percent, the effect of this smearing is exptected to be very small.

DRAFT

Table 3: Transverse momentum scaling factors for reconstructed PF particles

η_{min}	η_{max}	Residual JES	Photons	Neutral hadrons	Charged hadrons
-5.0	-5.0	0.999	1.027	0.9897	0.9897
-3.5	-5.0	0.982	1.027	0.967	0.967
-3.2	-3.5	1.005	1.027	0.9977	0.9977
-3.0	-3.2	0.9	1.027	0.8577	0.8577
-2.9	-3.0	0.93	1.027	0.8977	0.8977
-2.5	-2.9	0.948	1.027	0.9217	0.9217
-2.4	-2.5	0.972	1.027	0.9537	0.9537
-2.3	-2.4	0.988	1.027	0.975	0.975
-1.9	-2.3	0.999	1.027	0.9295	1
-1.5	-1.9	1.03	1.027	1.211	1
-1.3	-1.5	1.01	1.027	1.03	1
1.3	1.5	1.03	1.027	1.211	1
1.5	1.9	1.005	1.027	0.9841	1
1.9	2.3	1.002	1.027	0.9568	1
2.3	2.4	1.002	1.027	0.9937	0.9937
2.4	2.5	0.992	1.027	0.9803	0.9803
2.5	2.9	0.97	1.027	0.951	0.951
2.9	3.0	0.955	1.027	0.931	0.931
3.0	3.2	0.93	1.027	0.8977	0.8977
3.2	3.5	1.001	1.027	0.9923	0.9923
3.5	5.0	0.975	1.027	0.9577	0.9577
5.0	5.0	0.992	1.027	0.9803	0.9803

DRAFT

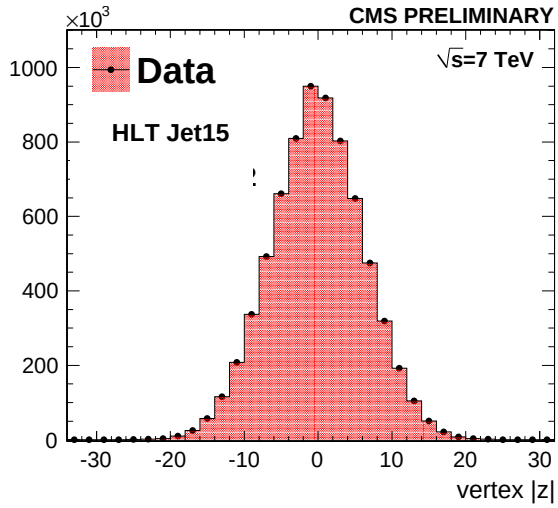

Figure 7: Position of the primary interaction along the beam direction

5 Cleaning

We use HBHENoiseFilter, noscraping to remove the non-physics events. Currently, we are not using beam halo filter or cosmic ray filter. Instead, we require that the fraction $\not{E}_T/\sum E_T$ is less than 0.5. The $\not{E}_T/\sum E_T$ and $\not{E}_T/\sqrt{\sum E_T}$ distributions before and after the cut are shown in Figs. 8 9. We require each jet to pass the jetID, given in Table 4[10] which requires that the jet energy is shared between both charged hadrons, photons and neutral stable hadrons. These cuts remove the jets which contain fake energy. We expect that the good vertex requirement and the jetID cuts remove the cosmic and beam-related background.

5.1 Vertex Selection Criteria

vents to have one and only one primary vertex. To minimize the contribution from any additional pp collisions which occurred in the same bunch crossing, the events are required to have one and only one primary vertex. Following CMS recommendations, the primary vertex is required to pass following requirements:

Number of degrees of freedom	ndof >5
z position of the vertex	$\lvert z\rvert < 24$ cm
Radial position of the vertex	$\sqrt{x^2+y^2} < 2$ cm

Position of the primary interaction along the beam direction is shown in Fig. 7.

6 Trigger Efficiency

Many single jet triggers with different p_{T} thresholds were employed during 2010 data taking. These trigger combined to span the $15-1000$ p_{T} ranged so that the trigger(s) used are 100% efficient for a given p_{T} bin. For this we follow the thresholds used by inclusive jet cross section measurement[10]. These thresholds were confirmed by our own study also.

DRAFT

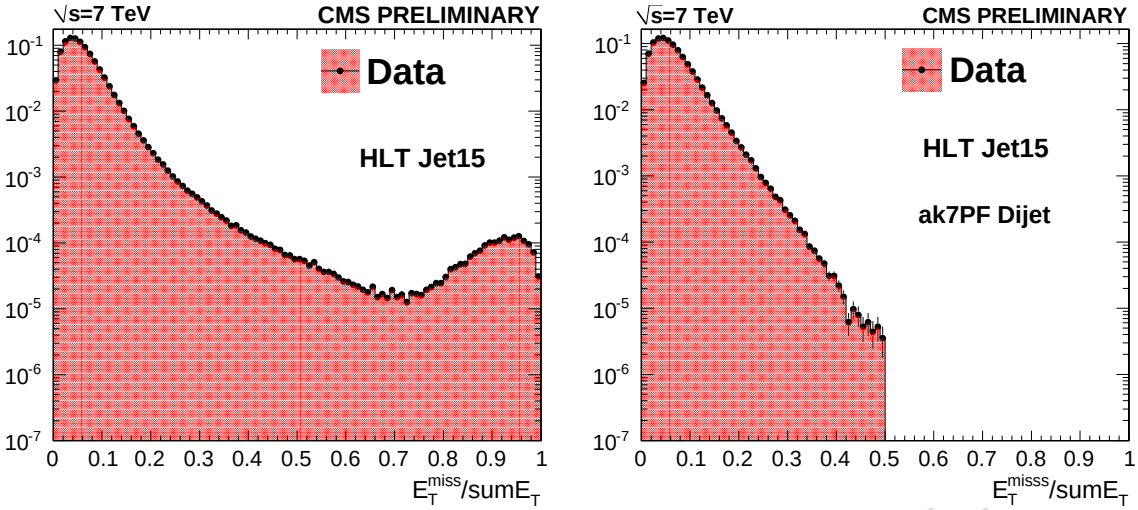

Figure 8: $\not{E}_T/\sum E_T$distribution of the data

DRAFT

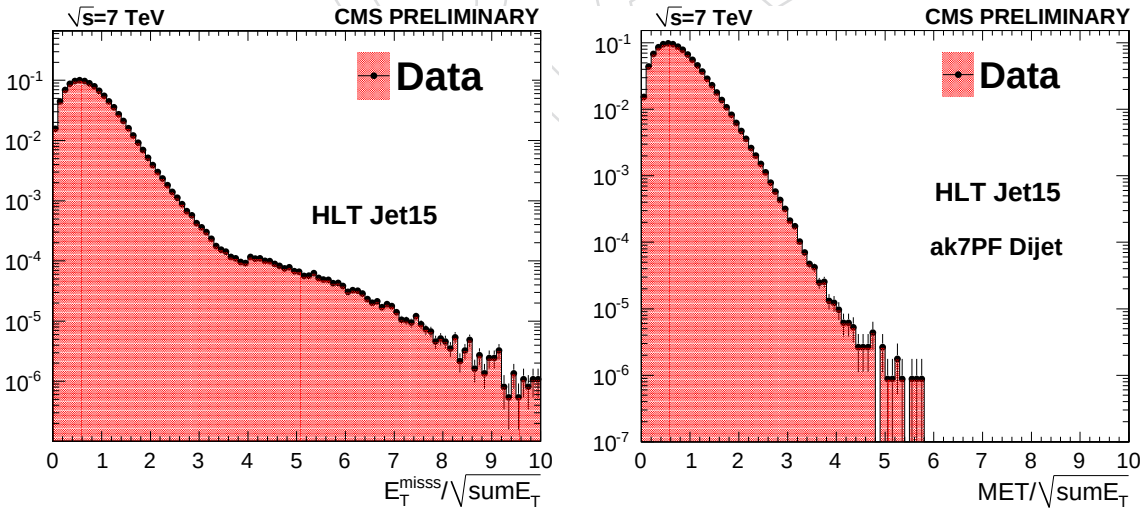

Figure 9: $\not{E}_T/\sqrt{\sum E_T}$ distribution before and after the $\not{E}_T/\sum E_T < 0.5$ cut

7 Jet Reconstruction

We use anti-k_T [11] jet algorithm to cluster the reconstructed particles (PF-particles) to form the jets using the size parameter D=0.7 for most of the studies described in this note. As each PF-particle is individually calibrated, the reconstructed jet, in principle, is fully calibrated also. However, in practice, a small $\sim$ 5% correction is needed to obtain the true energy of the jets. The jet energies are corrected using standard corrections which include MC-based L2L3 correction and the residual corrections[12] which account for the difference between the JES in the data and in the Monte Carlo.

For jetshape studies, multiplicity distributions, particle p_{T} and fragmentation functions only the axis of the reconstructed jet is used. However, for jet mass distributions, only the constituents of the jet as clustered by anti-kt algorithm are used. For all the distributions, we use only two leading jets in the event provided if they are within rapidity range. The distributions are studies for various jet p_{T} bins, given in 2.

The jet p_{T} distributions along with available number of jets are shown in Fig. 10.

DRAFT

Table 4: PF Jet ID

$\eta^{\text{Jet}} \leq 2.4$		
Number of particles in a jet	$>$	1
Number of charged hadrons in a jet	$>$	0
Jet p_{T} fraction carried by photons	$<$	0.90
Jet p_{T} fraction carried by neutrons	$<$	0.90

Table 5: Datasets and triggers

Version Tag	Date	Dataset	Start Run	Triggers with PS=1
Run2010/v1.1/HLT_LowInt_1E29/V1	2010-05-21	JetMETTau	136063	Jet15U/Jet30U/Jet50U
Run2010/v2.0/HLT_2E29/V1	2010-06-17	JetMETTau	138046	Jet30U/Jet50U
Run2010/v3.0/HLT_1.6E30/V1	2010-07-13	JetMETTau	140083	Jet50U
Run2010/4.0/HLT/V1	2010-07-28	JetMET	141950	Jet50U/Jet70U/Jet100U
Run2010/v5.0/HLT/V1	2010-08-16	JetMET	143317	Jet50U/Jet70U/Jet100U
Run2010/v6.0/HLT/V1	2010-09-03	Jet	135518	Jet50U/Jet70U/Jet100U
Run2010/V7.0/HLT/V2	2010-09-22	Jet	146428	Jet70U/Jet100U
Run2010/v8.0/HLT/V1	2010-10-03	Jet	147146	Jet100Uv2/Jet140Uv1
Run2010/v9.1/HLT/V1	2010-10-23	Jet	148783	Jet140Uv3

During 2010 datataking un-prescaled triggers are; **FIXME:** Check the run numbers

- minbias 0 - 138046
- Jet15U 0 - 138046
- Jet30U 138046 - 140083
- Jet50U 140083 - 146428
- Jet70U 146428 - 147146
- Jet100v2 147196 - 148783
- Jet140v3 148783 - 149294

8 Validation of PF Recontrunction Alorithm

The comparison of the reconstruction PF particles multiplicty with the Gen particles multiplicity is shown in Figs. 11 for charged hadrons and 12 for all particles, charged hadrons, neutral hadrons, photons and electrons and muons. No p_{T} threshold applied to particles used in the Gen distributions. The PF reconstruction for charged hadrons, primarily determined from tracks, is very close to the true distributions. The photon multiplicity at GEN level is higher as photons from decay of the neutral hadrons are reconstructed as a single photons. Low p_{T} neutral hadrons may not be reconstructed due to the calorimeter non-linear response to hadrons.

The fraction of jet p_{T} carried by photons, charged hadrons and neutral hadrons is compared with true distributions in Fig13. **FIXME:** The agreement is satisfactory as jetshapes do not distinguish the individual flavor of the particles. From these distributions and the fact that JES corrections are very close to unity, we conclude that PF reconstruction is reasonable. The remaining small differences can be taken into account in the un-folding process.

DRAFT

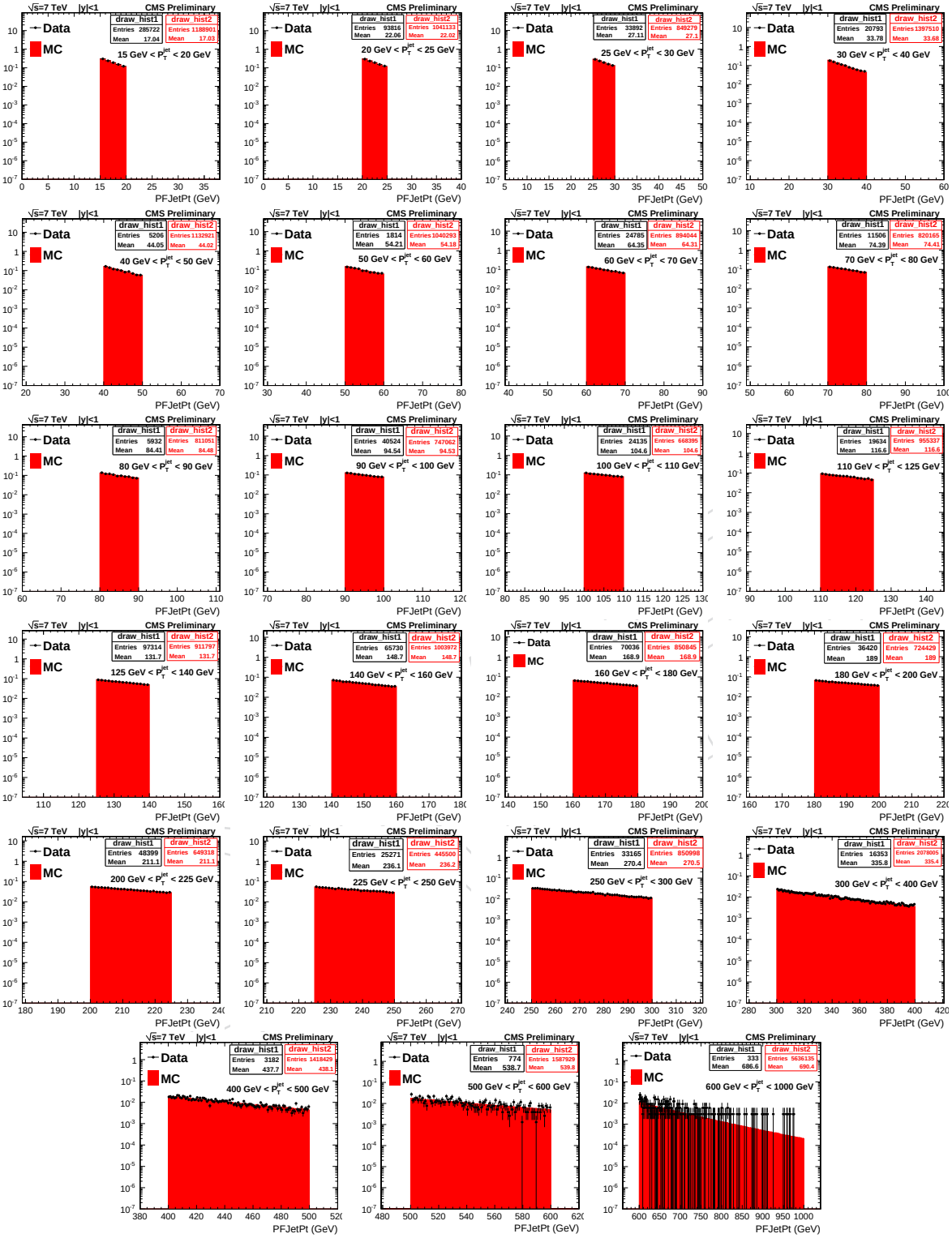

Figure 10: Jet p_T distributions in different bins in $y < 1$ region.

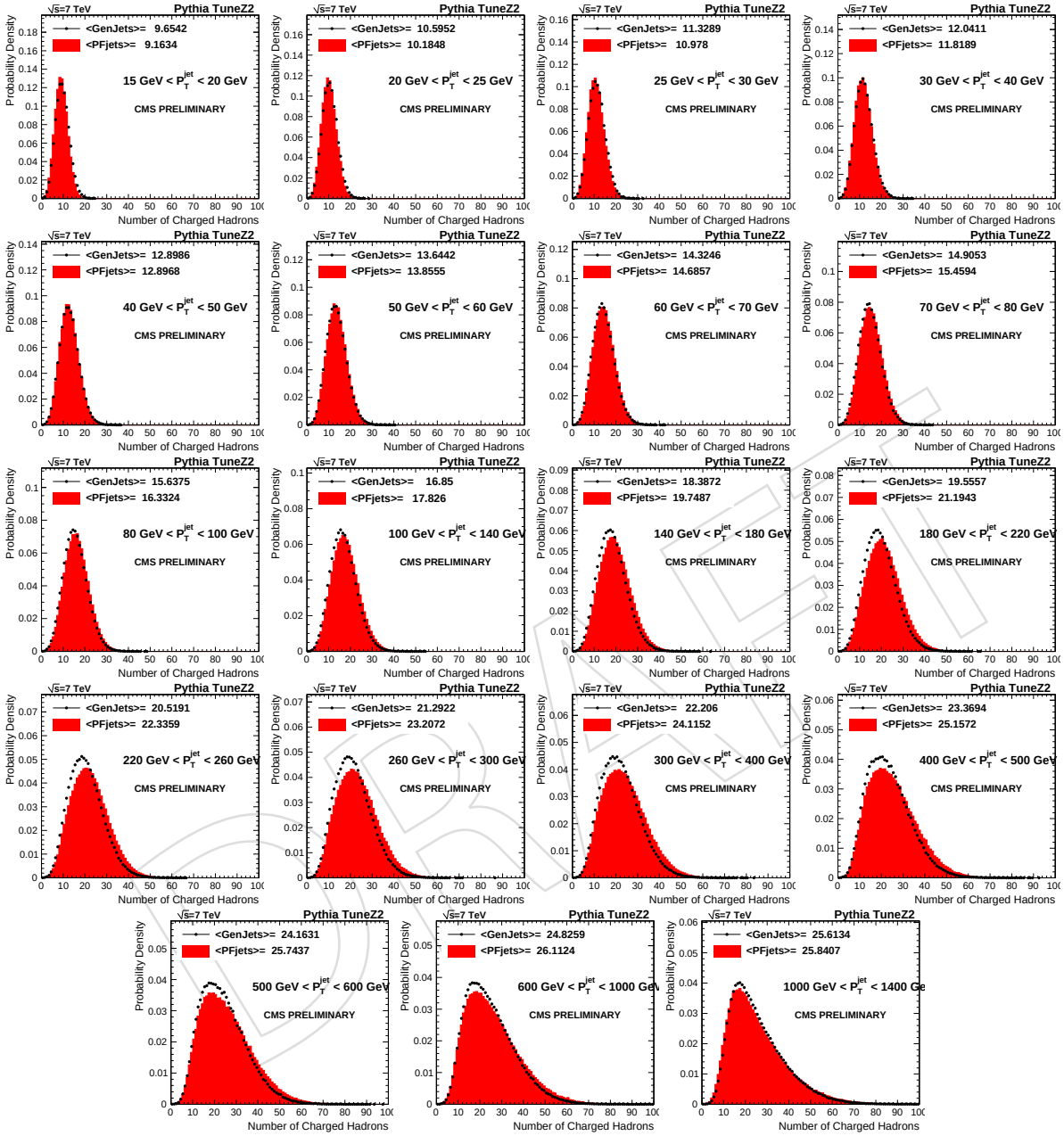

Figure 11: Comparison of reconstructed PF charged hadron multiplicity with the GEN distributions in $y < 1$ region using PYTHIA-Z2 event generator.

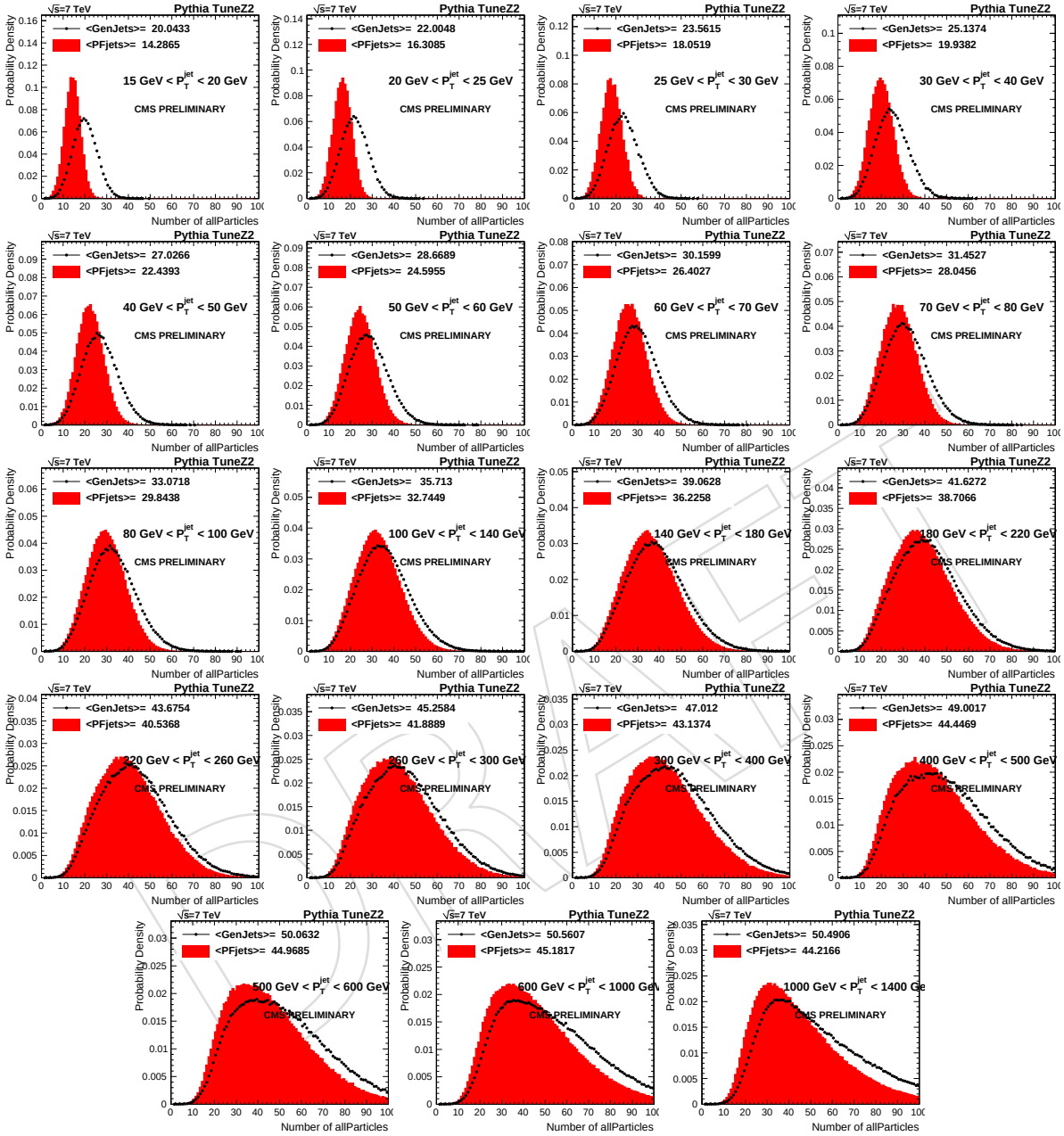

Figure 12: Comparison of reconstructed PF all multiplicity with the GEN distributions in $y < 1$ region using PYTHIA-Z2 event generator.

9 Gen and reconstructed Jetshape Distributions

The differential jet distributions from the reconstructed PF particles and generated particles are compared in Fig. 14. The GEN distributions are binned in particle jet p_{T}s where as the reconstructed distributions are binned in reconstructed jet p_{T}s which have been corrected to particle level. The difference in two distribution arises from (a) smearing of jets in and out of a given p_{T} bin (b) difference in the reconstruction of particles and (c) smearing of the reconstructed jet axis and (d) any smearing of the particles along the distance from the jet axis. These ratios will be used to corrected the reconstructed data. Associated uncertainties are discussed in Section13.

DRAFT

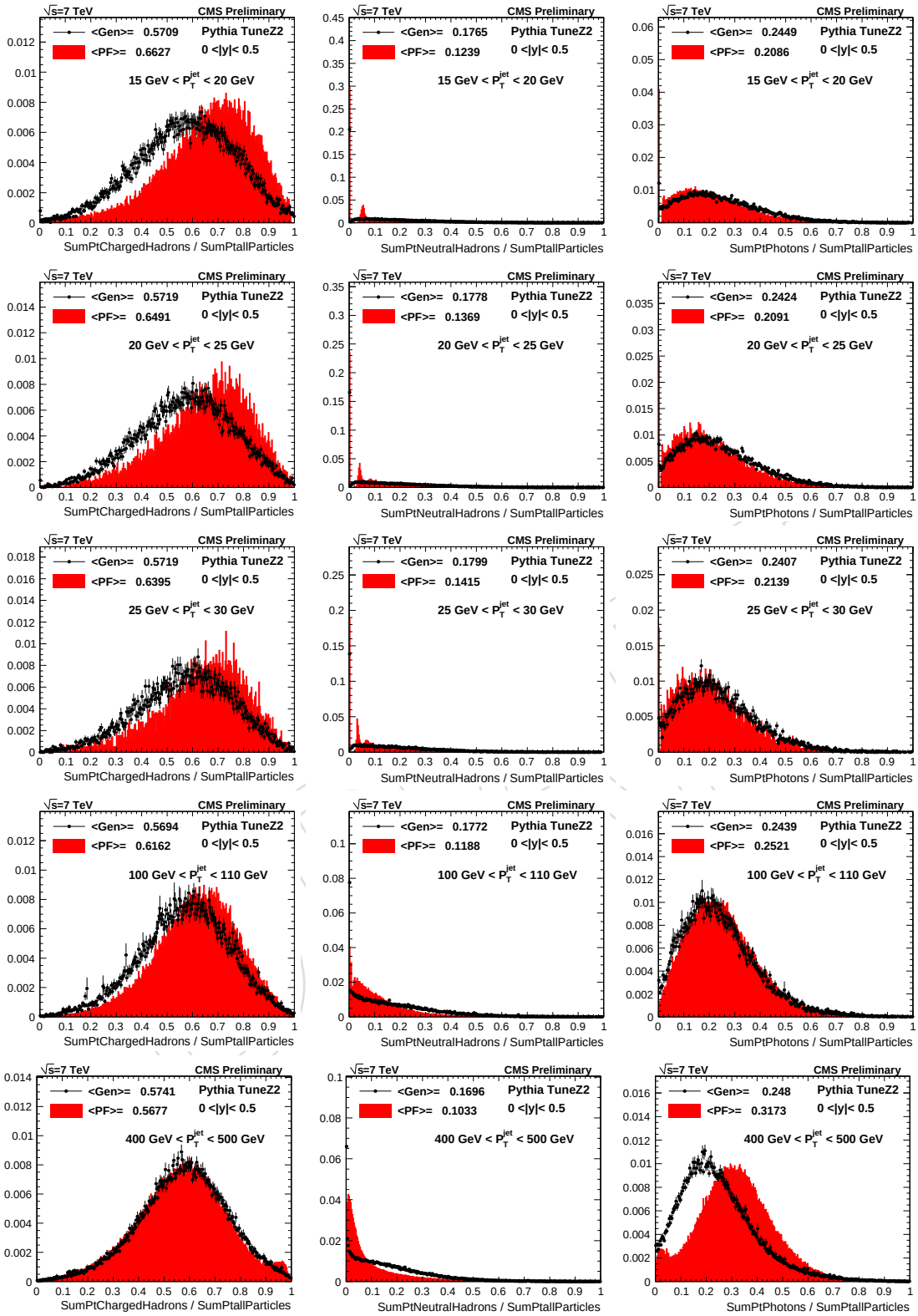

Figure 13: Fraction of jet p_{T} carried PYTHIA-Z2 event generators for low $p_{\mathrm{T}}^{\mathrm{Jet}}$ bins in $|y| < 0.5$ region. The small difference in the distributions does not effect the jetshape measurements.

10 Validation of QCD Parton Shower Modelling

10.1 Particles Multiplicity and Momentum Distributions

The reconstructed photon, charged hadron, neutral hadron, muon and electron multiplicity and momentum distributions were studies in data and compared with those in the QCD event generators. The agreement with PYTHIA Tune-Z2 predictions is quite good. These distributions are shown in Fig. 19, 20, 21, 22. The variation of multiplicities with jet p_{T} are shown in Fig. 23. Again data are well described by the PYTHIA-Z2 prediction for all the p_{T} ranged measured except for $p_{\mathrm{T}} \geq 600$ GeV. The multiplicity distribution vs jet p_{T} for different rapidity regions are shown in Fig. 24, 25, 26, 27, 28.

The fraction of jet p_{T} carried by charged hadrons, neutral hadrons and photons in $|y| < 1.0$ region is compared to PYTHIA-Z2 predictions in 30,31,32. The agreement is reasonable.

DRAFT

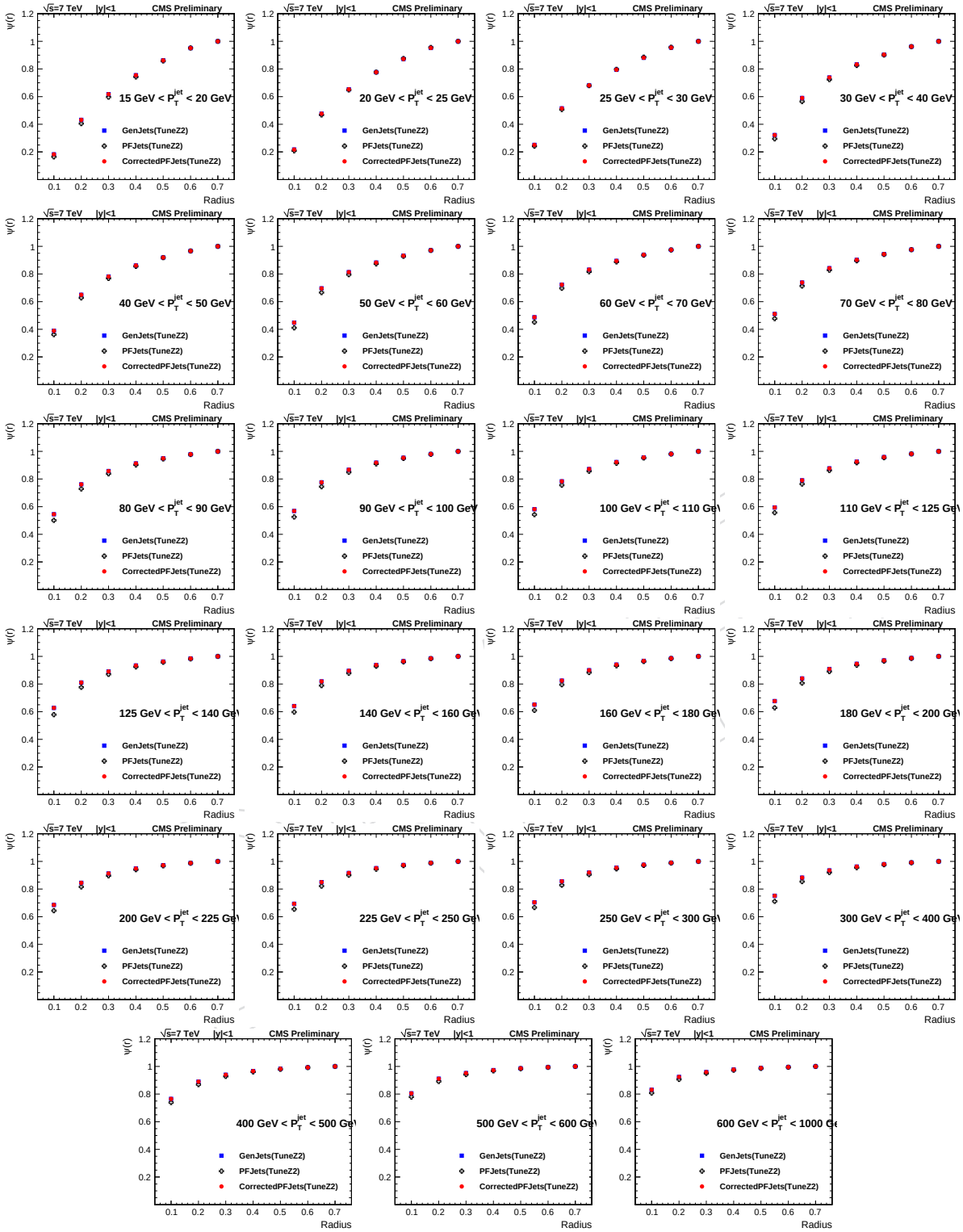

Figure 14: Raw and Corrected integrated jetshape distribution in PYTHIA-Z2 event generators.

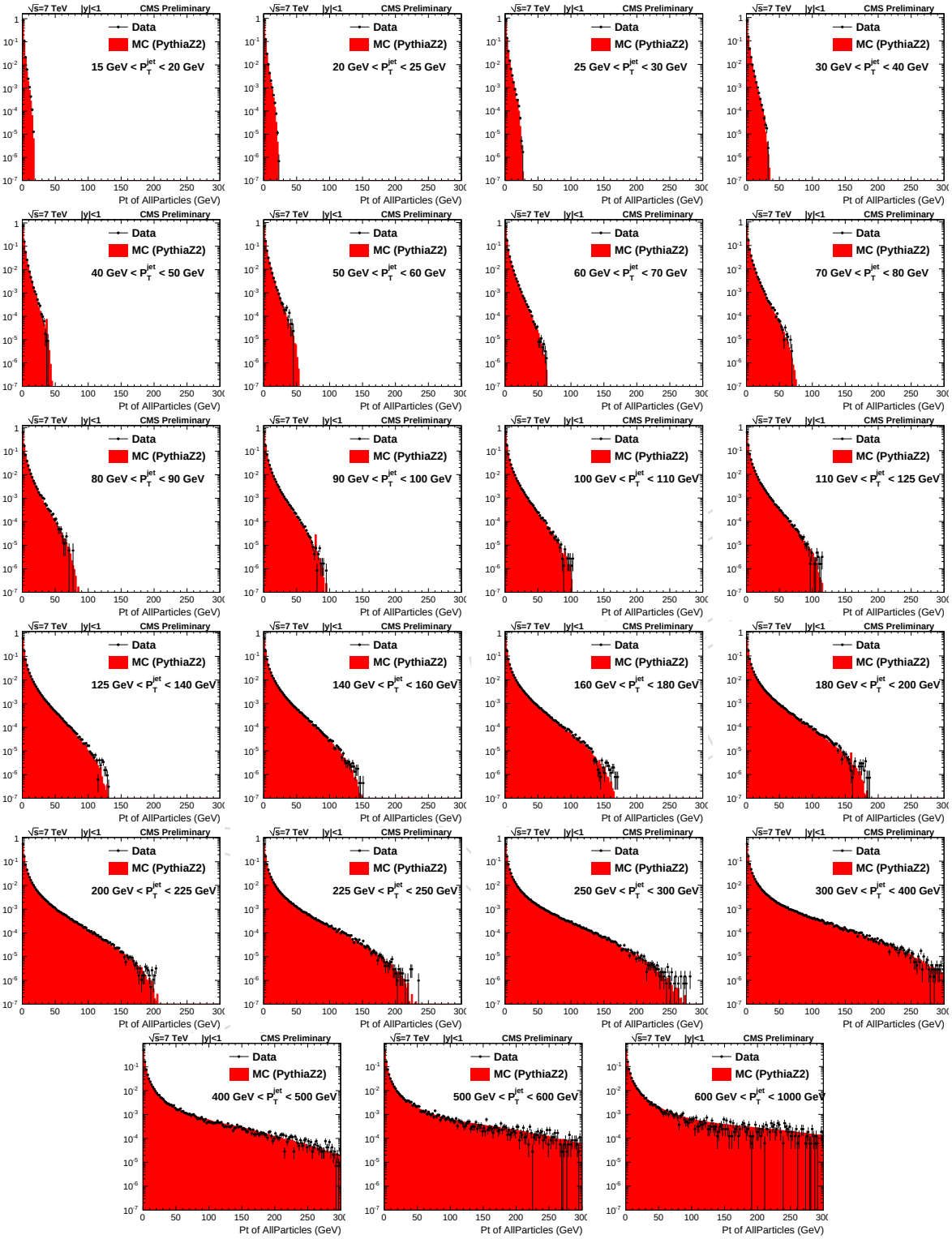

Figure 15: p_{T} distribution of all particles in two leading jets ($|y| < 1.0$) in jet p_{T} bins compared to PYTHIA-Z2 predictions

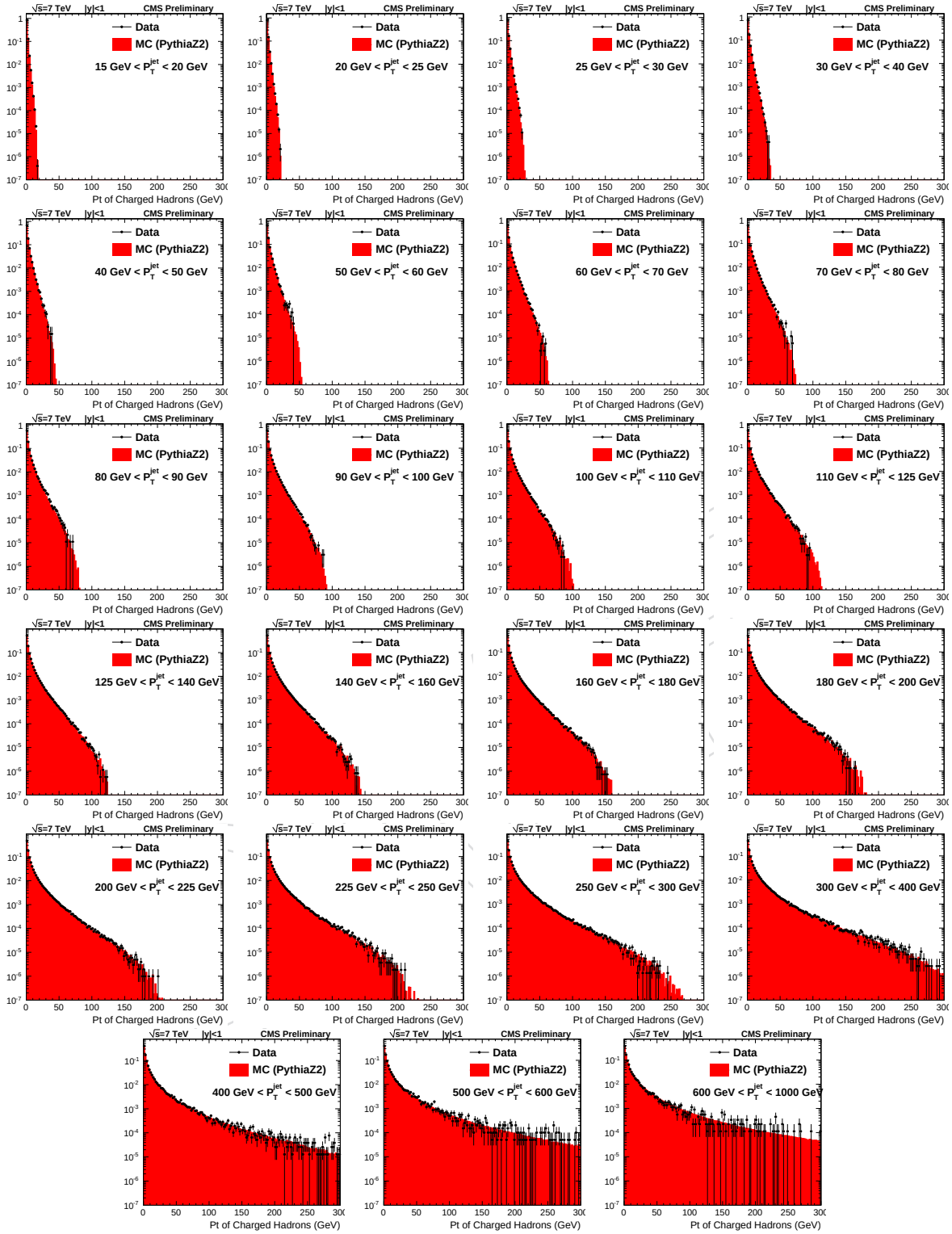

Figure 16: p_T distribution of charged hadrons in two leading jets ($|y| < 1.0$) in jet p_T bins compared to PYTHIA-Z2 predictions

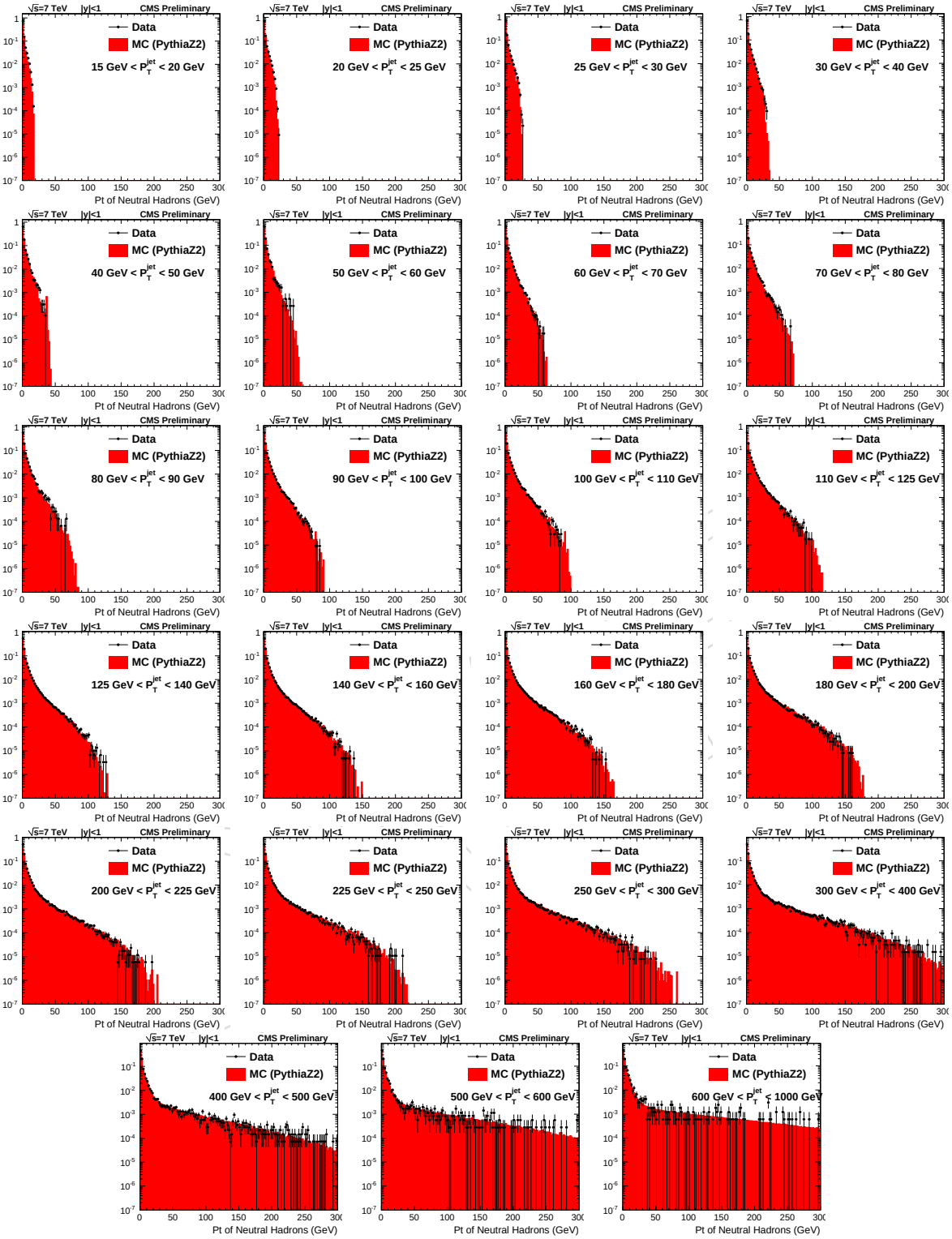

Figure 17: p_T distribution of neutral hadrons in two leading jets ($|y| < 1.0$) in jet p_T bins compared to PYTHIA-Z2 predictions

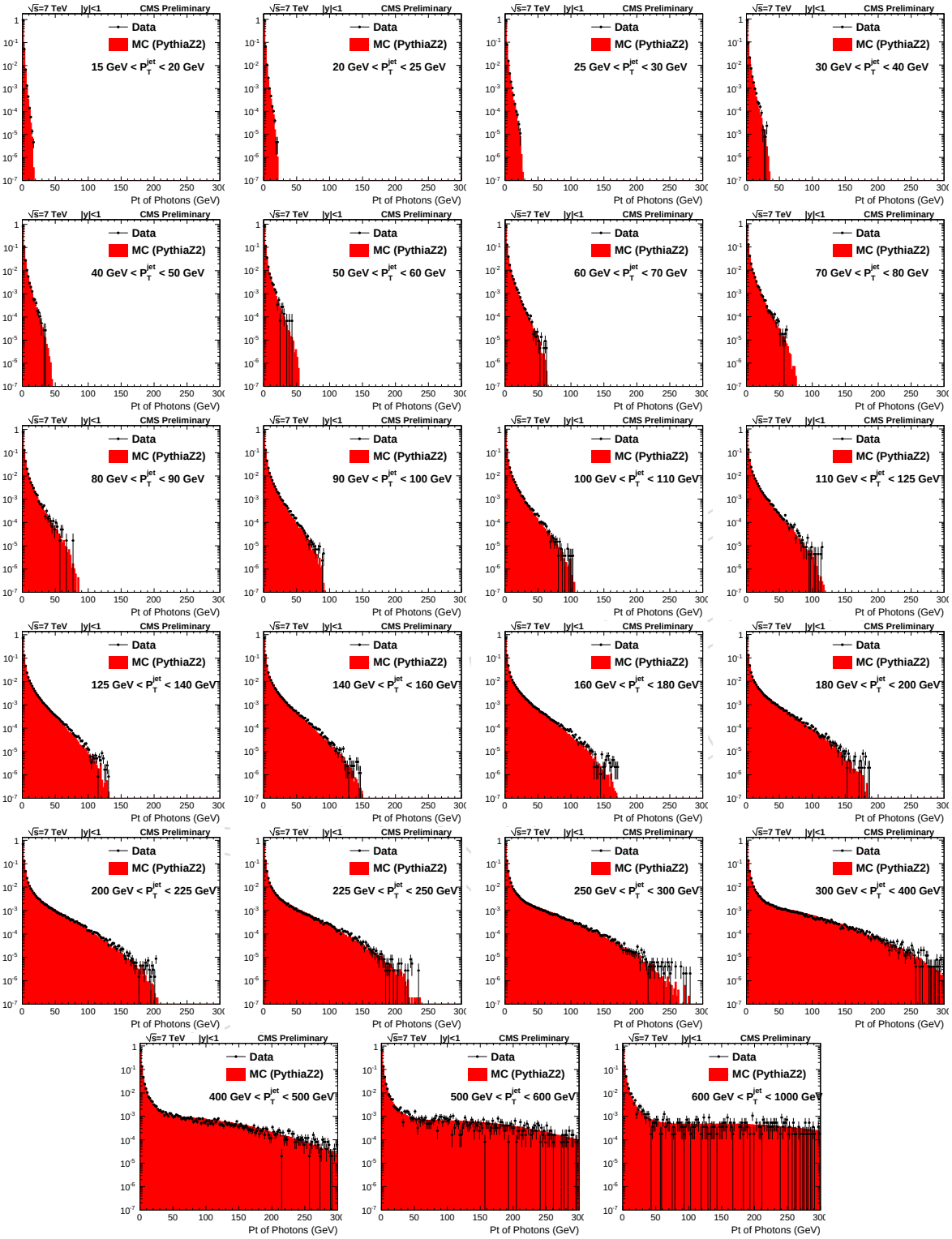

Figure 18: p_T distribution of photons in two leading jets ($|y| < 1.0$) in jet p_T bins compared to PYTHIA-Z2 predictions

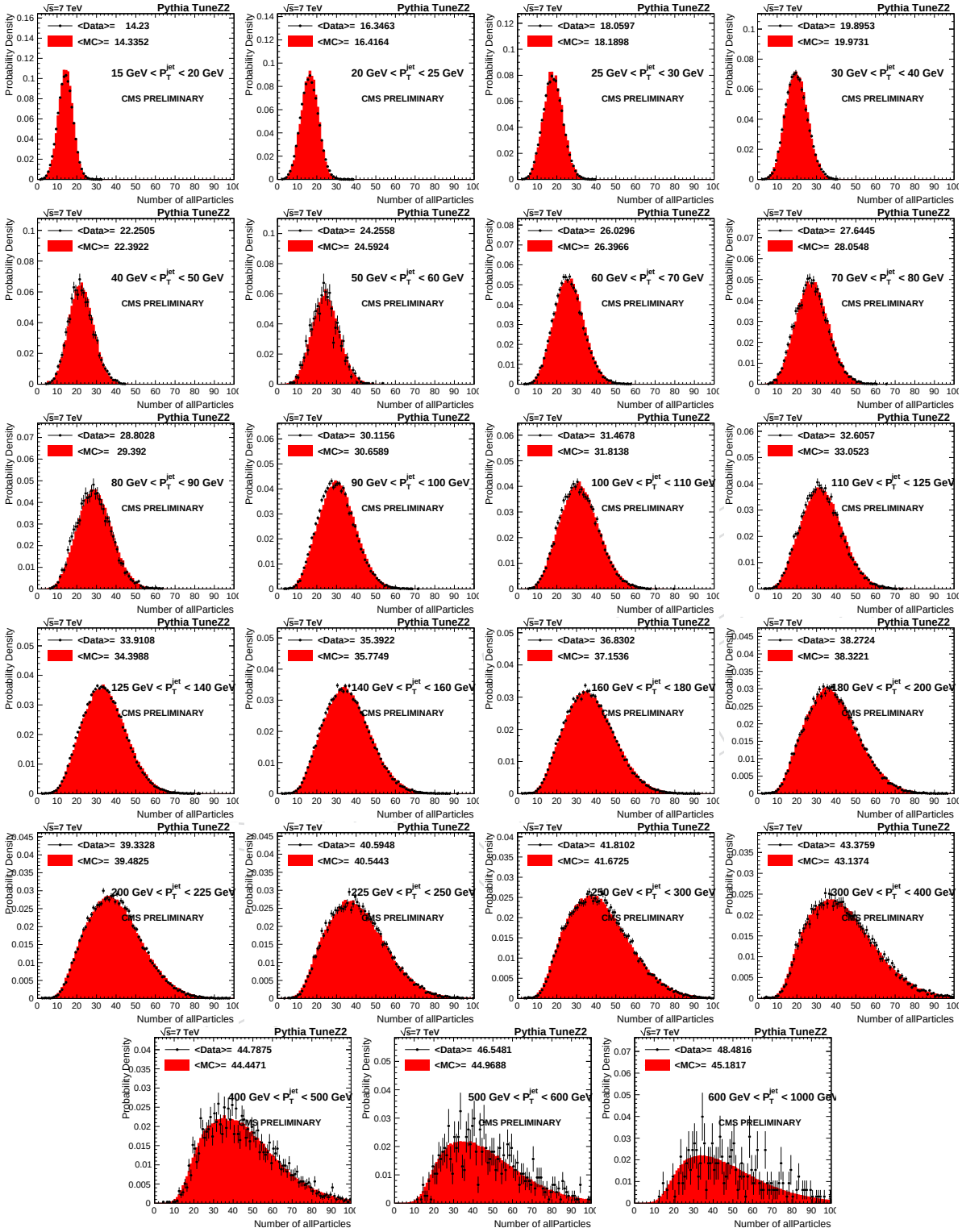

Figure 19: Multiplicity of all the reconstructed PF particles in two leading jets with $|y| \leq 1.0$ in various p_{T} bins in data compared with the predictions from PYTHIA.

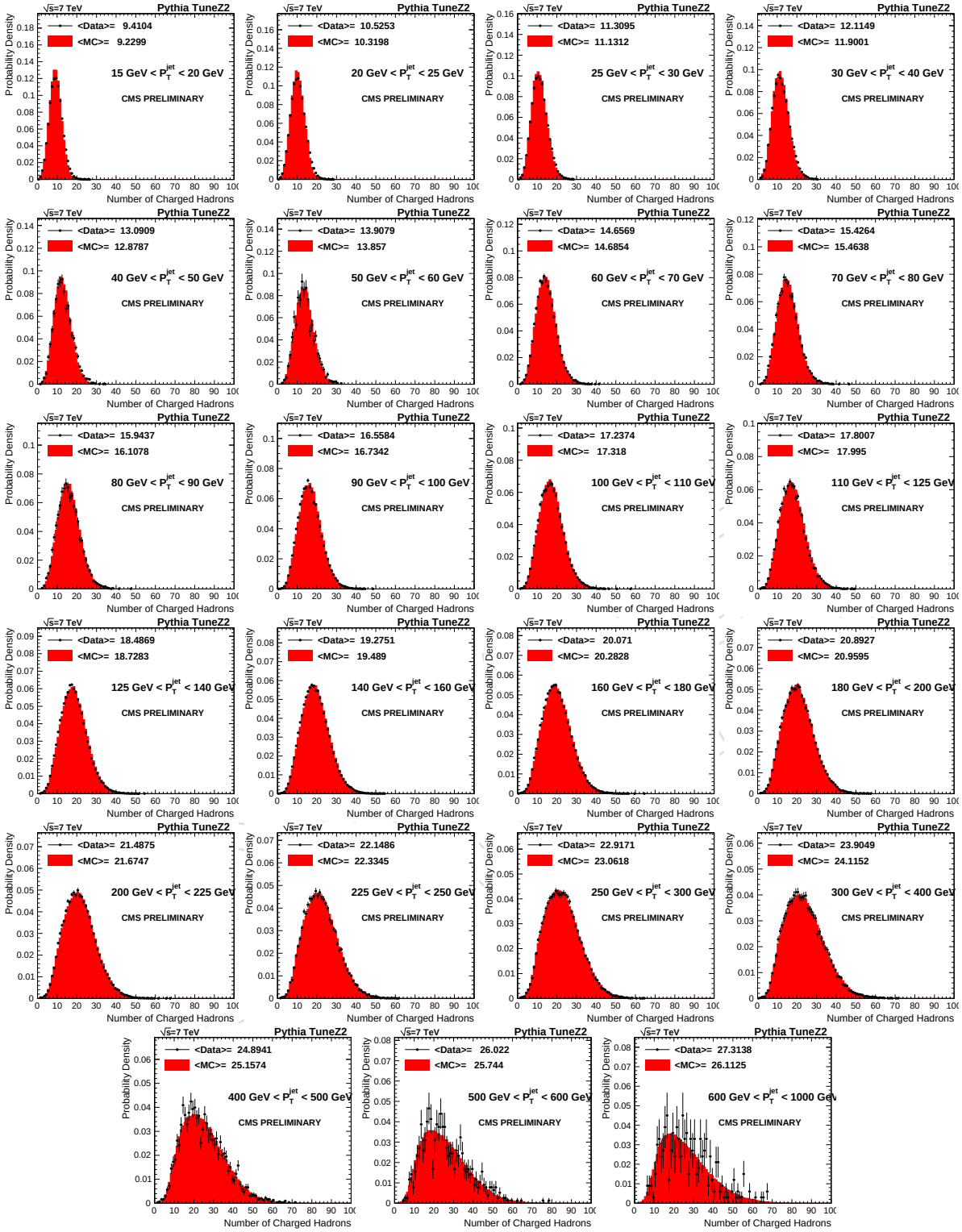

Figure 20: Multiplicity of the reconstructed charged hadrons in two leading jets with $|y| \leq 1.0$ in various p_{T} bins in data compared with the predictions from PYTHIA.

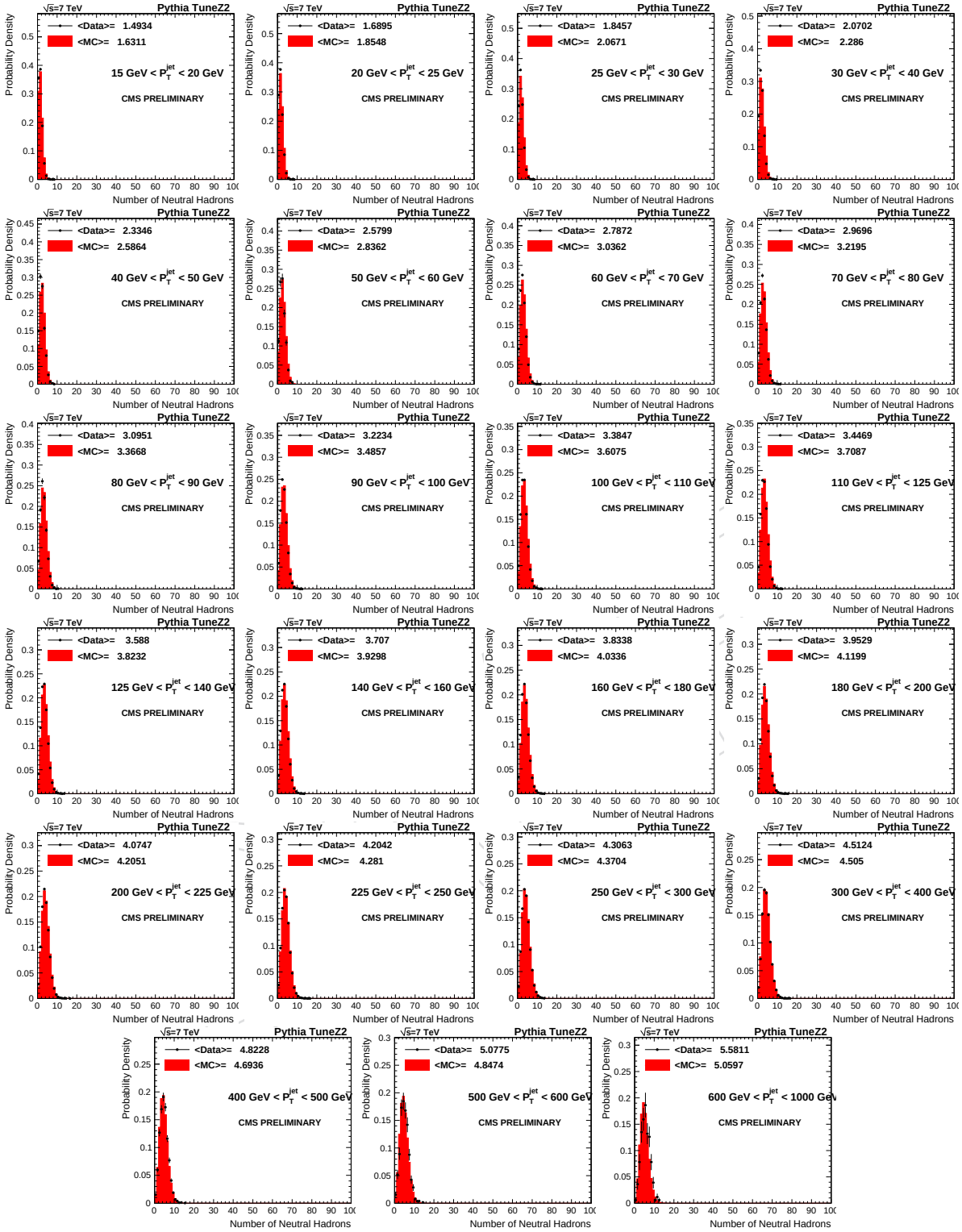

Figure 21: Multiplicity of the reconstructed neutral hadrons in two leading jets with $|y| \leq 1.0$ in various p_{T} bins in data compared with the predictions from PYTHIA.

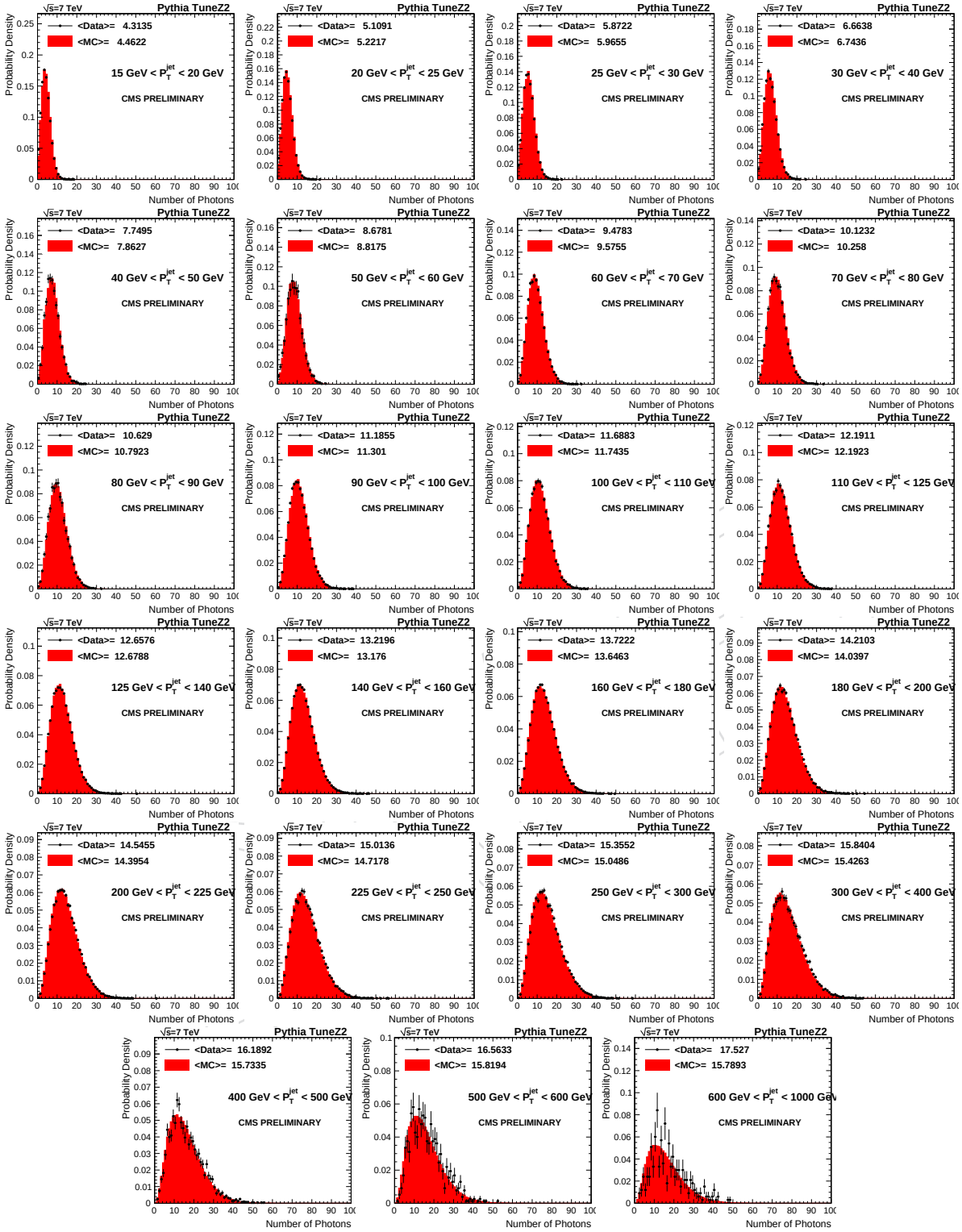

Figure 22: Multiplicity of the reconstructed photons in two leading jets with $|y| \leq 1.0$ in various p_T bins in data compared with the predictions from PYTHIA.

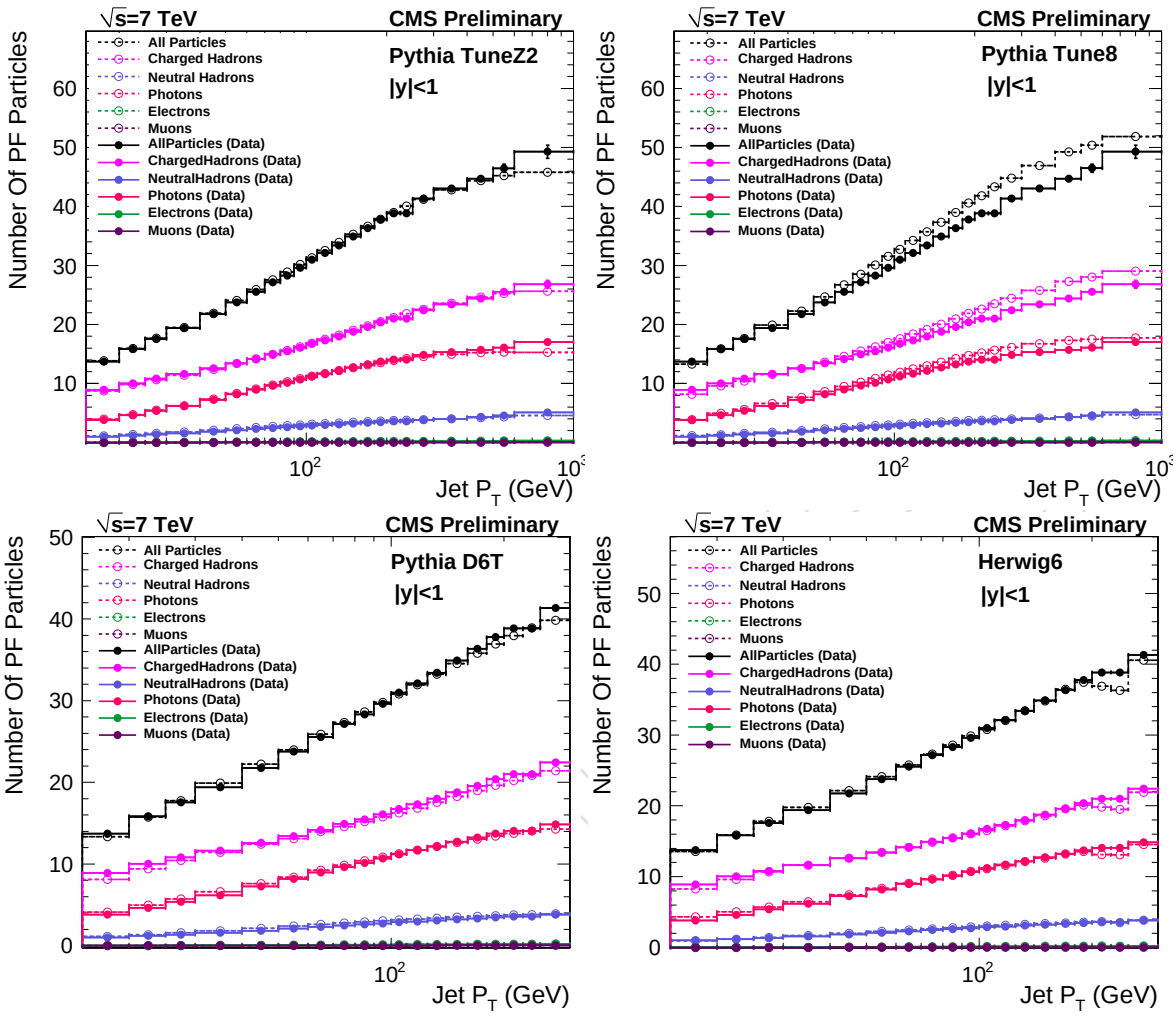

Figure 23: Multiplicity for PF particles in $|y| < 1.0$

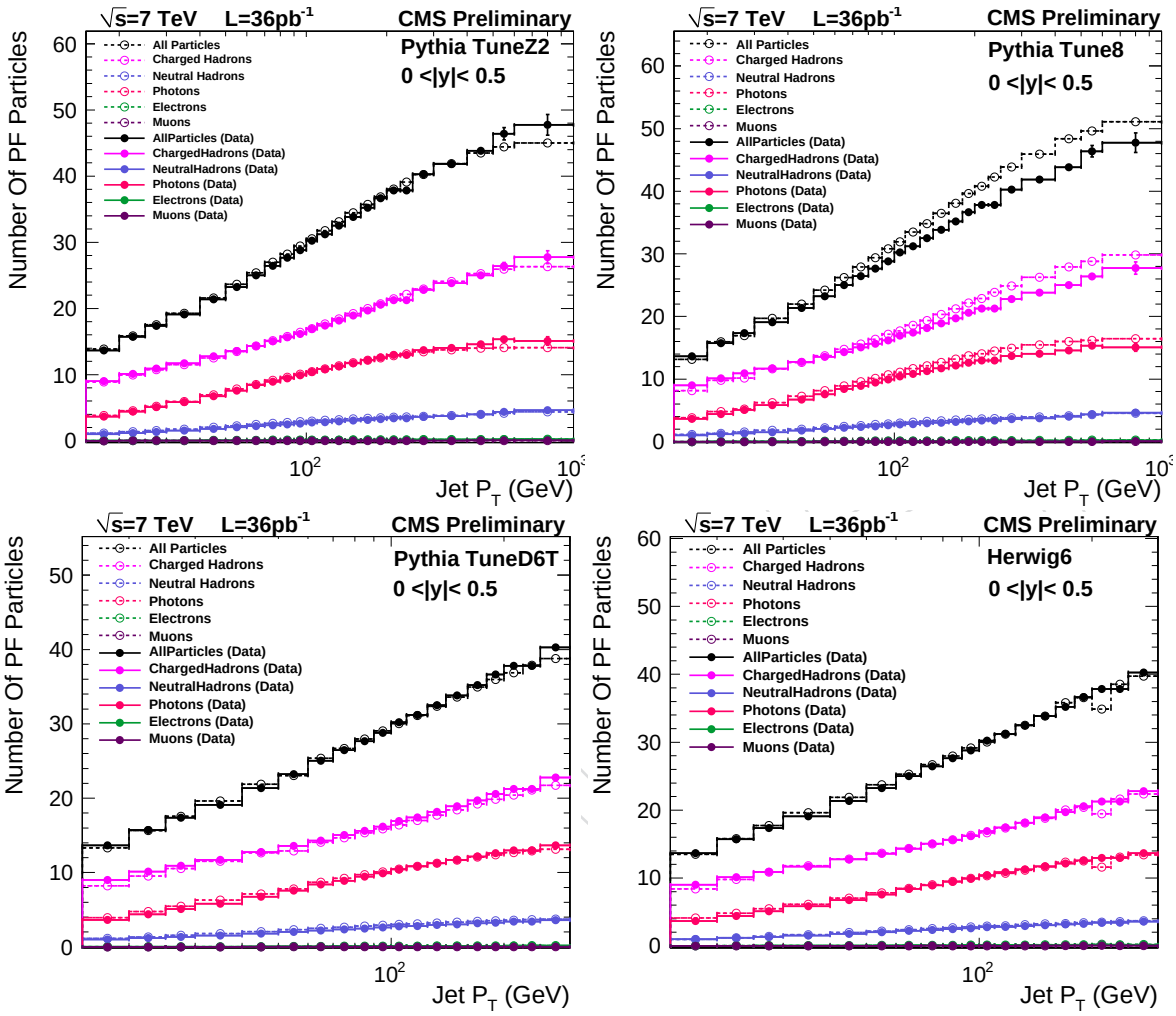

Figure 24: Multiplicity for PF particles in $|y| < 0.5$

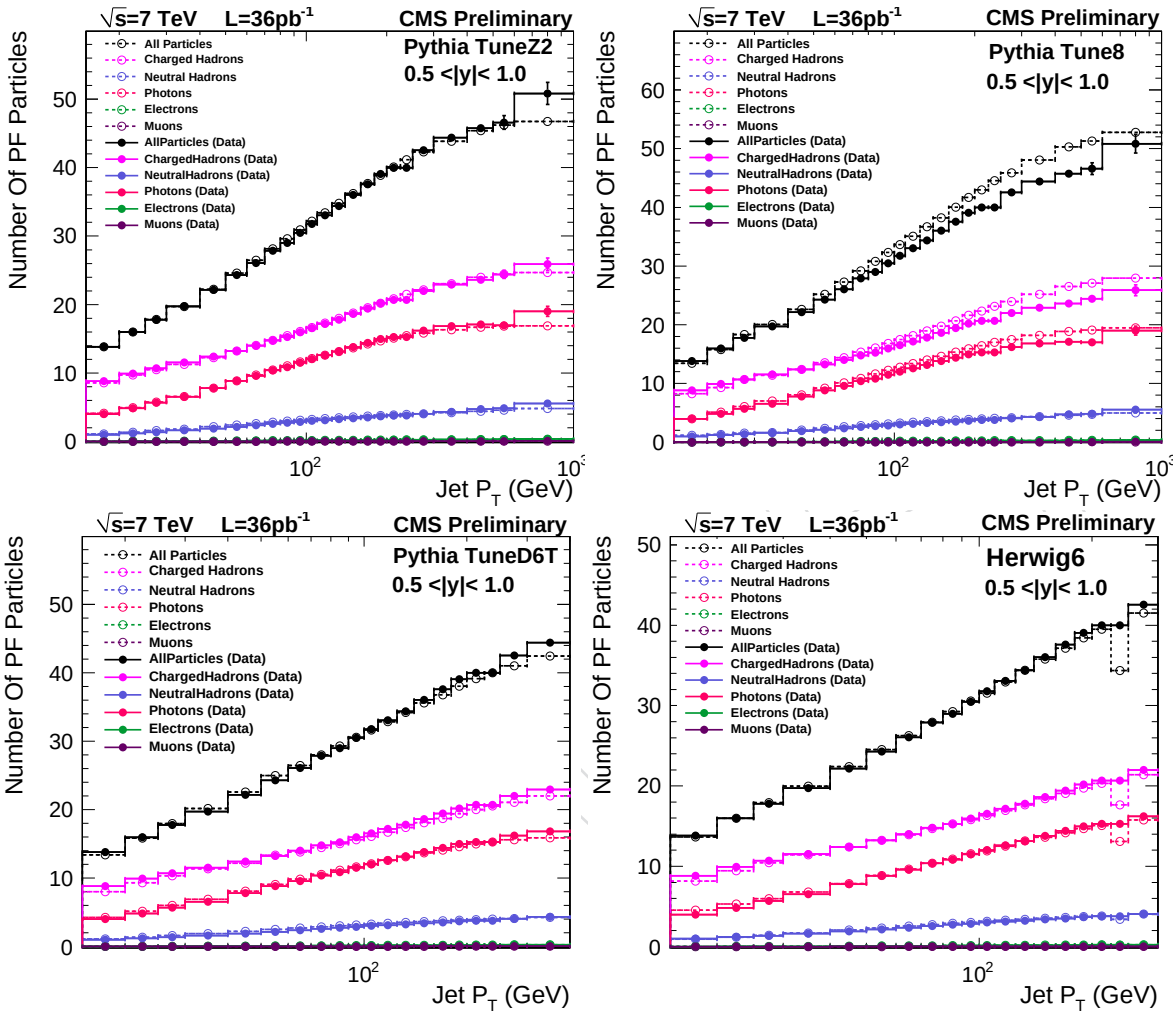

Figure 25: Multiplicity for PF particles in $0.5 < |y| < 1.0$

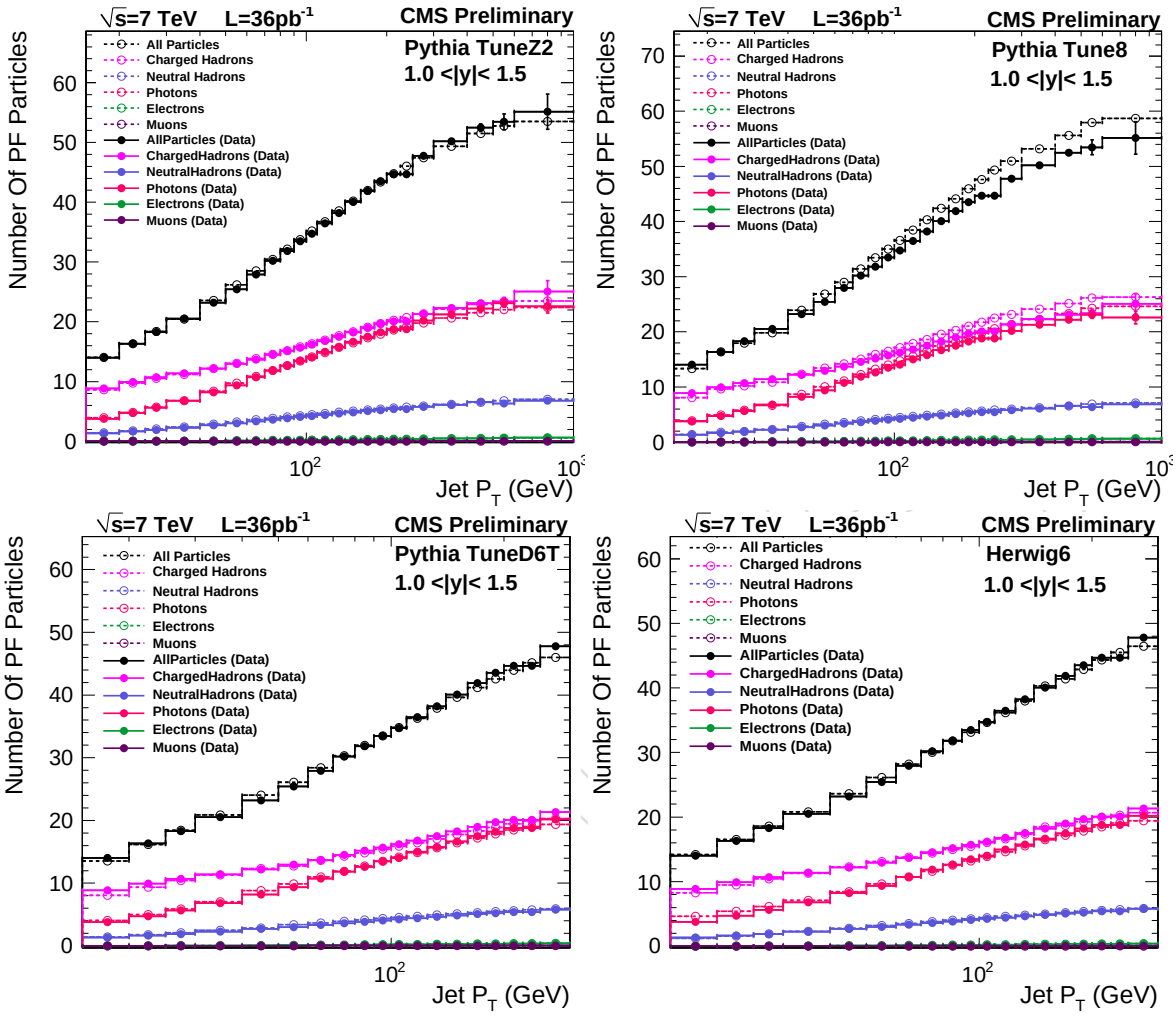

Figure 26: Multiplicity for PF particles in 1.0< $|y|$ <1.5

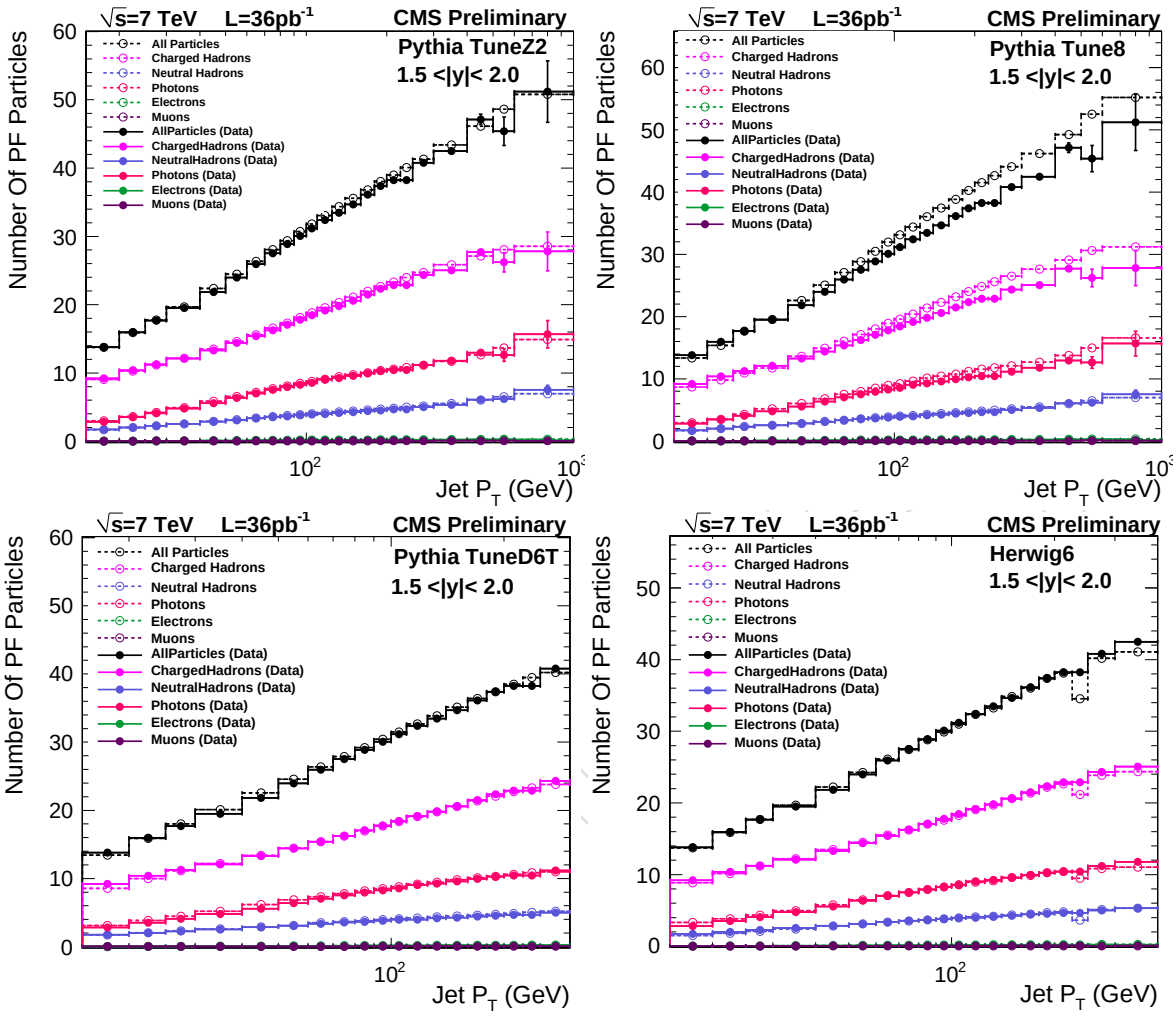

Figure 27: Multiplicity for PF particles in 1.5< $|y|$ <2.0

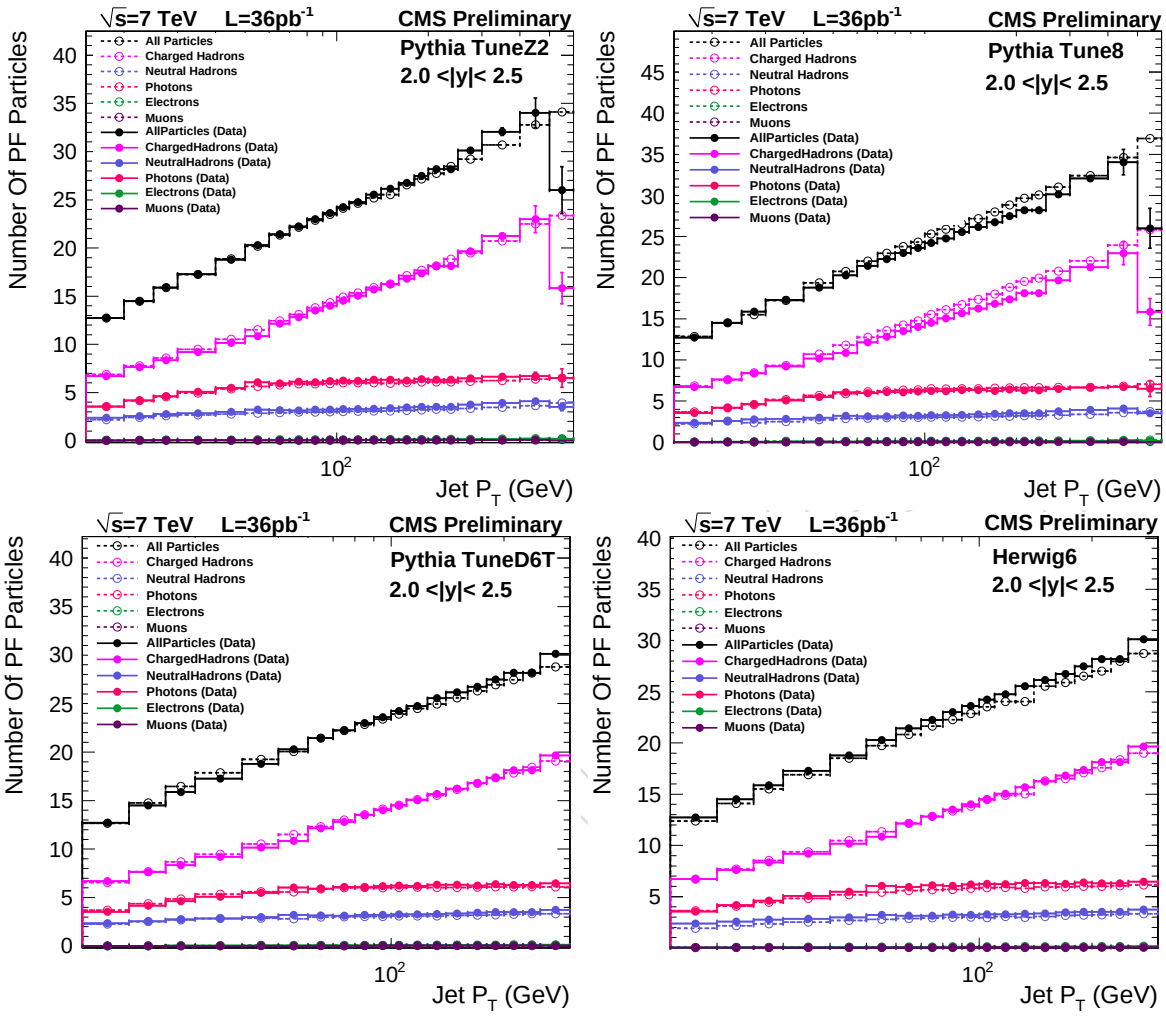

Figure 28: Multiplicity for PF particles in 2.0< $|y|$ <2.5

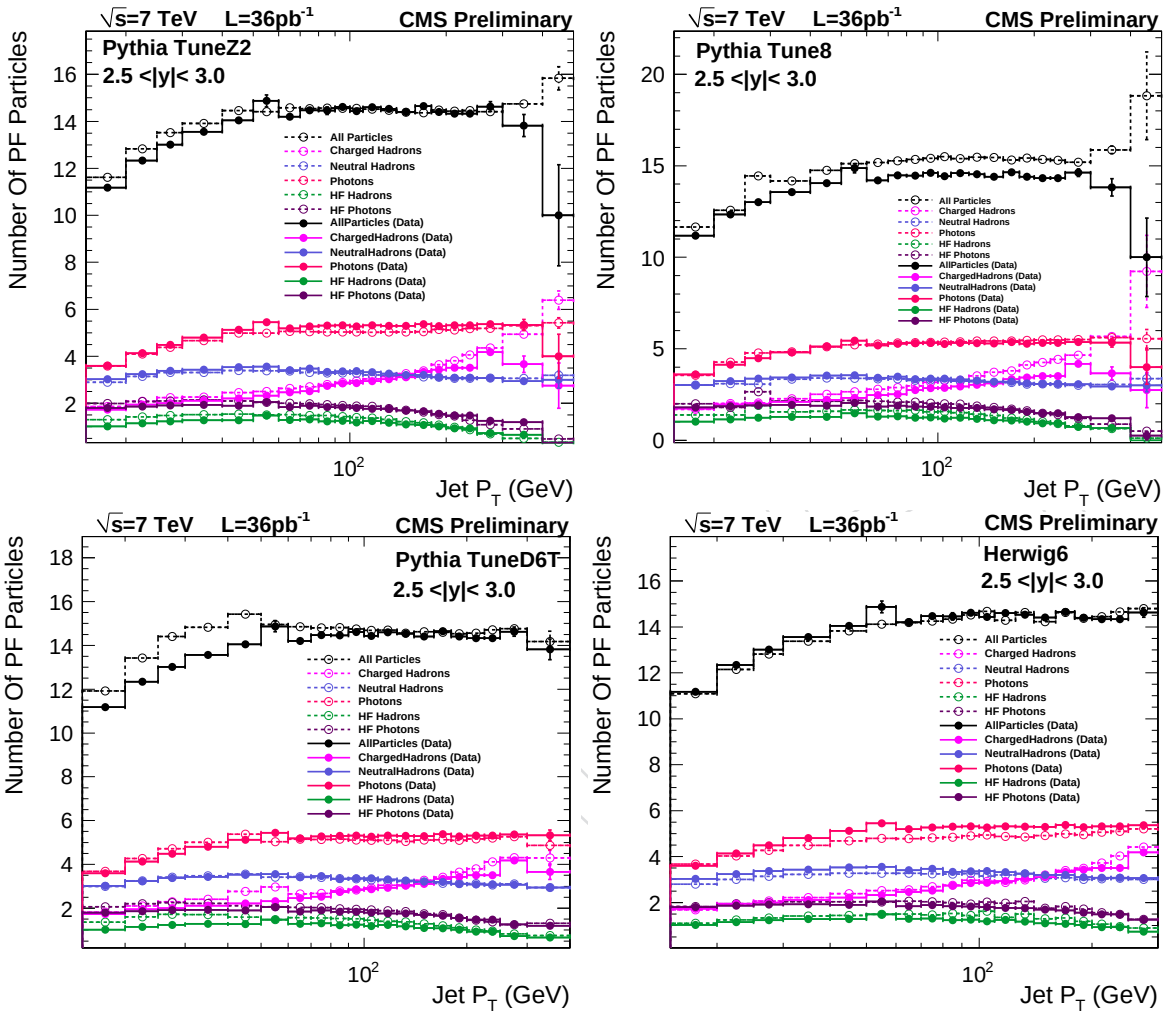

Figure 29: Multiplicity for PF particles in 2.5< $|y|$ <3.0

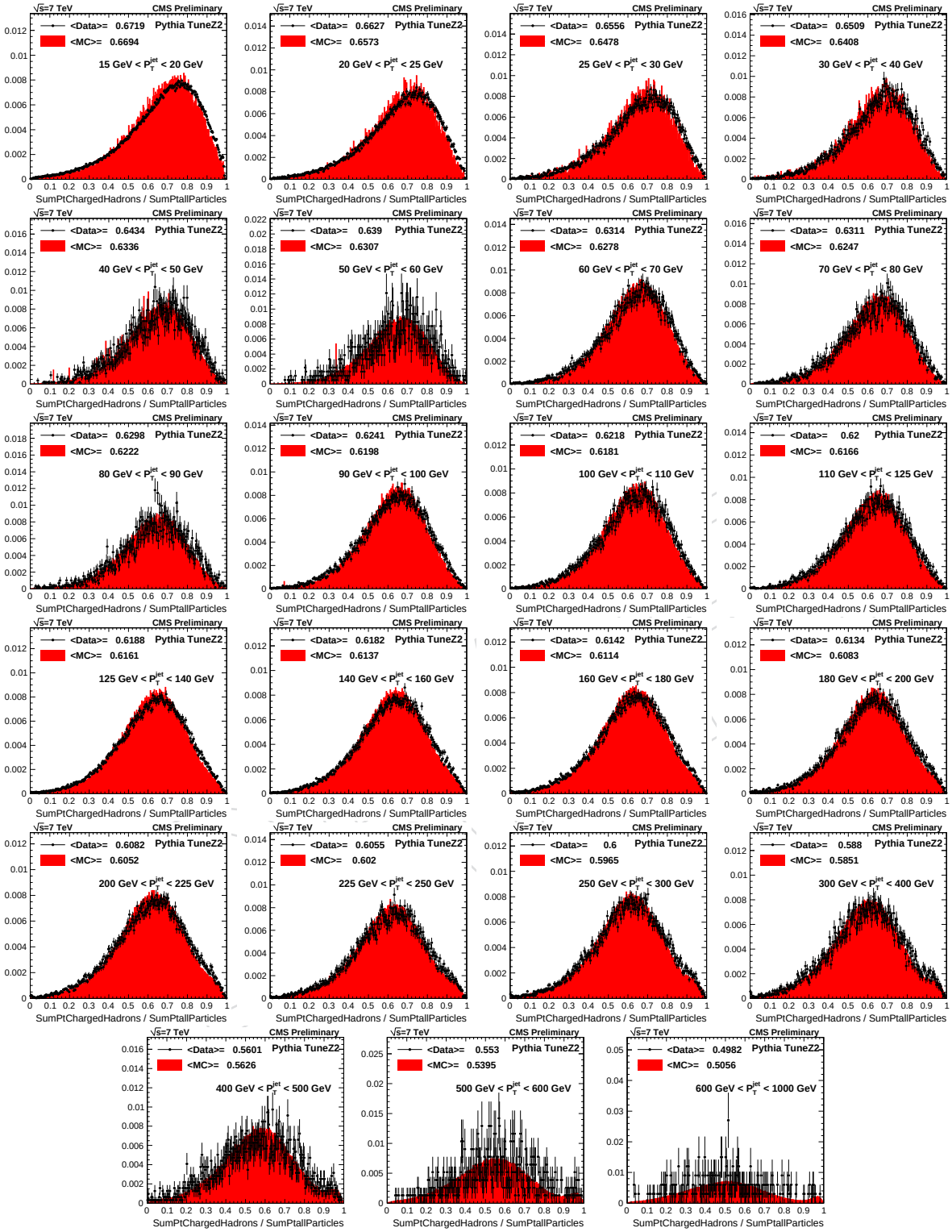

Figure 30: TuneZ2-SumPtFraction-hadrons

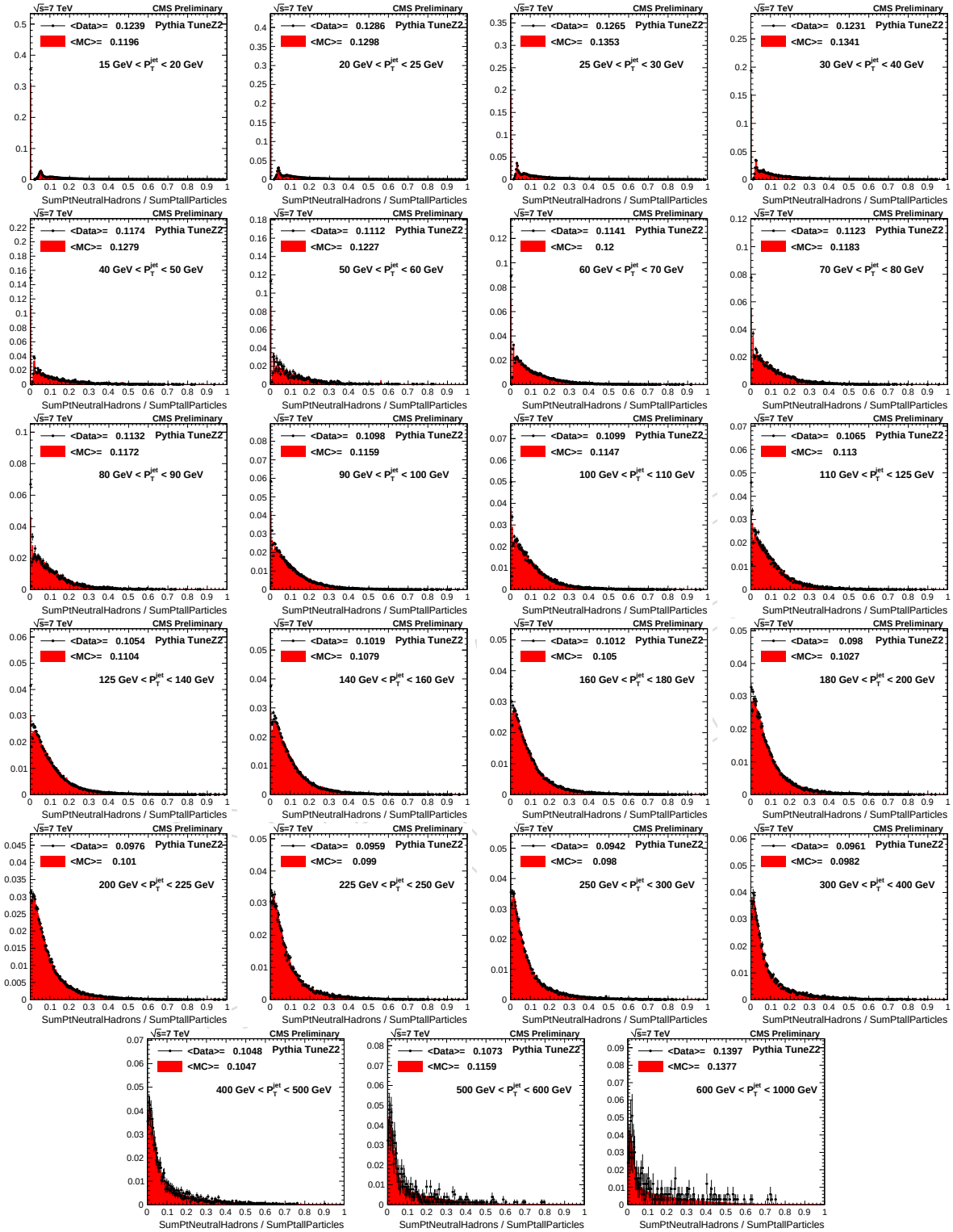

Figure 31: TuneZ2-SumPtFraction-neutrals

10.2 Jet Fragmentation Functions

Jet fragmentation functions defined as $\log(1/z)$ where z is the momentum fraction of the jet carried by an individual particle, $z = p_{\mathrm{T}}^{\mathrm{particle}} / p_{\mathrm{T}}^{rmJet}$ are shown in Fig. 33. The MC described the data for charged hadrons, photons, neutrals hadrons, electrons and muons and combined distributions reasonable well, though not perfectly.

DRAFT

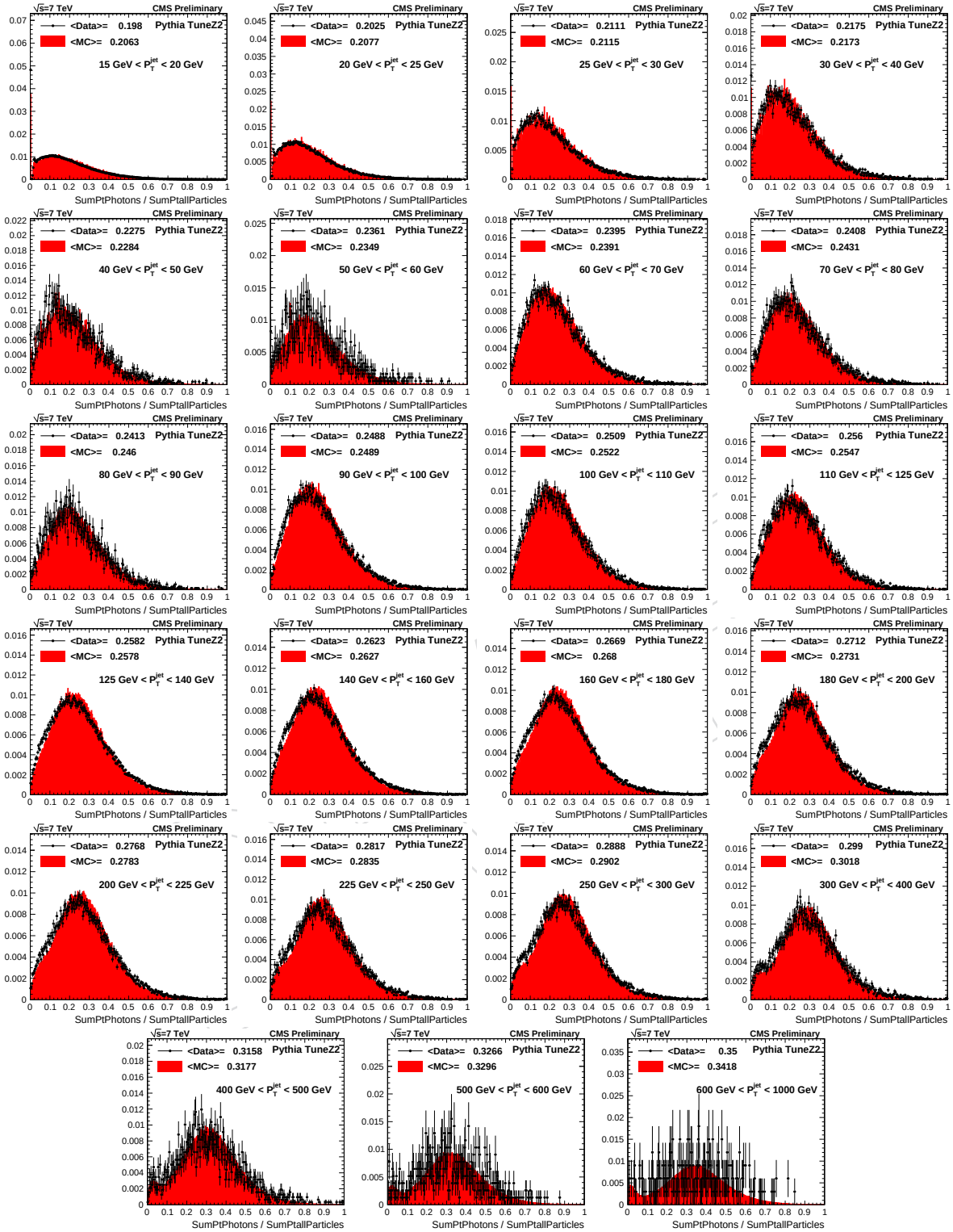

Figure 32: TuneZ2-SumPtFraction-photons

10.3 Single Jet Mass Distributions

The single jet mass distributions, an other measure of the QCD showering and hadromization process, are compared with PYTHIA-Z2 in Fig. 34 and agreement is reasonable. The variation of mean jet mass with jet momenta for different models is shown in Fig. 35. Figure 36 shows the ratio of average jet mass to the jet p_{T} compared with PYTHIA-Z2, PYTHIA8,PYTHIAD6T and HERWIG6 event generators.

DRAFT

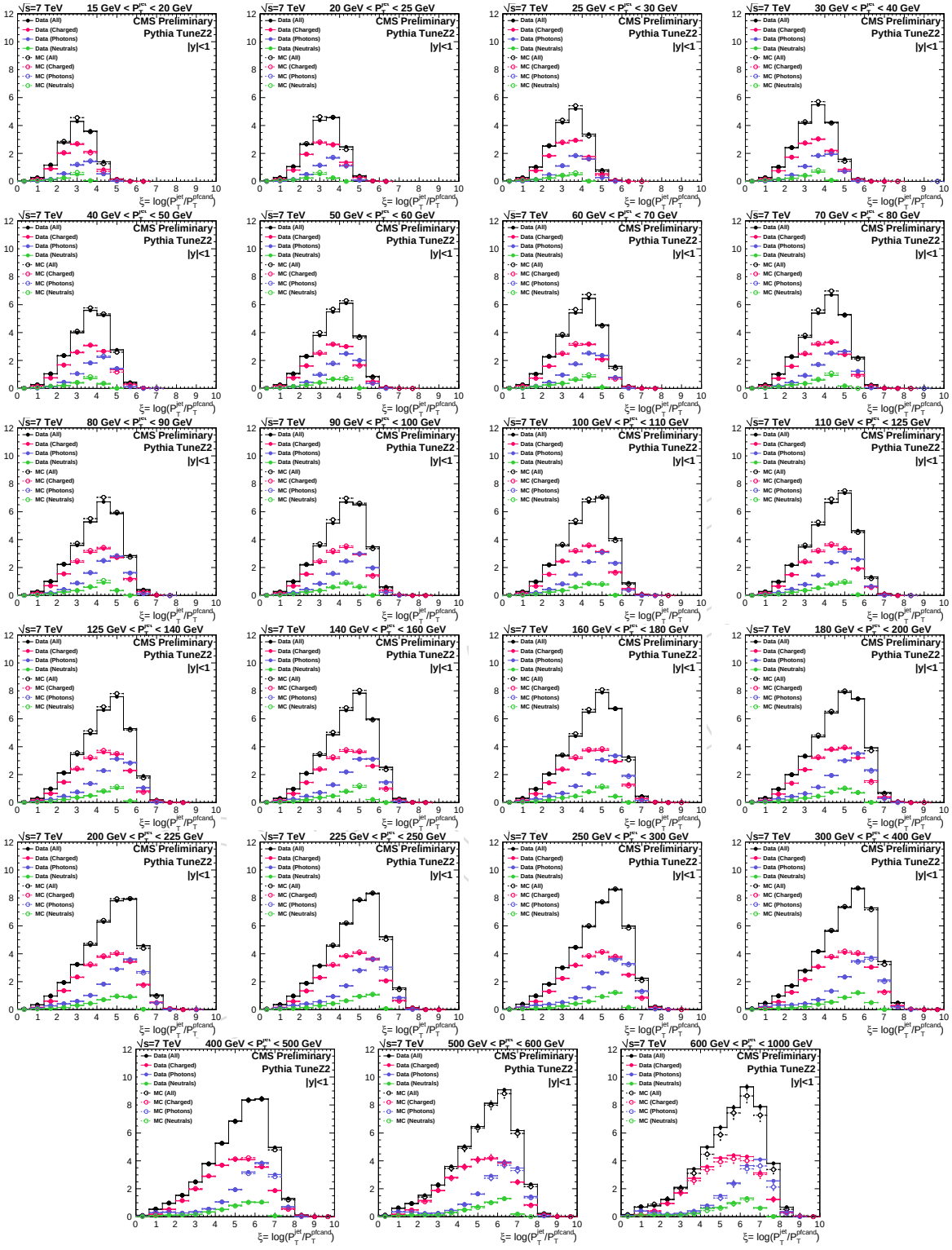

Figure 33: TuneZ2-JetFragmentation comparison of all particles

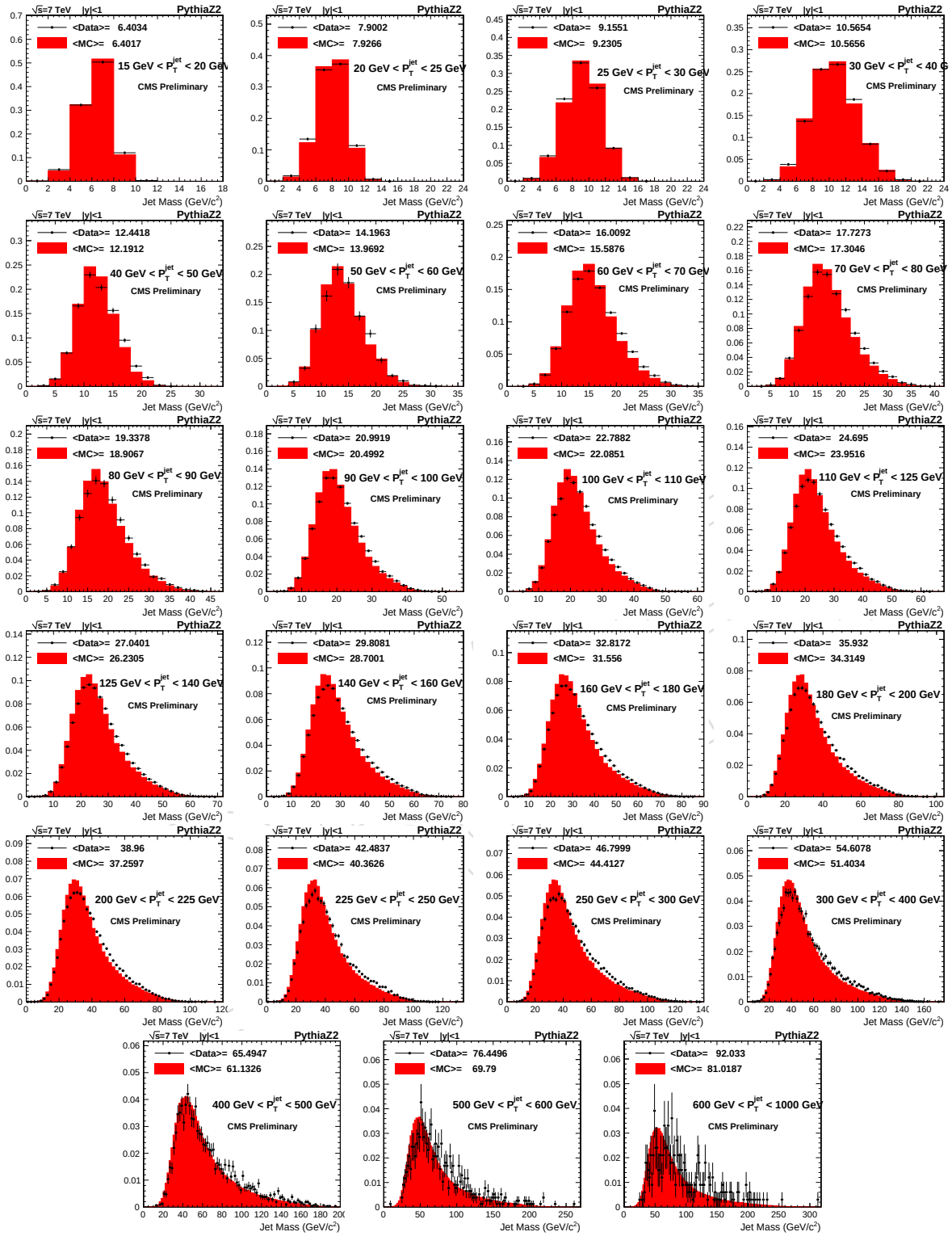

Figure 34: Jet Mass distributions in MC (TuneZ2) and Data where $y < 1$

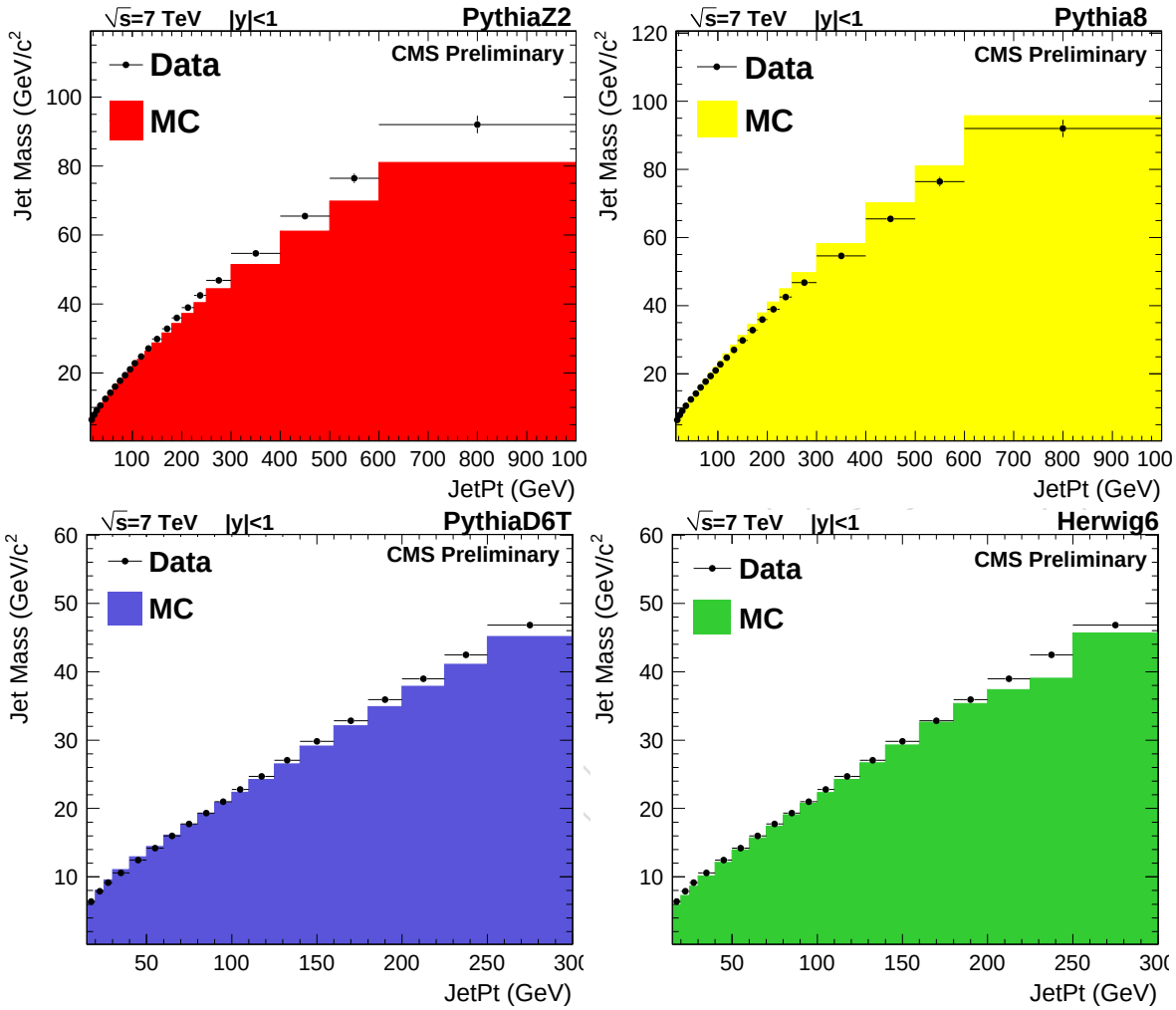

Figure 35: Jet Mass vs Pt for Data and different MC tunes in $|y| < 1.0$

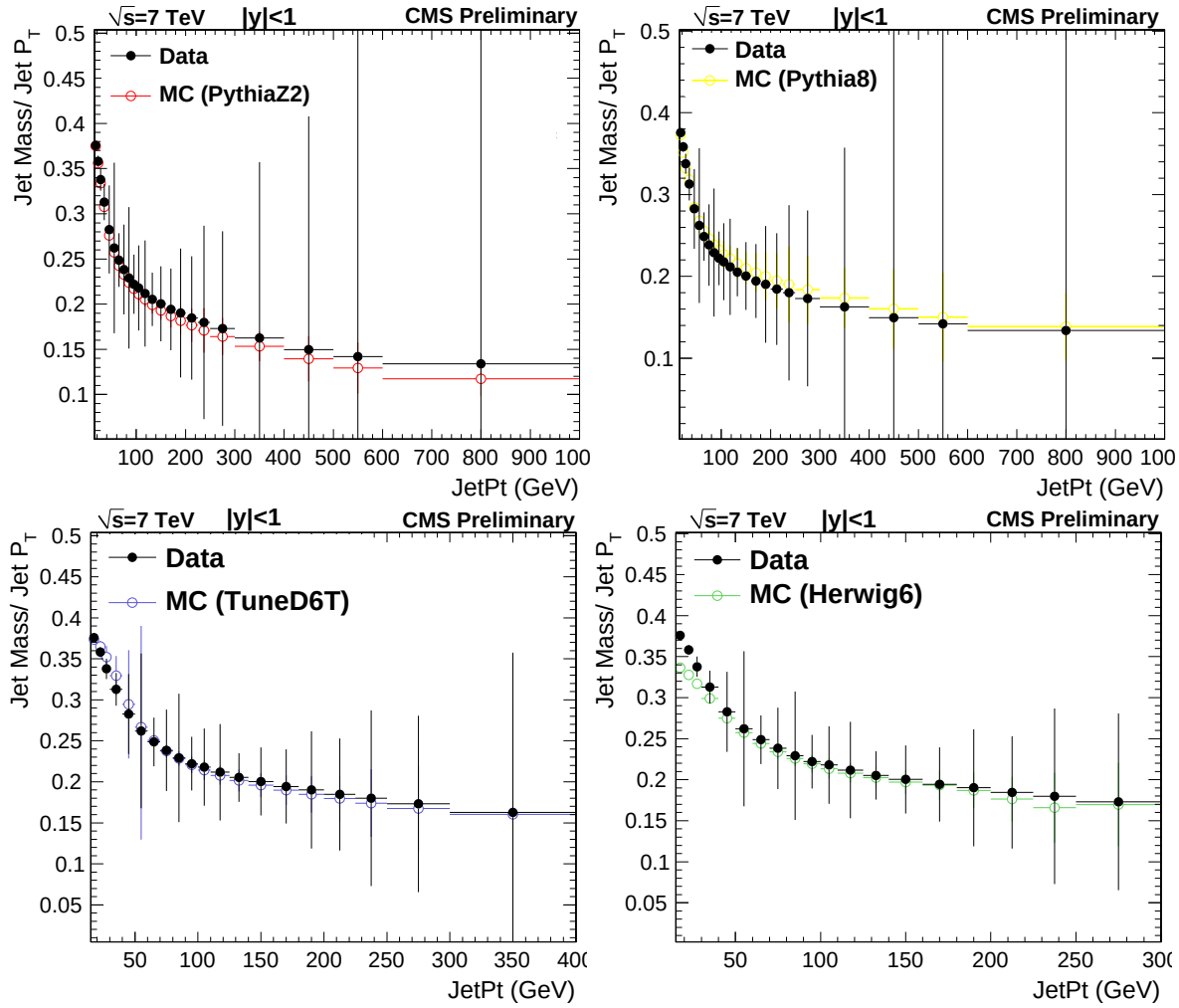

Figure 36: Jet Mass over JetPt vs JetPt for Data and different MC tunes in $|y| < 1.0$

11 Jet Shapes

12 Unfolding of the jetshapes

The reconstructed jetshapes differ from the "true" jetshapes due to smearing in the jet energy resolution and single particle energy and position resolutions. To extract the true jetshapes (i.e. unfold the jetshapes), we use simulated events. The ratio of particle jetshapes and reconstructed jetshapes is obtained events simulated using PYTHIA-Z2. These correction factors, along with correction factors using other generators are shown in Fig. 37. The corrections are small and decrease with the p_T of the jets. The ratio of various corrections to the correction factors for PYTHIA-Z2 tune are shown in 38. This ratio shows the sensitivity of the unfolding corrections to the modeling of jetshapes. We take the maximum difference between the correction determined using Z2 tune and the correction determined from any other event generator as the systematic uncertainty. This uncertainty is significant only for low jet p_T bins and at low r.

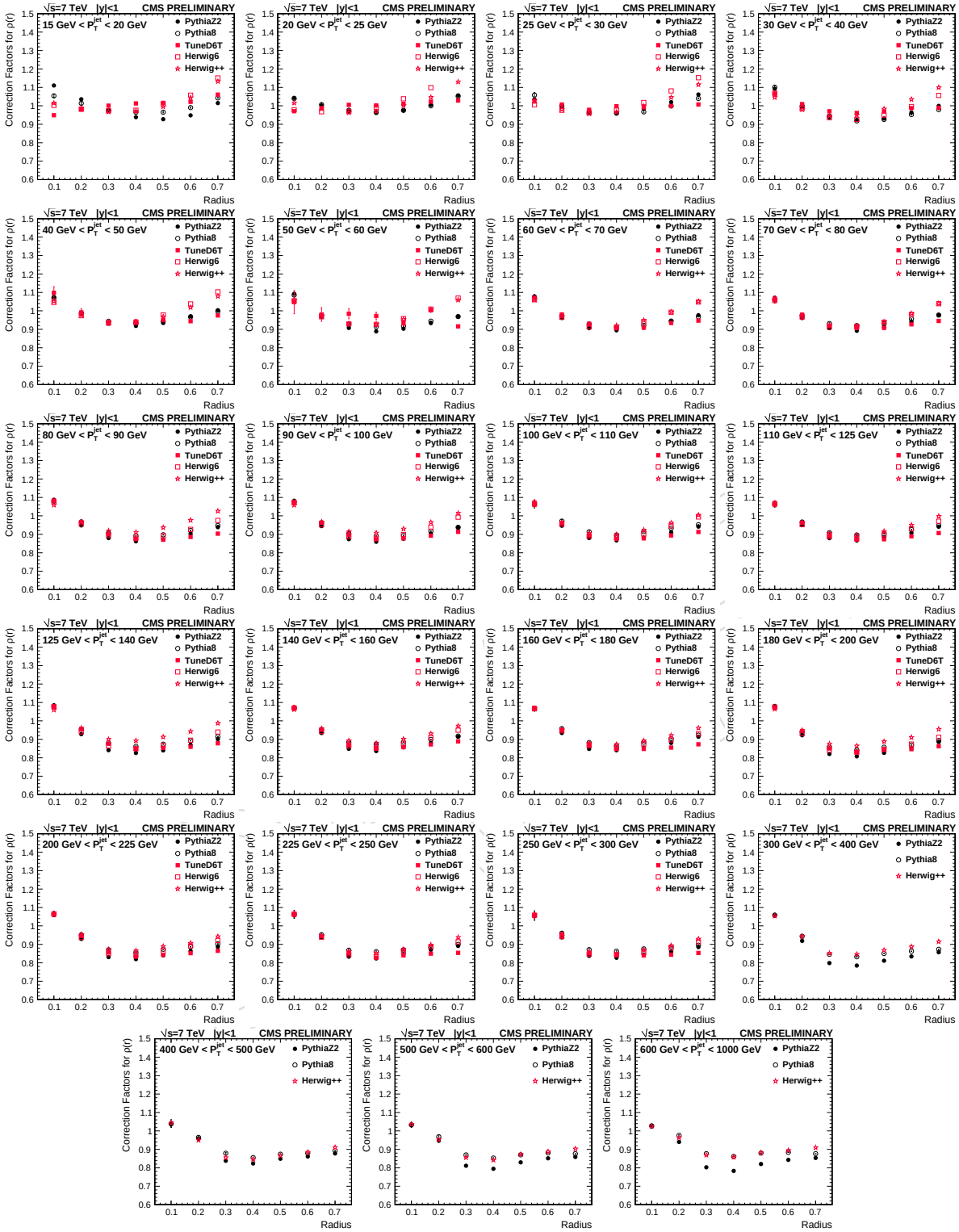

Figure 37: Correction Factors for Differential Jet Shapes for all Tunes

13 Systematic Uncertainties

We consider following systematic uncertainties on the jetshapes measurements.

13.1 Jet Energy Scale

We present the jetshapes in bins of the corrected p_T of the jets and jet can move in and out of the bin if the jet energy scale changes. We use official JES uncertainty which depends on the p_T and η of the jet on the data. For modified energy, we repeat the analysis and obtained new jetshapes. The difference in the jetshapes from the nominal jetshape is taken as the systematic uncertainty.

13.2 PF Particle Calibration

The PF particles used to measure the jetshapes are well calibrated. For charged hadrons, the measurement is dominated by the tracker resolution for low p_T particles. At high p_T, the energy measurement is a combination of calorimeter measurement and the tracker measurement. The charged hadron the energy measurement is uncertain by $\pm 1\%$ for $p_T < 1.5$ GeV/c and $\pm 0.7\%$ for $p_T >= 1.5$ GeV/c. The photons are measured by excellent crystal calorimeter and their energy is uncertain by 1% independent of p_T. The p_T of neutral hadrons is uncertainty by $\pm 3\%$. The effect on these uncertainties on jetshapes is minimal as change in the energy deposition verses radius is the same and thus laargely cancel out. We determine the uncertainty by changing the response independently for each type of particle and add them in quadrature.

13.3 Jet Energy Resolution

Smearing of the jet energy can also result is migration of jets between bins. Bin to bin corrections are determined using simulated events. The simulated data, which is used to determine bin-to-bin corrections agrees with the data to within 10%. We have not evaluated the systematic uncertainty from this effect yet but expect it to be smaller then the JES uncertainty.

13.4 Unfolding Uncertainty

The unfolding correction were determined using the PYTHIA 6 with Z2 tune as is officially recommended by CMS. We compare the correction factors obtained using other event generators and assign the difference in the correction factors is used as the systematic uncertainty. This correction factors depend in the p_T spectrum of the jets and detector response to the jet. The detector response depends on the jet fragmentation which we are measuring. However, we expect that bulk of correction is due to jet p_T corrections.

14 Jet Shapes

The unfolded jetshape for different p_T bins for range $15 \leq p_T \leq 1000$ GeV for various rapidity bins are shown in Fig. 40, 41, 42, 43, 44, 44. As expected, jets become more collimated with increasing p_T. This trend is summarized in Fig. 52. where energy outside a fixed cone of $r = 0.3$ is shown as a function of the jet transverse energy for $|y| < 1.0$ bin. The fraction of jet p_T outside fixed $\eta\phi$ cone decreases with increases p_T of the jet. This due to combination of two effects. Firstly, as discussed above the quarks jets are narrower than gluon jets due to color factor associated with parton emission and the fraction of quark jets increasing with the jet p_T due to change in the parton density distribution in the proton. Secondly, the parton showering changes with increasing p_T of the parton as strong coupling constant α_s decreases.

DRAFT

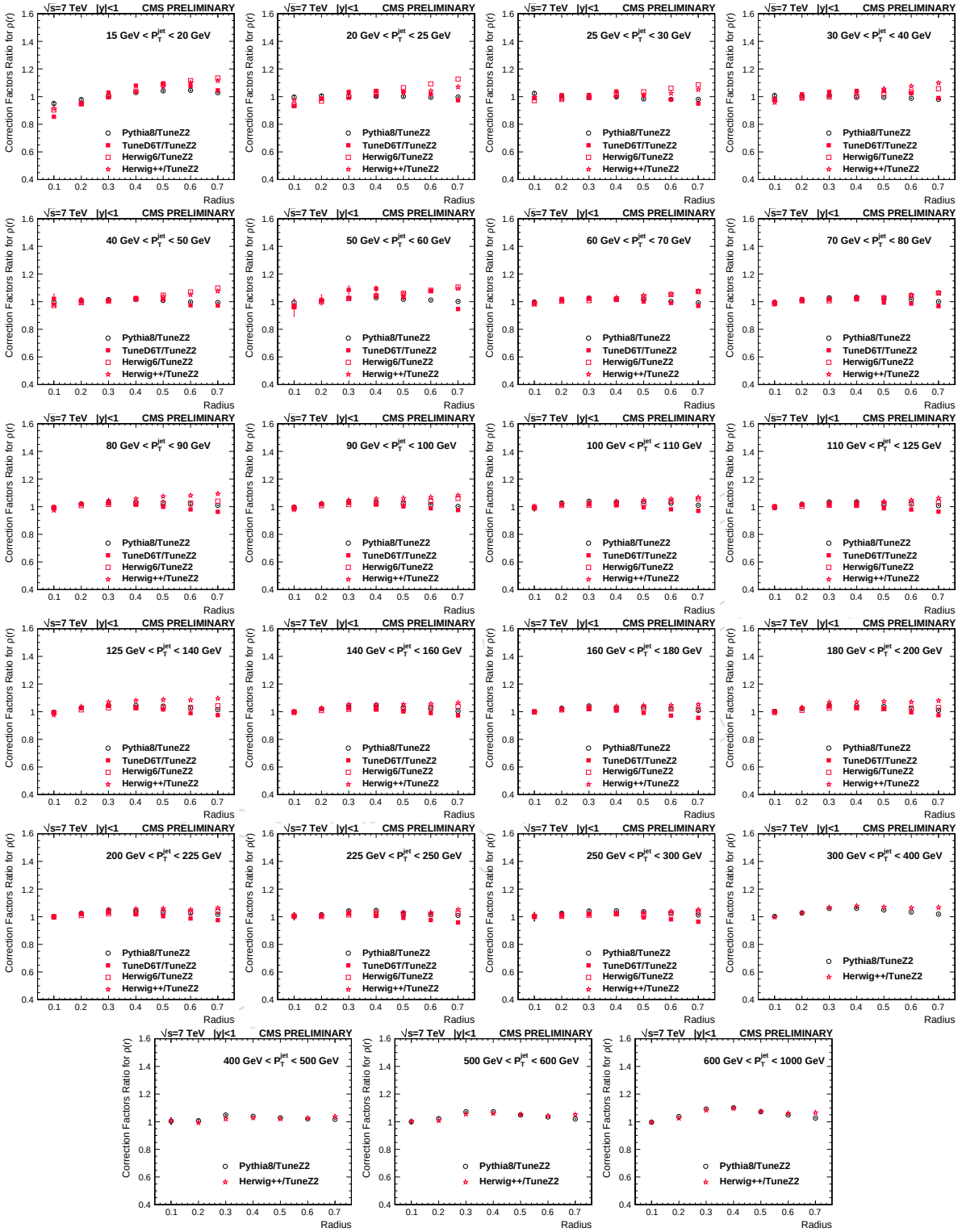

Figure 38: Ratio for Correction Factors for Differential Jet Shapes for all Tunes

QCD inspired events generators show that the second effect is the dominant effect. As shown in Fig. 53, similar trend is observed on all the rapidity bins.

Figure 54 shows the jet shapes changed with the rapidity of the jet very mildy. The p_{T} outside a fixed cone of $R = 0.3$ decreases by $\sim$ 5% when the jet rapidity changes from $y = 0$ to —y—=3.0 for fixed jet p_{T}, in agreement with the QCD-inspired event generators. The same trend is observed for all the p_{T} ranges studied.

Table 6: The p_{T} fraction of jet outside $R = 0.3$ for different jet p_{T} bin for $|y| < 0.5$ region

PtBin	Njet	$1-\psi(0.3)$ raw	corrFactor (TuneZ2)	$1-\Psi(0.3)$ Corrected	sytematics $\pm$	$\Psi(0.3)$ Raw TuneZ2	$\Psi(0.3)$ Gen TuneZ2
15- 20	148024	0.45316	1.04067	0.430918	0.0784845	0.592966	0.617084
20- 25	49091	0.416781	1.00915	0.411441	0.0471831	0.646017	0.651931
25- 30	17736	0.37243	1.00512	0.36922	0.0541343	0.677467	0.680934
30- 40	10917	0.320622	1.02226	0.305497	0.0733645	0.721782	0.73785
40- 50	2715	0.26707	1.01662	0.25489	0.0672304	0.767627	0.780384
50- 60	940	0.214897	1.02165	0.197898	0.0765827	0.794624	0.81183
60- 70	12711	0.20168	1.01731	0.187868	0.0626024	0.815947	0.830067
70- 80	5932	0.185125	1.01674	0.171487	0.0607483	0.827527	0.841376
80- 90	3052	0.1727	1.02159	0.154838	0.0665651	0.838432	0.856534
90- 100	20910	0.162691	1.01986	0.146064	0.0692568	0.849194	0.866057
100-110	12529	0.160108	1.01758	0.145343	0.0532165	0.856366	0.87142
110-125	10150	0.14959	1.01684	0.135281	0.0589159	0.861537	0.876041
125-140	50447	0.141613	1.02124	0.12338	0.0690439	0.870592	0.889084
140-160	33891	0.136562	1.01837	0.120704	0.0639153	0.878461	0.894595
160-180	36754	0.127851	1.01726	0.112799	0.0579018	0.883467	0.898714
180-200	19336	0.124874	1.01984	0.107516	0.0622908	0.890543	0.908207
200-225	25782	0.118736	1.01711	0.103655	0.061038	0.896396	0.911736
225-250	13431	0.11475	1.01591	0.10067	0.0539237	0.900016	0.914332
250-300	17753	0.107257	1.01524	0.0936522	0.049849	0.904252	0.918032
300-400	8785	0.098147	1.01561	0.0840697	0.0638453	0.919388	0.933739
400-500	1774	0.0917456	1.01146	0.0813375	0.0575386	0.927747	0.938378
500-600	435	0.0871136	1.01051	0.0775215	0.0622393	0.940793	0.950678
600-1000	168	0.070001	1.00931	0.0613472	0.110964	0.949597	0.958434

15 Conclusions

The internal structure of the jet was measured in the pp collisions at $\sqrt{s} = 7$ TeV using 36 pb^{-1} of data collected during 2010. The data are in general in agreement with QCD-inspired event generators. At high p_{T}, all different event generators describe the data well. At low p_{T}, event generators differ from each other and data prefers PYTHIA Tune Z2.

References

[1] S. D. Ellis, Z. Kunszt, and D. E. Soper, "Jets at hadron colliders at order alpha-s**3: A Look inside", *Phys. Rev. Lett.* **69** (1992) 3615–3618, `arXiv:hep-ph/9208249`. `doi:10.1103/PhysRevLett.69.3615`.

Table 7: The p_T fraction of jet outside $R = 0.3$ for different jet p_T bin for $0.5 < |y| < 1.0$ region

PtBin	Njet	$1-\psi(0.3)$ raw	corrFactor (TuneZ2)	$1-\Psi(0.3)$ Corrected	sytematics $\pm$	$\Psi(0.3)$ Raw TuneZ2	$\Psi(0.3)$ Gen TuneZ2
15-20	137919	0.450775	1.03022	0.434179	0.0257205	0.600763	0.618916
20-25	44792	0.412141	1.00375	0.40994	0.0189904	0.65157	0.65401
25-30	16183	0.367588	1.00009	0.36753	0.0220145	0.681625	0.681687
30-40	9891	0.317954	1.02014	0.304216	0.024781	0.725222	0.73983
40-50	2494	0.255058	1.01594	0.243184	0.0168201	0.769993	0.782266
50-60	875	0.223876	1.02265	0.206297	0.01539	0.795969	0.813998
60-70	12087	0.198911	1.0188	0.183851	0.00985095	0.816598	0.83195
70-80	5581	0.186808	1.01656	0.173338	0.00597811	0.828876	0.842605
80-90	2885	0.171891	1.02328	0.152612	0.00930473	0.838542	0.858064
90-100	19635	0.162403	1.02152	0.144381	0.007141	0.849559	0.867839
100-110	11619	0.155324	1.01937	0.138966	0.00655786	0.856418	0.873004
110-125	9495	0.149904	1.01884	0.133885	0.00616983	0.861962	0.878204
125-140	46934	0.141416	1.02394	0.120865	0.00748744	0.870663	0.891503
140-160	31879	0.138347	1.02025	0.1209	0.00541902	0.87859	0.896379
160-180	33336	0.13086	1.02026	0.113249	0.00527391	0.88281	0.900698
180-200	17110	0.126214	1.0222	0.10682	0.00652195	0.890629	0.910398
200-225	22639	0.119186	1.01933	0.102156	0.00531151	0.896488	0.913821
225-250	11851	0.114751	1.01826	0.0985846	0.00498509	0.90076	0.91721
250-300	15417	0.107014	1.01754	0.0913545	0.00469016	0.90512	0.920992
300-400	7569	0.0973223	1.01769	0.0813505	0.00506246	0.92021	0.936492
400-500	1408	0.0798454	1.01289	0.0679885	0.00329575	0.929215	0.941188
500-600	339	0.0722141	1.01197	0.0611048	0.00617953	0.941813	0.95309
600-1000	165	0.0656195	1.0109	0.0554314	0.00417174	0.950034	0.960393

[2] M. H. Seymour, "Jet shapes in hadron collisions: Higher orders, resummation and hadronization", *Nucl. Phys.* **B513** (1998) 269–300, arXiv:hep-ph/9707338. doi:10.1016/S0550-3213(97)00711-6.

[3] CDF Collaboration, "A Measurement of jet shapes in $p\bar{p}$ collisions at $\sqrt{s} = 1.8$ TeV", *Phys. Rev. Lett.* **70** (1993) 713–717. doi:10.1103/PhysRevLett.70.713.

[4] D0 Collaboration, "Transverse energy distributions within jets in $p\bar{p}$ collisions at $\sqrt{s} = 1.8$ TeV", *Phys. Lett.* **B357** (1995) 500–508. doi:10.1016/0370-2693(95)00889-S.

[5] CDF Collaboration, "Study of jet shapes in inclusive jet production in $p\bar{p}$ collisions at $\sqrt{s} = 1.96$ TeV", *Phys. Rev.* **D71** (2005) 112002, arXiv:hep-ex/0505013. doi:10.1103/PhysRevD.71.112002.

[6] H1 Collaboration, "Measurements of transverse energy flow in deep inelastic scattering at HERA", *Eur. Phys. J.* **C12** (2000) 595–607, arXiv:hep-ex/9907027. doi:10.1007/s100520000287.

[7] ZEUS Collaboration, "Measurement of jet shapes in high-Q**2 deep inelastic scattering at HERA", *Eur. Phys. J.* **C8** (1999) 367–380, arXiv:hep-ex/9804001. doi:10.1007/s100520050471.

[8] CMS Collaboration, "JetShapes",. AN-10-098.

[9] CMS Collaboration, "JetShapes",. AN-10-014.

Table 8: The p_T fraction of jet outside $R = 0.3$ for different jet p_T bin for $1.0 < |y| < 1.5$ region

PtBin	Njet	$1-\psi(0.3)$ raw	corrFactor (TuneZ2)	$1-\Psi(0.3)$ Corrected	sytematics $\pm$	$\Psi(0.3)$ Raw TuneZ2	$\Psi(0.3)$ Gen TuneZ2
15- 20	129928	0.455818	1.05535	0.425699	0.0253163	0.590041	0.622698
20-25	41270	0.416711	1.02325	0.403151	0.0208848	0.642964	0.65791
25-30	14711	0.372986	1.01953	0.360744	0.0197551	0.674228	0.687392
30-40	8975	0.319986	1.04004	0.292759	0.0260866	0.716082	0.744753
40-50	2225	0.261318	1.03276	0.237119	0.0191553	0.761017	0.785947
50-60	720	0.225929	1.04007	0.194908	0.0161636	0.786314	0.817826
60-70	10582	0.203835	1.03625	0.174974	0.015274	0.806229	0.835454
70-80	5042	0.193767	1.03233	0.167701	0.0107851	0.819328	0.845817
80-90	2497	0.182947	1.04034	0.149985	0.0114988	0.828572	0.862
90-100	16761	0.171968	1.03854	0.140058	0.0138992	0.839124	0.871462
100-110	9627	0.163679	1.03497	0.134436	0.0104178	0.847375	0.877004
110-125	8076	0.159157	1.03486	0.129846	0.0101111	0.852789	0.882516
125-140	38523	0.149558	1.04063	0.115004	0.011441	0.860559	0.895524
140-160	25766	0.144779	1.03643	0.113626	0.0101548	0.86937	0.901039
160-180	26566	0.137657	1.03621	0.106432	0.00940202	0.874106	0.905757
180-200	13948	0.133184	1.03841	0.0998857	0.0101333	0.881297	0.915152
200-225	17399	0.123877	1.03473	0.0934528	0.00970192	0.887785	0.918615
225-250	8770	0.119353	1.0325	0.090735	0.0081911	0.892751	0.921762
250-300	11664	0.112406	1.03135	0.0845766	0.00789438	0.897989	0.926144
300-400	5430	0.104604	1.03324	0.0748443	0.00838631	0.910746	0.941016
400-500	956	0.0928803	1.02608	0.0692253	0.00711029	0.922209	0.946257
500-600	214	0.0695014	1.02632	0.0450061	0.0076324	0.932382	0.956927
600-1000	62	0.0787178	1.02451	0.0561378	0.00801079	0.940125	0.963167

[10] Inclusive Jet group Collaboration, "Measurement of Inclusive Jet Cross section",. AN-10-439.

[11] M. Cacciari, G. P. Salam, and G. Soyez, "The anti-k_T jet clustering algorithm", *JHEP* **04** (2008) 063, arXiv:0802.1189. doi:10.1088/1126-6708/2008/04/063.

[12] CMS Collaboration, "Jet Energy Calibration and Transverse Momentum Resolution in CMS",. JME-10-011.

DRAFT

Table 9: The p_{T} fraction of jet outside $R = 0.3$ for different jet p_{T} bin for $1.5 \leq |y| < 2.0$ region

PtBin	Njet	$1-\psi(0.3)$ raw	corrFactor (TuneZ2)	$1-\Psi(0.3)$ Corrected	sytematics $\pm$	$\Psi(0.3)$ Raw TuneZ2	$\Psi(0.3)$ Gen TuneZ2
15 - 20	118936	0.456573	1.06562	0.420912	0.0272126	0.590593	0.629349
20 - 25	36649	0.41671	1.03488	0.396365	0.0212816	0.642576	0.664988
25 - 30	12835	0.372017	1.03171	0.352101	0.0193852	0.672945	0.694286
30 - 40	7610	0.321798	1.05262	0.286109	0.0255472	0.71386	0.751425
40 - 50	1922	0.268596	1.0467	0.234442	0.0199651	0.757225	0.792584
50 - 60	664	0.228994	1.05263	0.188412	0.0205936	0.783006	0.82422
60 - 70	8654	0.214525	1.04681	0.177756	0.0151182	0.804134	0.841776
70 - 80	3754	0.201369	1.04658	0.164173	0.0155833	0.814711	0.852657
80 - 90	1920	0.187589	1.05133	0.145886	0.0159016	0.826538	0.868966
90 - 100	12877	0.175486	1.04789	0.136	0.01464	0.838196	0.878338
100- 110	7325	0.16942	1.04517	0.131905	0.0135825	0.845622	0.883817
110- 125	6047	0.158702	1.04452	0.121247	0.0135688	0.850667	0.888539
125- 140	28842	0.148548	1.04722	0.108347	0.0142598	0.862019	0.90272
140-160	18965	0.141538	1.0414	0.105999	0.0123102	0.871984	0.908084
160-180	19554	0.132538	1.04212	0.0960034	0.0124651	0.87608	0.912977
180-200	9987	0.126399	1.04099	0.0905937	0.0123108	0.88605	0.922365
200-225	12629	0.117193	1.03648	0.0849901	0.0108185	0.893306	0.925892
225-250	6304	0.110356	1.0335	0.080553	0.0100193	0.898756	0.928865
250-300	7949	0.10127	1.03174	0.0727395	0.0097135	0.904192	0.932896
300-400	3500	0.0901991	1.03206	0.0610298	0.00976416	0.917276	0.946685
400-500	465	0.0762471	1.02524	0.0529328	0.00850511	0.928503	0.951937
500-600	81	0.0616168	1.02419	0.0389163	0.0099803	0.938597	0.961303
600-1000	15	0.0538563	1.02516	0.0300524	0.00764925	0.943308	0.96704

DRAFT

Table 10: The p_T fraction of jet outside $R = 0.3$ for different jet p_T bin for $2.0 \leq |y| < 2.5$ region

PtBin	Njet	$1-\psi(0.3)$ raw	corrFactor (TuneZ2)	$1-\Psi(0.3)$ Corrected	sytematics $\pm$	$\Psi(0.3)$ Raw TuneZ2	$\Psi(0.3)$ Gen TuneZ2
15 - 20	91544	0.415687	1.01297	0.422302	0.0223467	0.630776	0.638955
20 - 25	28192	0.372642	0.99232	0.391874	0.0216696	0.680122	0.674901
25 - 30	10058	0.324765	0.99559	0.346665	0.0163566	0.708114	0.704987
30 - 40	6129	0.276636	1.01909	0.28038	0.0217207	0.748705	0.762999
40 - 50	1554	0.227196	1.01684	0.230083	0.0165646	0.788069	0.801337
50 - 60	495	0.198071	1.02761	0.200445	0.0143236	0.811572	0.833979
60 - 70	6793	0.167429	1.02393	0.176607	0.010423	0.831336	0.85123
70 - 80	2996	0.148337	1.02437	0.161288	0.0093411	0.841653	0.862161
80 - 90	1486	0.13624	1.03041	0.140223	0.0135836	0.852792	0.878722
90 - 100	10005	0.129824	1.02665	0.134281	0.00992106	0.865004	0.888059
100 - 110	5596	0.116053	1.02322	0.126713	0.00893893	0.872665	0.892933
110 - 125	4562	0.112275	1.02531	0.118294	0.00921007	0.876767	0.898961
125 - 140	20806	0.100224	1.02682	0.106712	0.0112951	0.888167	0.911984
140 - 160	13653	0.0915661	1.02177	0.101832	0.00807904	0.898304	0.917858
160 - 180	13030	0.0855579	1.02297	0.0909654	0.00888357	0.901572	0.92228
180 - 200	6501	0.0738195	1.02266	0.085685	0.00879635	0.909883	0.930504
200 - 225	7472	0.0687338	1.01751	0.0804577	0.00715144	0.917647	0.933715
225 - 250	3469	0.0662942	1.01682	0.0771925	0.00692561	0.921761	0.937269
250 - 300	3540	0.059699	1.01484	0.0743322	0.00649533	0.927689	0.941459
300 - 400	976	0.043393	1.01738	0.0647488	0.00635894	0.935945	0.952209
400 - 500	53	0.0525818	1.01178	0.0502518	0.011647	0.947158	0.958319
500 - 600	6	1	1.01254	0.0149343	0.0116868	0.954754	0.966726
600 - 1000	0	-	-	-	-	0.960884	0.976281

DRAFT

Table 11: The p_{T} fraction of jet outside $R = 0.3$ for different jet p_{T} bin for $2.5 \leq |y| < 3.0$ region

PtBin	Njet	$1-\psi(0.3)$ raw	corrFactor (TuneZ2)	$1-\Psi(0.3)$ Corrected	sytematics $\pm$	$\Psi(0.3)$ Raw TuneZ2	$\Psi(0.3)$ Gen TuneZ2
15-20	77916	0.415687	1.02479	0.401204	0.0210321	0.636987	
20-25	23755	0.372642	1.00462	0.369745	0.0171094	0.686251	
25-30	8405	0.324765	1.00549	0.321061	0.0127774	0.717352	
30-40	5017	0.276636	1.02655	0.25743	0.0201147	0.758459	
40-50	1224	0.227196	1.01779	0.213449	0.0157772	0.801372	
50-60	406	0.198071	1.02695	0.176462	0.0127464	0.826153	
60-70	5491	0.167429	1.0197	0.151028	0.0119249	0.848691	
70-80	2359	0.148337	1.01614	0.134589	0.00980283	0.861396	
80-90	1153	0.13624	1.02433	0.115226	0.0123012	0.870555	
90-100	7631	0.129824	1.01851	0.11372	0.0110395	0.883993	
100-110	4214	0.116053	1.01277	0.104764	0.00896666	0.894136	
110-125	3186	0.112275	1.01337	0.100407	0.00738338	0.899032	
125-140	14504	0.100224	1.01734	0.0846242	0.0106462	0.90704	
140-160	8670	0.0915661	1.00926	0.0831551	0.00676727	0.91879	
160-180	7509	0.0855579	1.0111	0.0754098	0.00729175	0.922205	
180-200	3330	0.0738195	1.01169	0.062992	0.00783231	0.92864	
200-225	3117	0.0687338	1.00677	0.0624261	0.00563984	0.936396	
225-250	1195	0.0662942	1.00656	0.0601736	0.00473939	0.940703	
250-300	924	0.059699	1.00521	0.0548018	0.00543286	0.947306	
300-400	133	0.043393	1.01045	0.0333956	0.00667517	0.951395	
400-500	4	0.0525818	1.01308	0.040185	0.504339	0.955803	
500-600	0	-	-	-	-	-	
600- 1000	0	-	-	-	-	-	

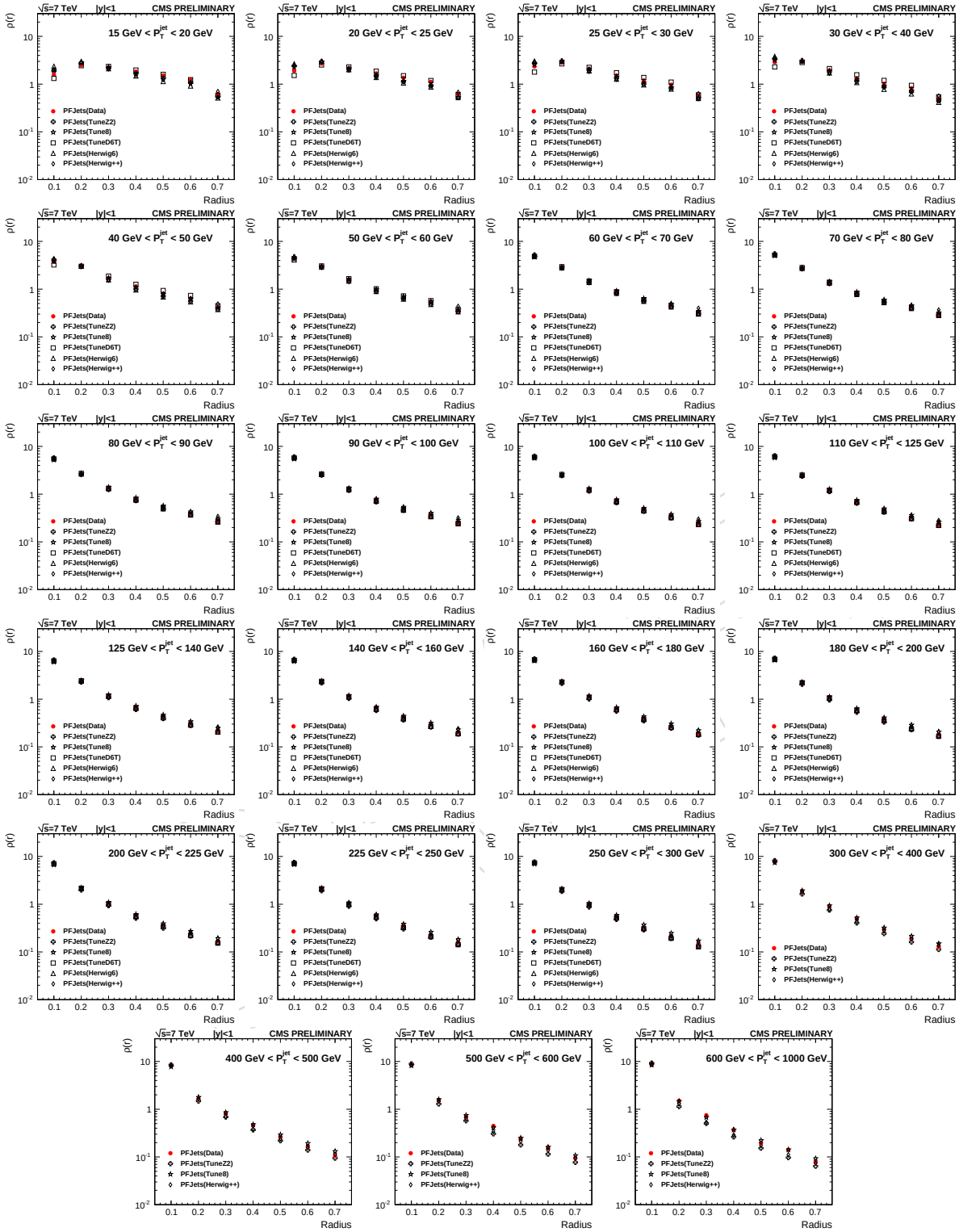

Figure 39: Differential Jet Shapes for all Tunes

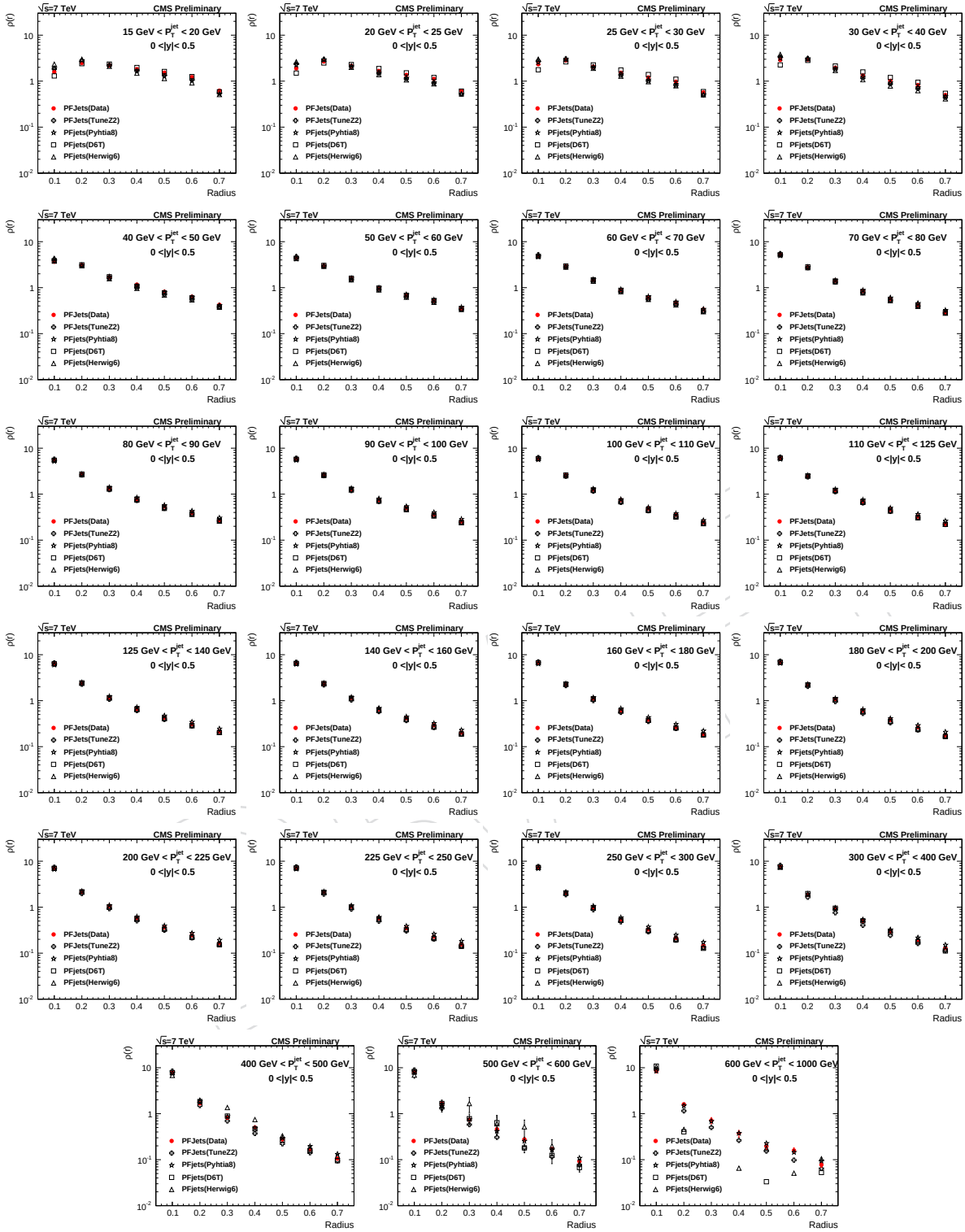

Figure 40: Differential Jet Shapes for all Tunes for $|y|$ <0.5

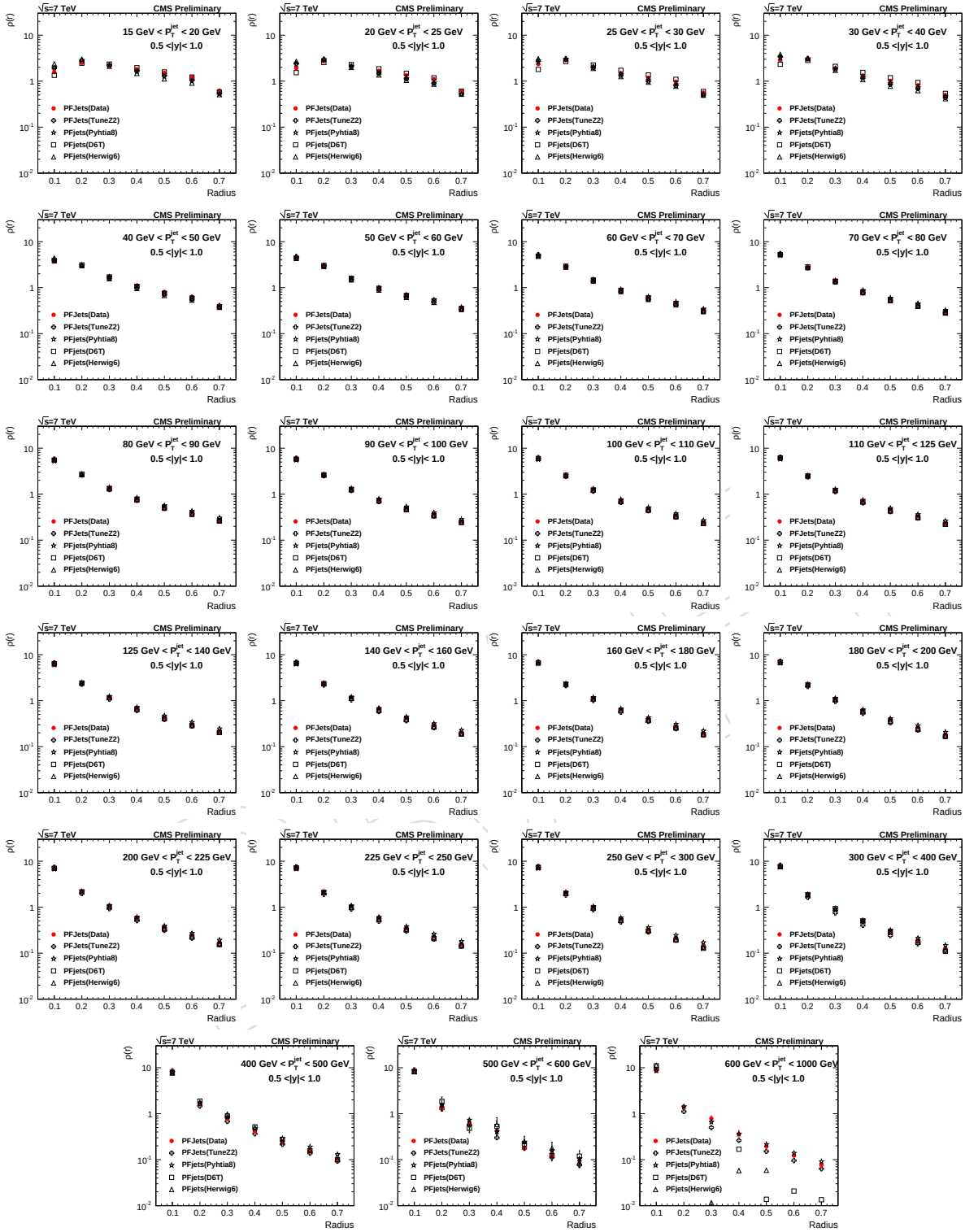

Figure 41: Differential Jet Shapes for all Tunes for $0.5 < |y| < 1.0$

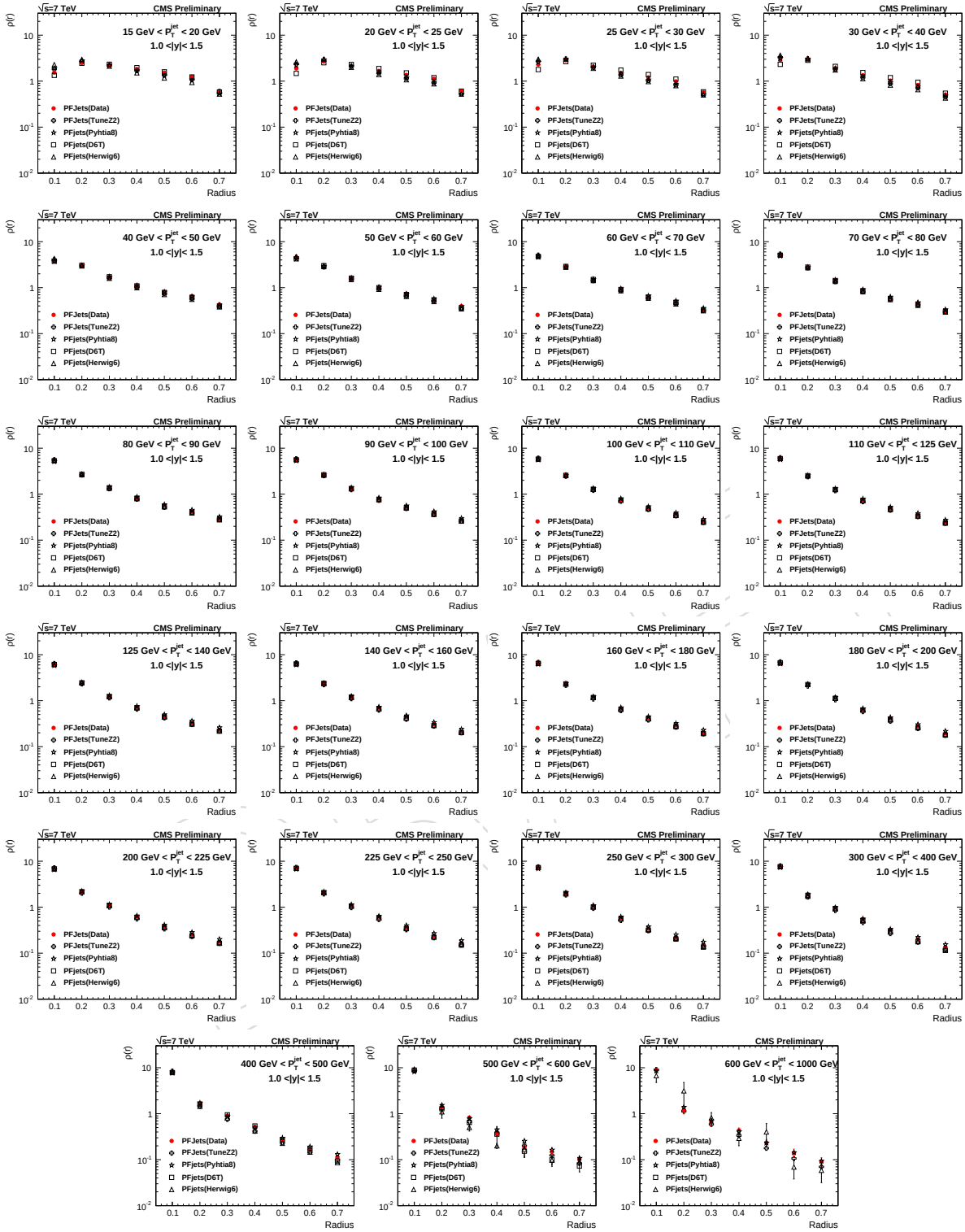

Figure 42: Differential Jet Shapes for all Tunes for $1.0 < |y| < 1.5$

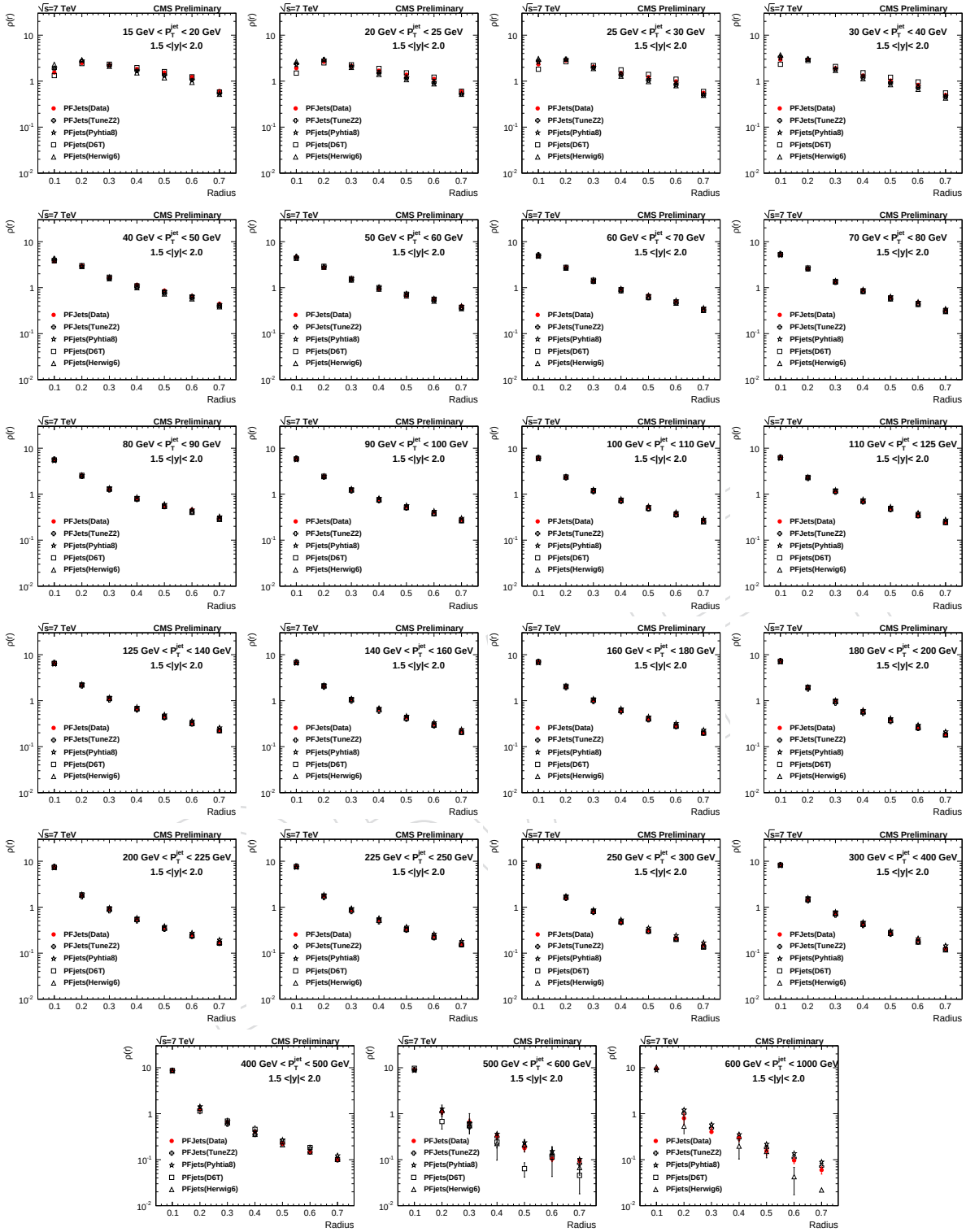

Figure 43: Differential Jet Shapes for all Tunes for $1.0 < |y| < 1.5$

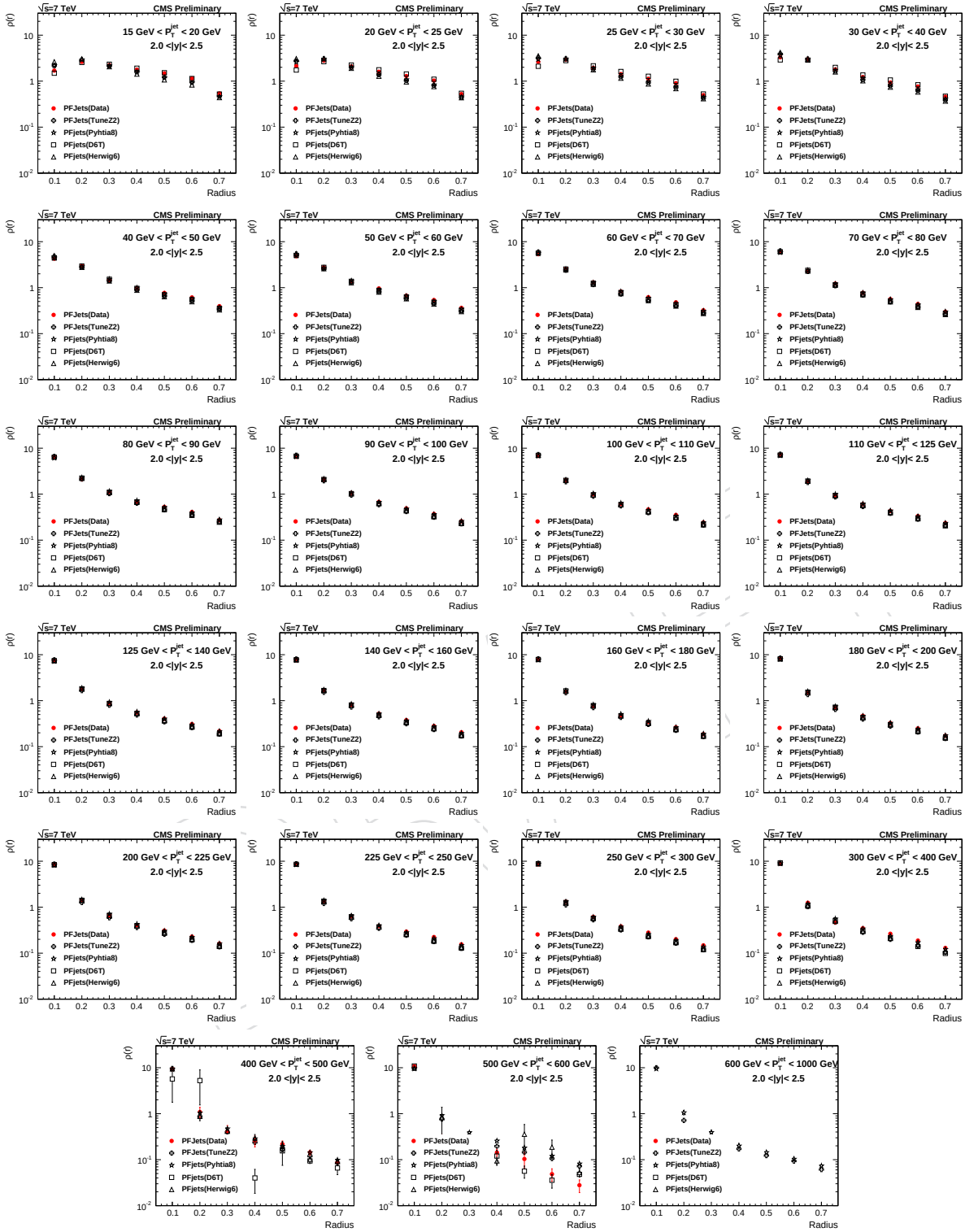

Figure 44: Differential Jet Shapes for all Tunes for $2.0 < |y| < 2.5$

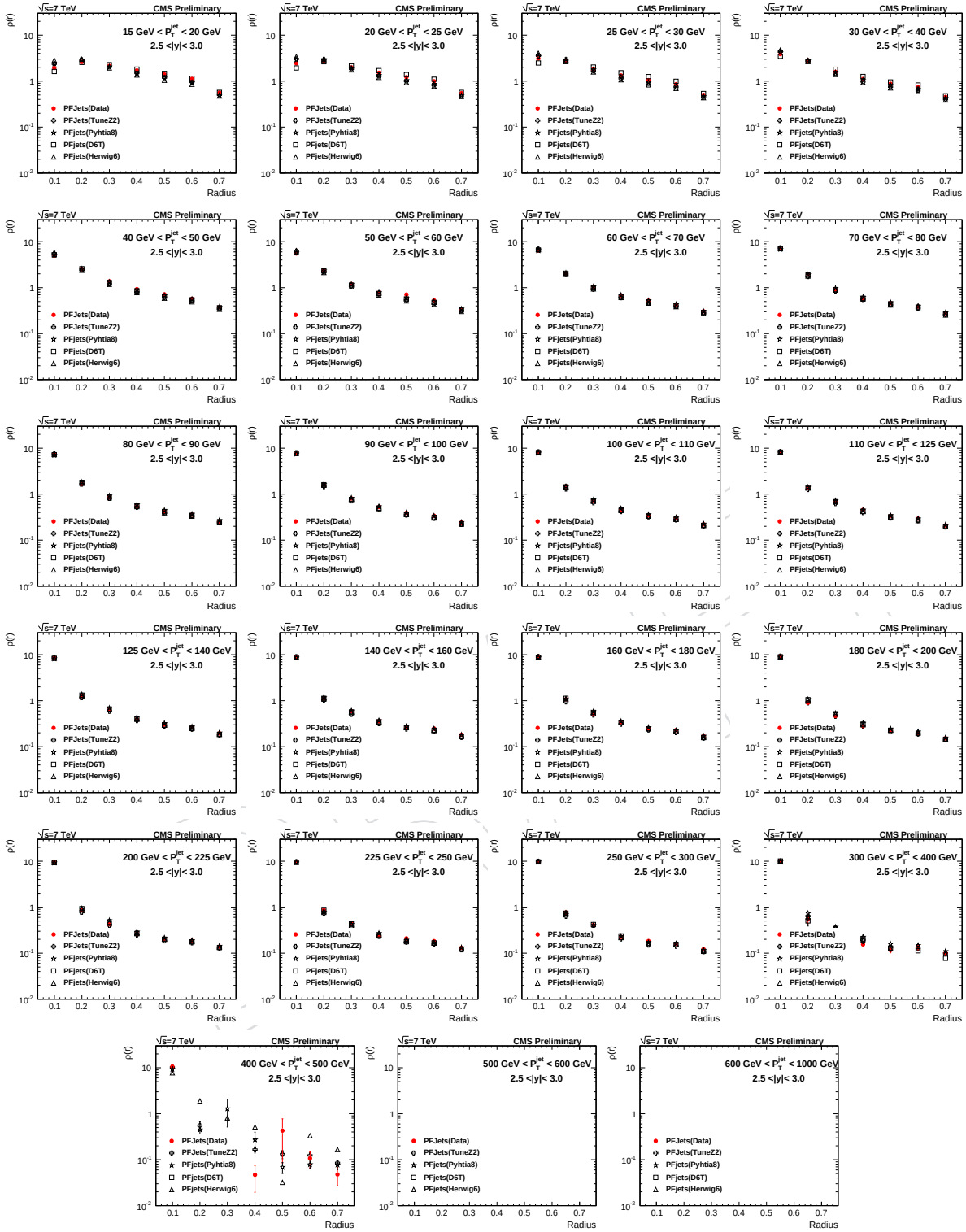

Figure 45: Differential Jet Shapes for all Tunes for 2.5< $|y|$ <3.0

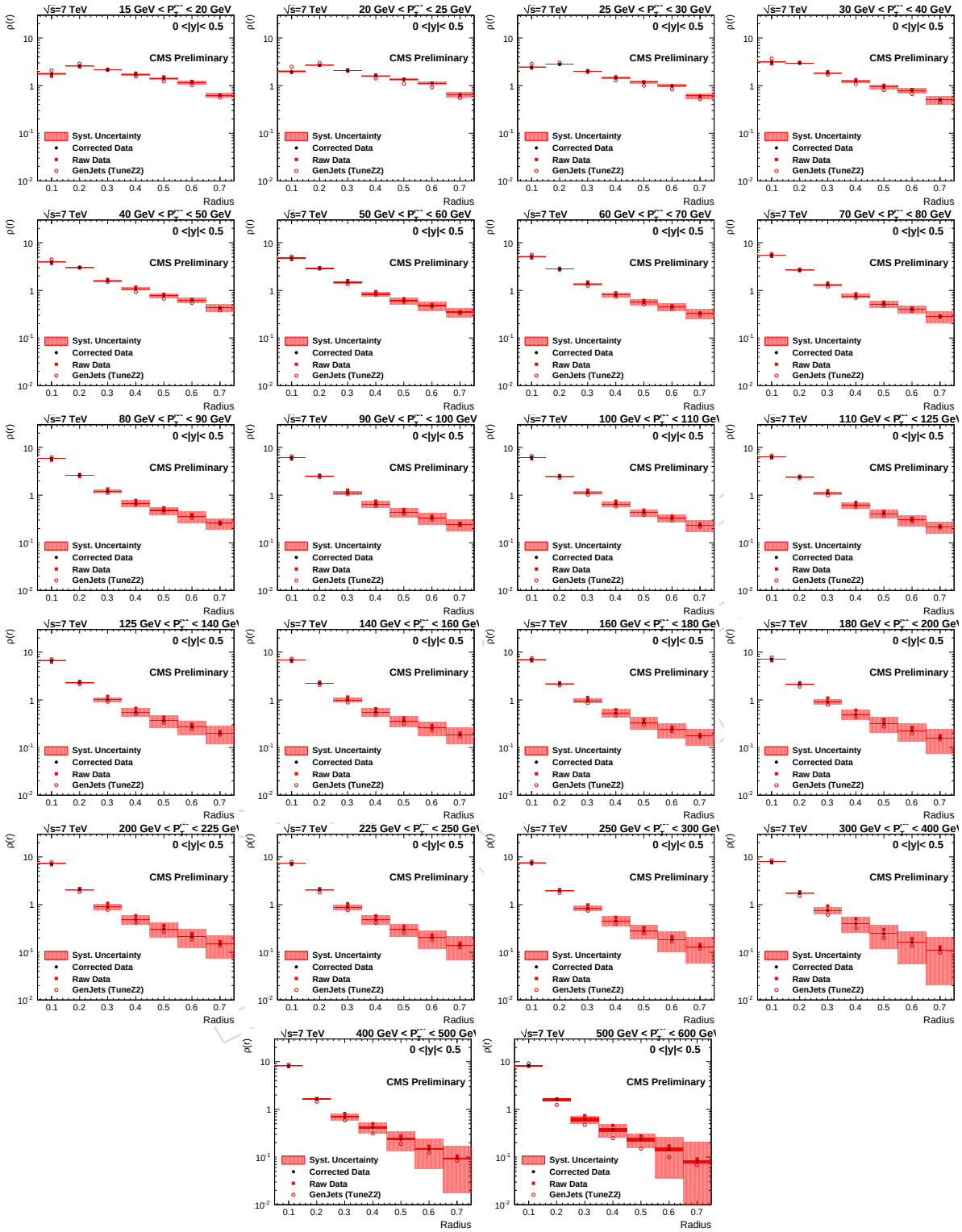

Figure 46: Corrected Differential JetShapes for $|y| < 0.5$

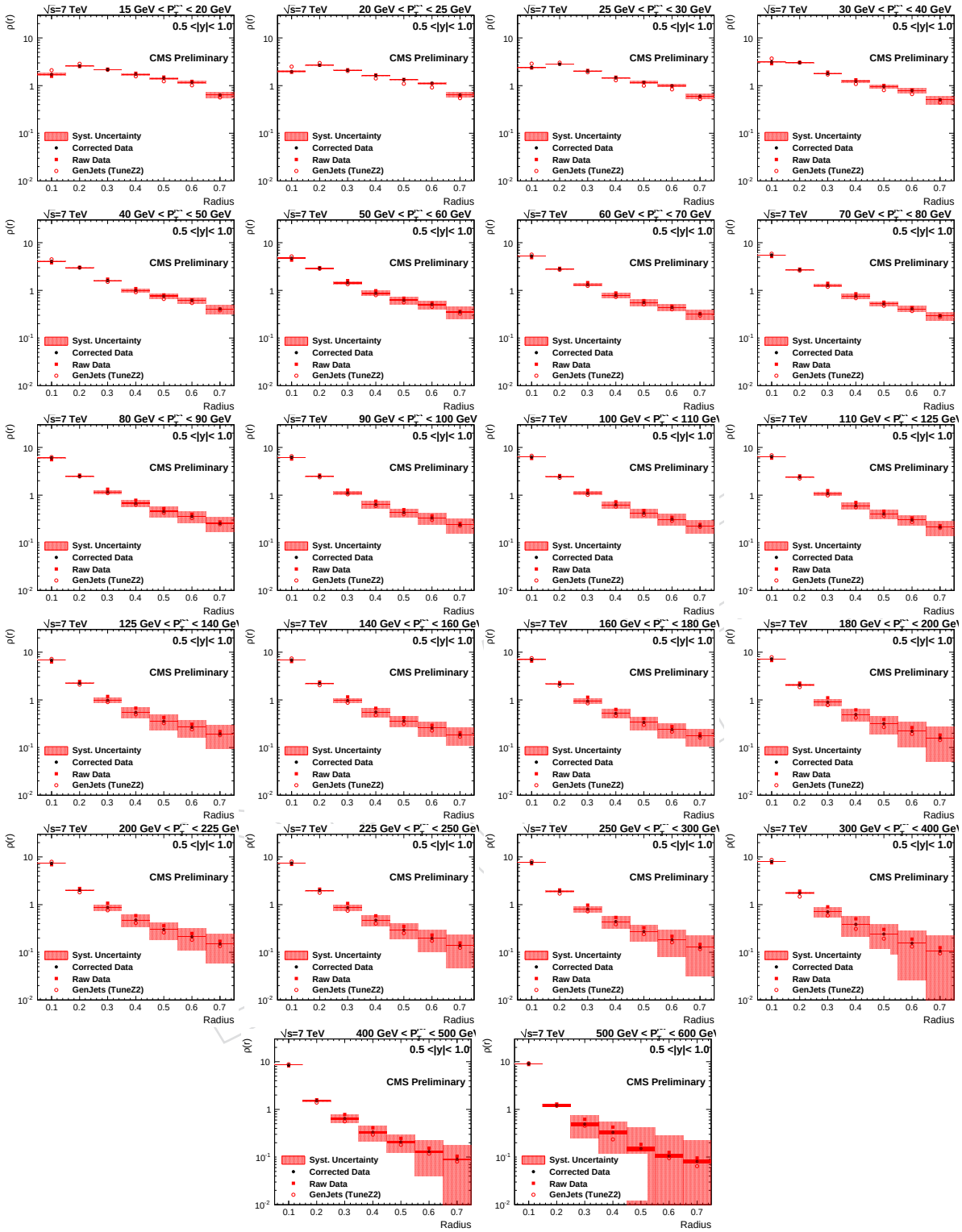

Figure 47: Corrected Differential JetShapes for 0.5< $|y|$ <1.0

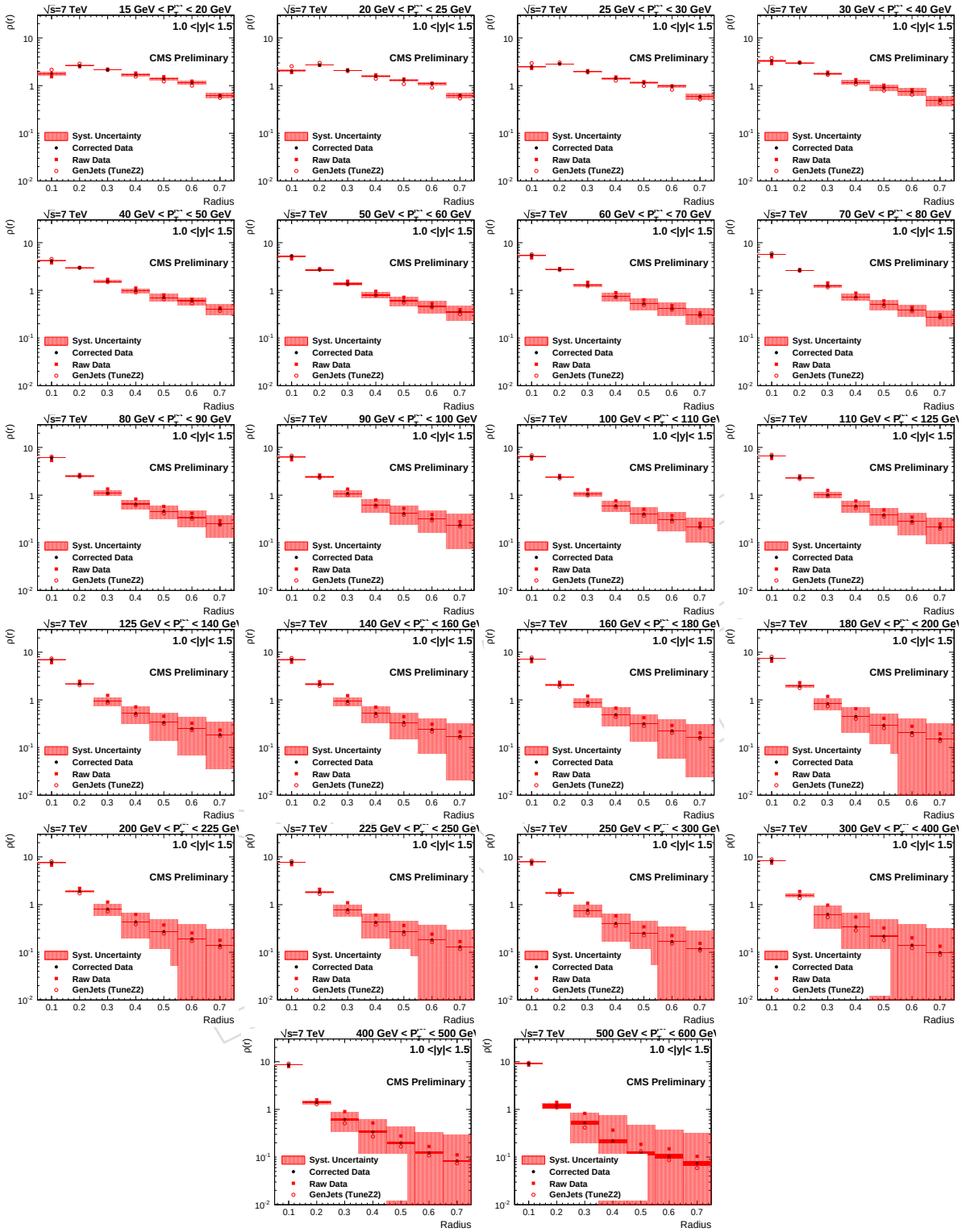

Figure 48: Corrected Differential JetShapes for 1.0< $|y|$ <1.5

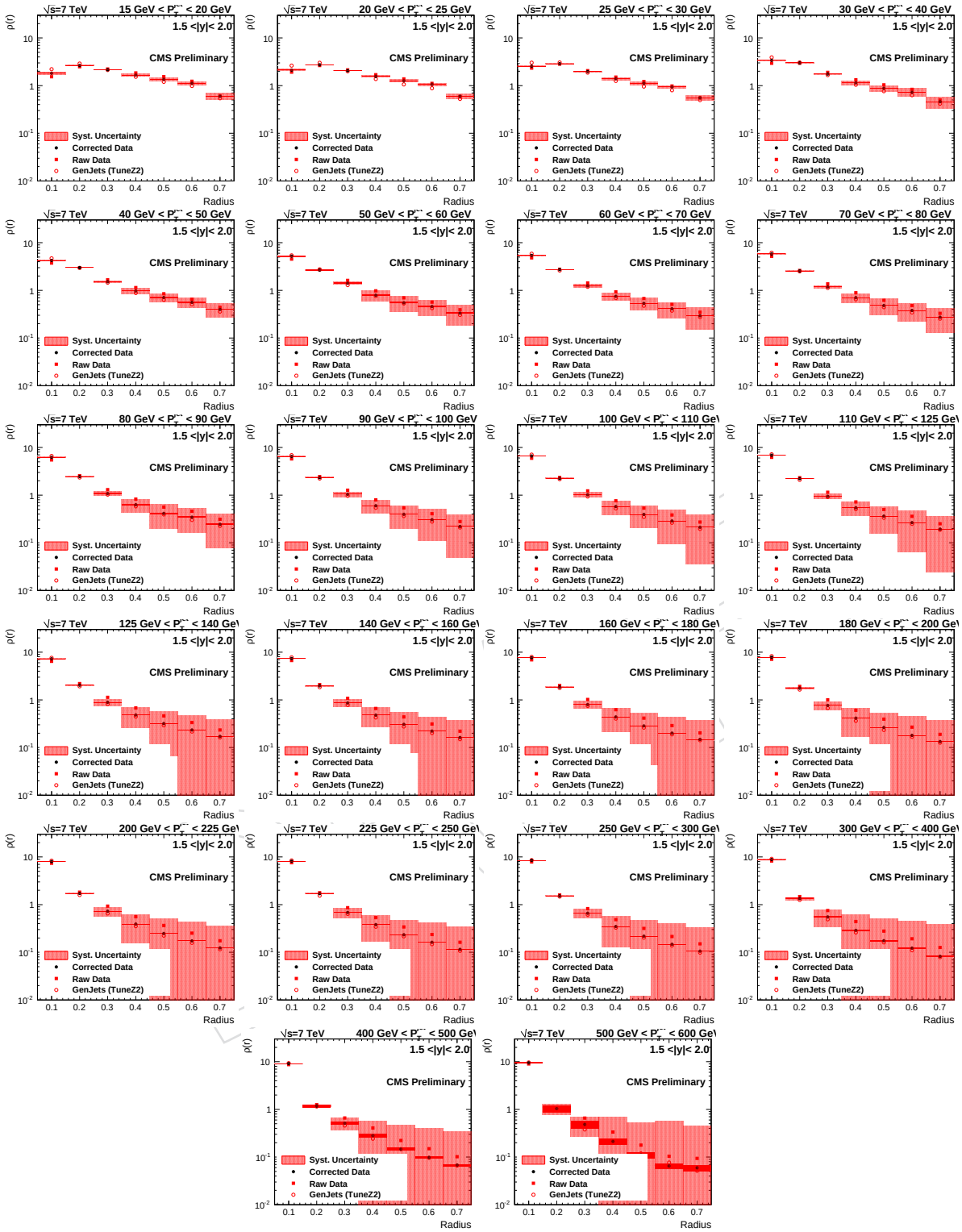

Figure 49: Corrected Differential JetShapes for 1.5< $|y|$ <2.0

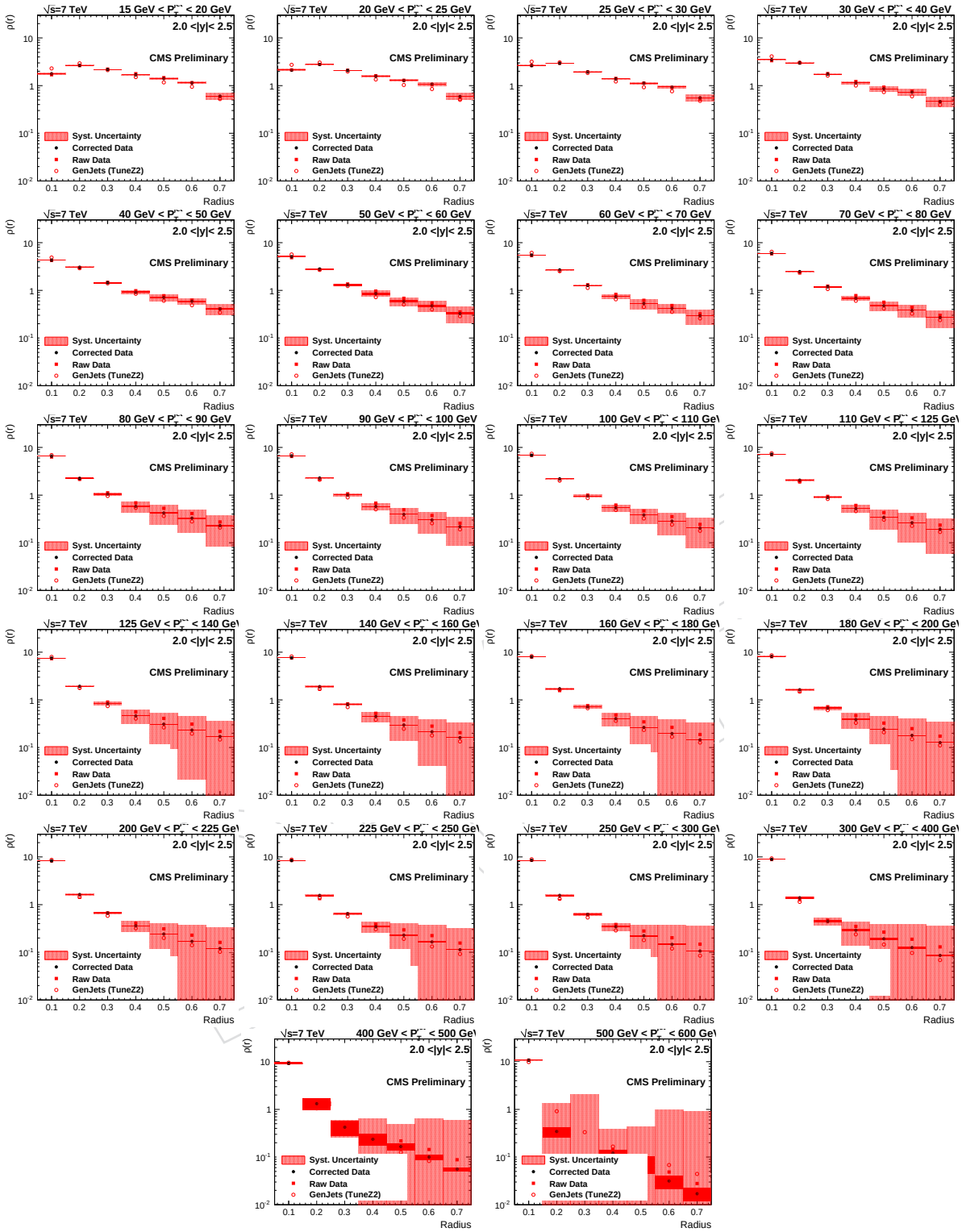

Figure 50: Corrected Differential JetShapes for 2.0< $|y|$ <2.5

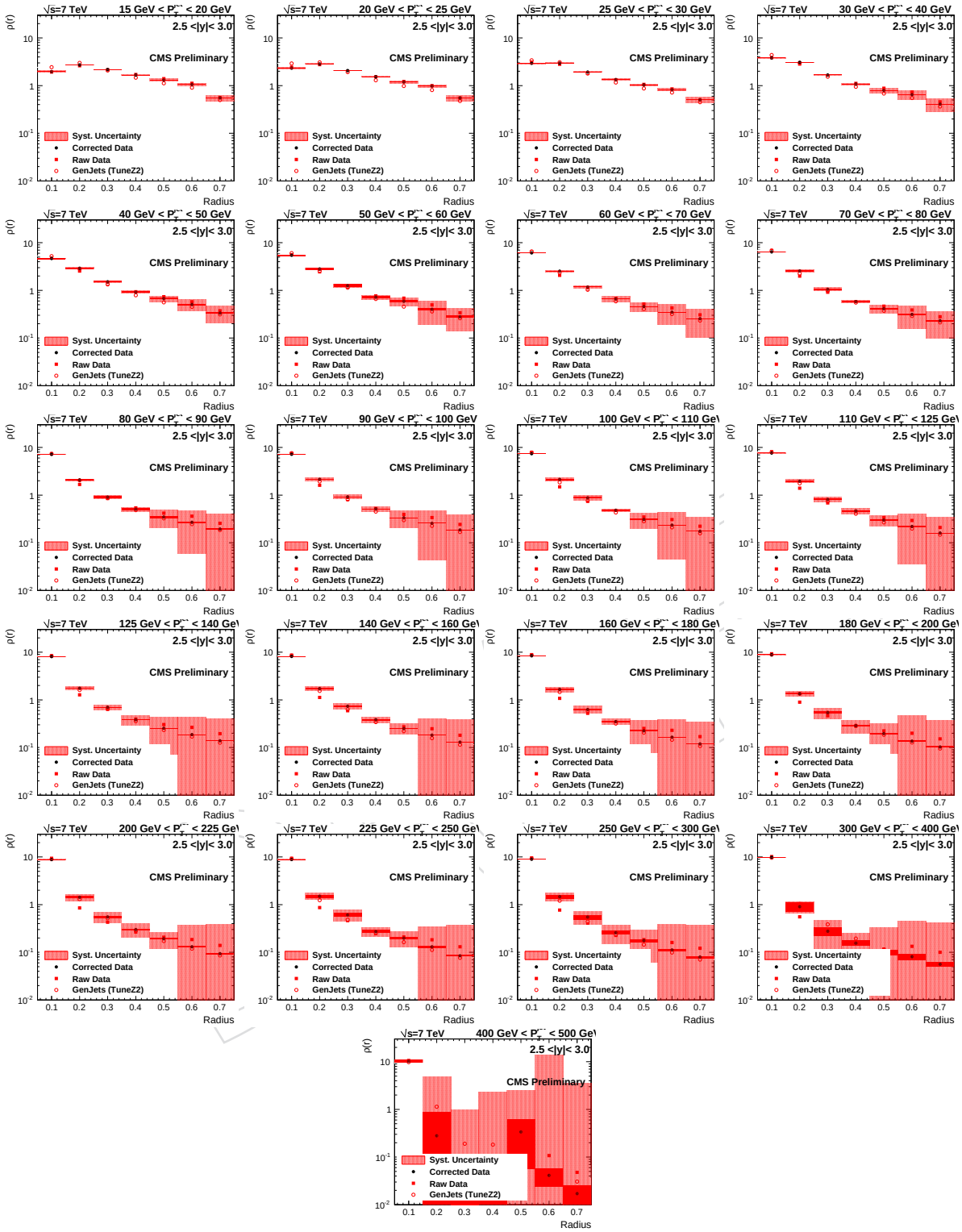

Figure 51: Corrected Differential JetShapes for 2.5< $|y|$ <3.0

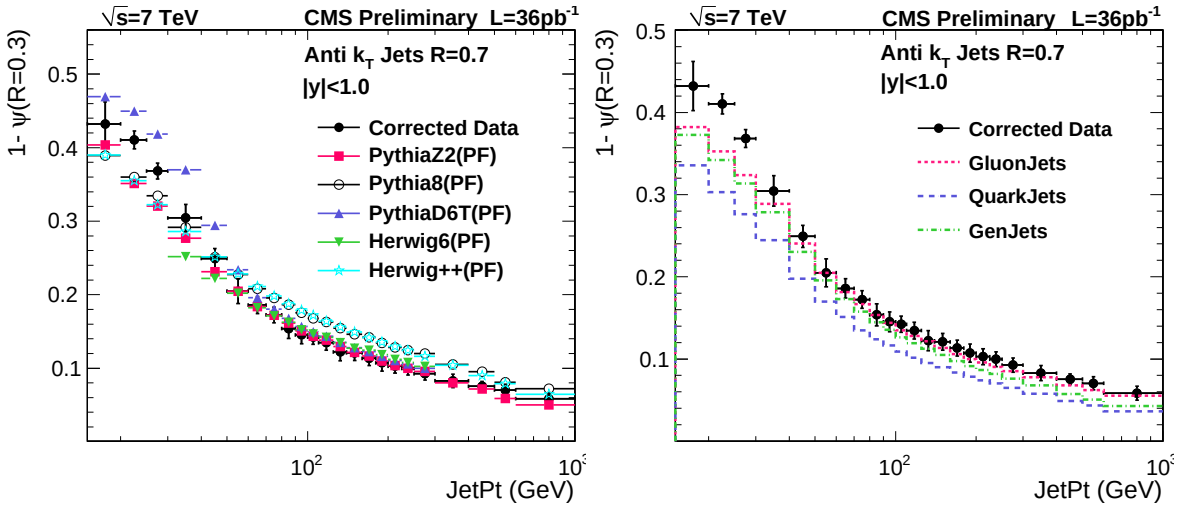

Figure 52: 1- psi(R=0.3) vs Jet pt for $|y| < 1$

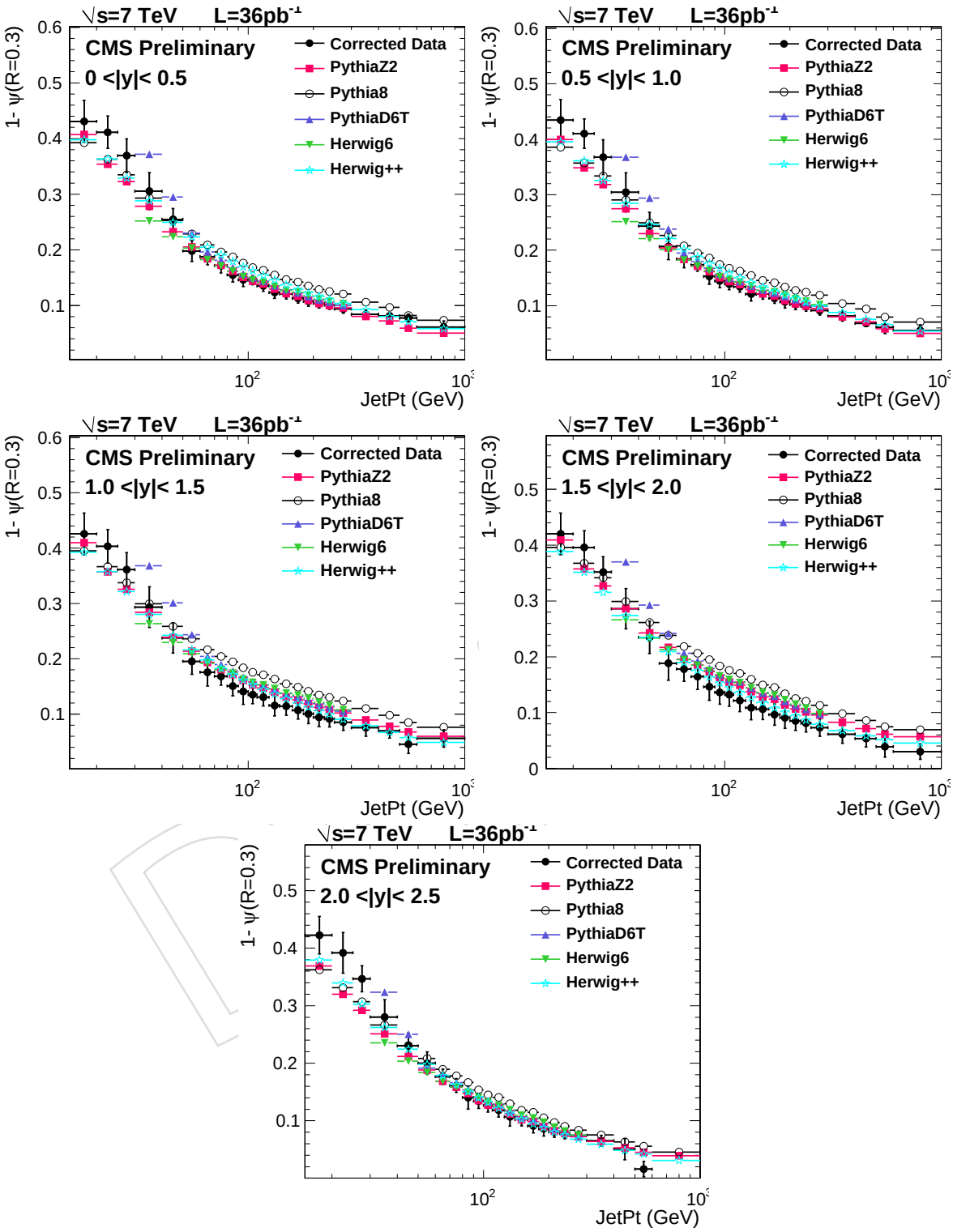

Figure 53: 1-psi(R=0.3) vs Jet pt for different rapidity bins

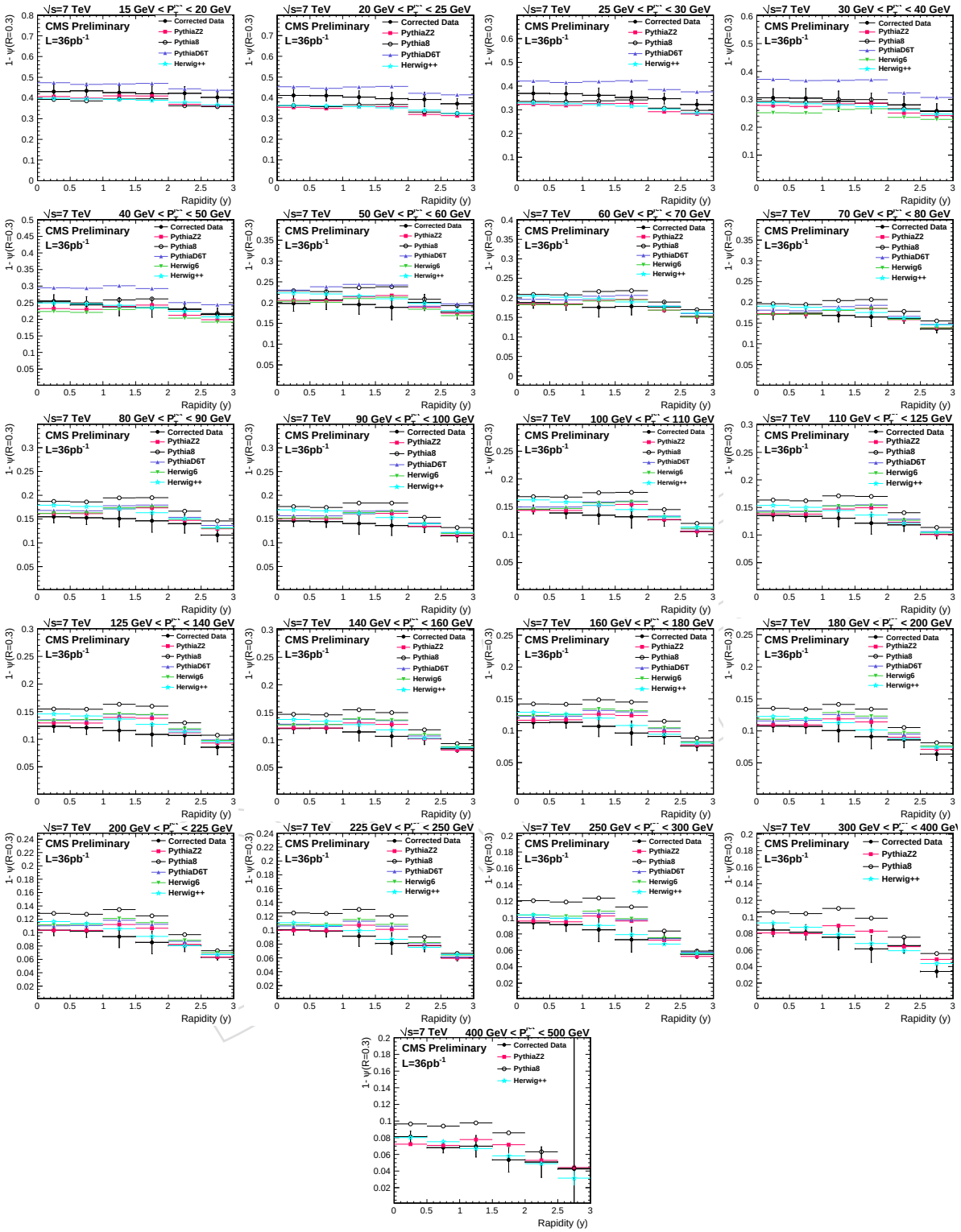

Figure 54: 1-psi(R=0.3) vs rapidity